Non-Intrusive Efficiency Estimation of Induction Machines under Various Power Supplies

Chetan Sudhir Gajjar

A dissertation submitted to the Department of Electrical Engineering,
University of Cape Town, in fulfilment of the requirements
for the degree of Master of Science in Engineering.

Cape Town, October 2013

Declaration

I declare that this dissertation is my own, unaided work. It is being submitted for the degree of Master of Science in Engineering in the University of Cape Town. It has not been submitted before for any degree or examination in any other university.

Signature of Author .....

Cape Town
October 2013

Abstract

Considering that 45% of the world's generated electricity is consumed by induction machines, determining an induction motors efficiency non-intrusively is of great importance in that it enables the machine to operate productively whilst ensuring that the energy consumed by the machine is utilized efficiently. International efficiency testing methods such as the IEEE 112-B can determine a motors efficiency accurately at the cost of hindering the machines productivity. Alternatively, various methods used to determine a machines efficiency in-situ do so at the cost of accuracy.

This research proposes a method that determines an induction machines efficiency over a range of load conditions from tests conducted and centered around one thermally stable load point in the least intrusive manner possible. Coupled with vibration sensors used to determine a motor's speed, measured input voltages and currents are used to deduce a machine efficiency-load profile through the use of a modified evolutionary algorithm, the Non-Intrusive Efficiency Estimation using Population-Based Incremental Learning (NIEE-PBIL) algorithm. Five temporal load measurements are taken, centered around one thermally stable load point, to determine the machines efficiency profile from two equivalent circuit implementations; the Standard Circuit NIEE-PBIL and the Iron-Loss NIEE-PBIL.

In order to assess the performance of the proposed method, international testing standards are employed as benchmarks for comparison of accuracy. 7.5kW and 11kW standard efficiency and premium efficiency induction machines, each supplied by balanced sinusoidal power, are tested and compared

against the IEEE 112-B and IEC 60034-2-1 standards at rated load conditions. Additionally, tests are conducted on a machine supplied by a PWM-VSI at two separate switching frequencies and results are compared against the direct efficiency method, also at rated load-torque conditions.

Results attained indicate that the proposed method accurately determines a machines efficiency. In a machines main operating region of $50 - 100\%$ of rated load, the proposed Standard Circuit NIEE-PBIL determines efficiency to an accuracy of $0.09 - 2.98\%$ and $0.04 - 2.57\%$ when compared to the IEEE 112-B and IEC 60034-2-1 standards respectively. In the same region, the proposed Iron-Loss Circuit NIEE-PBIL determines efficiency to an accuracy of $0.13 - 1.20\%$ and $0.11 - 1.95\%$ when compared to the IEEE 112-B and IEC 60034-2-1 standards respectively. The proposed Standard Circuit NIEE-PBIL determines a machines efficiency with an accuracy of $0.02 - 0.44\%$ and $0.07 - 1.04\%$ at high loading conditions $(125 - 150\%)$ when compared to the IEEE 112-B and IEC 60034-2-1 standards respectively. Alternatively, the proposed Iron-Loss Circuit NIEE-PBIL determines a machines efficiency with an accuracy of $0.18 - 2.12\%$ and $0.09 - 1.64\%$ at low loading conditions $(25 - 50\%)$ when compared to the IEEE 112-B and IEC 60034-2-1 standards respectively. However, the proposed algorithm cannot provide a consistent core loss evaluation of an induction machine, resulting in an efficiency estimate deviation of $\pm 0.25\%$ and $\pm 0.5\%$ at low loading conditions for the Standard and Iron-Loss NIEE-PBIL implementations respectively. As a result, improvements in the core loss and thermal model is recommended.

With regards to PWM-VSI testing, the proposed algorithm accurately estimates a machines efficiency by $0.14 - 3.04\%$ and $0.13 - 5.65\%$ in the $40 - 100\%$ load range for the Standard and Iron-Loss NIEE-PBIL implementations respectively. However, only a single machine using two switching frequencies, each under a single open-loop control scheme was tested. Thus further tests on various machines and various VSD implementations is recommended.

Acknowledgements

The author would like to thank the following:

My parents and brothers for their unconditional love and support, without whom none of this would be possible.

To Nirupa Mohee, a friend since my first day at the University of Cape Town, who assisted with the preparation of this document.

My supervisors, Assoc. Prof. Azeem Khan and Assoc. Prof. Paul Barendse for their advice, guidance and support for the duration of this thesis.

All the post-graduate members of the UCT AMES Group (past and present) who are not only colleagues but friends.

The lab support staff, Mr Chris Wozniak and Mr Phillip Titus, who assisted in the technical aspects of this research.

Contents

List of Figures

List of Tables

List of Symbols

$f_{carrier}$	—	frequency of carrier signal
f_{mod}	—	frequency of modulating signal
f_s	—	Fundamental frequency of the power supply
h	—	Harmonic order
I_c	—	Current through the core reluctance
I_m	—	Current through the core reactance
I'_r	—	Rotor current referred to the stator side
I_s	—	Stator current (or input line current)
I_ϕ	—	Total core current
m_a	—	Amplitude modulation ratio for PWM inverter
m_f	—	Frequency modulation ratio for PWM inverter
n	—	shaft speed of an IM in RPM
n_s	—	Synchronous speed of IM in RPM
P	—	Number of poles in an IM
P_{core}	—	Power loss incurred in the stator core
P_{FW}	—	Friction and Windage power loss
P_{elec}	—	Electrical power supplied to an IM
P_{in}	—	Input power supplied to an IM (Mech. or Elec. dependent on IM mode of operation)
P_{losses}	—	Losses incurred in an IM
P_{mech}	—	Mechanical power delivered by an IM
P_{out}	—	Output power delivered by an IM (Mech. or Elec. dependent on IM mode of operation)
P_{Rr-Cu}	—	Power loss incurred in the rotor winding

P_{Rs-Cu}	—	Power loss incurred in the stator winding
P_{SLL}	—	Stray load power loss
R_m	—	Electrical equivalent resistance of core reluctance
R'_r	—	Rotor resistance referred to the stator side
R_s	—	Stator resistance
s	—	slip of an IM under sinusoidal supply
v_{AN}, v_{BN}	—	Instantaneous phase voltages
v_{AB}	—	Instantaneous line voltages
$v_{control}$	—	modulating signal for PWM inverter
V_p	—	RMS phase voltage
v_{tri}	—	carrier signal for PWM inverter
X_m	—	Core leakage reactance
X'_r	—	Rotor leakage reactance referred to the stator side
X_s	—	Stator leakage reactance
η_{IM}	—	Efficiency of an IM

Nomenclature

AC	—	Alternating Current
ADC	—	Analog to Digital Converter
DC	—	Direct Current
GA	—	Genetic Algorithm
HVF	—	Harmonic Voltage Factor
IC	—	Integrated Circuit
IEC	—	International Electrotechnical Commission
IEEE	—	Institute of Electrical and Electronic Engineers
IM	—	Induction Machine
MCSA	—	Machine Current Signature Analysis
MMF	—	Magnetomotive force
MRAS	—	Model Reference Adaptive System
NIEE	—	Non-Intrusive Efficiency Estimation
PBIL	—	Population-Based Incremental Learning
PSD	—	Power Spectral Density
PWM	—	Pulse-Width Modulation
RMS	—	Root Mean Square
RPM	—	Revolutions Per Minute
THD	—	Total Harmonic Distortion
VSD	—	Variable Speed Drive
VSI	—	Voltage-Source Inverter

Chapter 1

Introduction

1.1 Background

Increasing demand of energy combined with rising energy costs has led to a desire to increase the efficiency of products and processes that utilize said energy. According to a report published by the International Energy Agency (IEA), electric motors account for $43-46\%$ of global electrical energy consumption [12]. Thus, one of the main reasons for monitoring an induction machine's efficiency is to ensure that productive mechanical power output is achieved from the least amount of electrical energy input.

In order to ensure that a machines operation and productivity are not hindered there is a need for determining a motors efficiency in the least intrusive possible manner. Unfortunately, the most common adopted strategies involved with determining an induction machine's efficiency implement methods whereby intrusiveness of tests used to determine efficiency directly correlate to accuracy of the estimate: the more intrusive the method, the more accurate the result.

1.2 Literature Review

Based on the importance of determining induction motor efficiency, the accuracy and methodology of measuring efficiency has been scrutinized. In [13] and [14] international standards for determining motor efficiency are analyzed and compared against each other. Due to the increasing accuracy of measurement equipment, [13] concluded that the indirect methods such as the IEEE 112-B provide the most accurate way of determining efficiency. Indirect methods involve segregating losses in an induction motor. By independently determining each of the losses the impact of instrumentation error is reduced when compared to directly determining a machines efficiency. The differences in efficiency estimates between the IEEE 112-B and IEC 60034-2 standards are a result of the differences in the methodology of determining each of the losses. Nevertheless both standards provide an efficiency estimate to a high degree of accuracy for a machine's entire load range [14].

The disadvantage of implementing the IEEE 112-B and IEC 60034-2 standards lie in that fact that the tests required in determining efficiency are intrusive. Whilst tests are conducted the productive output of a machine is hindered, thus non-intrusive efficiency estimation methods have been developed [15], [16]. In [17], efficiency estimation methods are grouped according their physical natures and the intrusiveness versus accuracy of the methods are analyzed. It was found that the more intrusive the method, the more accurate the efficiency estimate.

In [18] the efficiency of a motor is determined by non-intrusively determining the air-gap torque power. Rotor speed and stator resistance are determined from the measured input current and a DC voltage injection circuit. No-load and stray load losses are determined from empirical values suggested by the IEEE 112 standard. Using this method, [18] found that the motor efficiency can be estimated with less that a 2% error under a machines normal load condition.

The disadvantage of the method described in [18] is the intrusiveness of the DC voltage injection circuit whose impact on machine performance has not been analyzed; as well as the fact that the method can only determine efficiency for tested loading condition. In [19] the efficiency of a machine is derived from a genetic algorithm that utilizes voltage and current measurements taken from five load points. Rather than using a DC injection circuit to estimate stator resistance, a method of determining the machines temperature is introduced given that the stator resistance at ambient temperature is known. Additionally, the speed on the machine is determined from current measurements using a non-linear adaptive algorithm [20]. The proposed method described in [19] estimates a machines efficiency to an accuracy of $1-5\%$ error depending on the machine's loading condition.

In addition to determining an induction machines efficiency, it is becoming more common for Variable Speed Drives (VSD) to be implemented in industry in order to optimize the process system [21]. Numerous electrical equivalent circuits have been proposed for dealing with induction machines under harmonic power supply. A simple equivalent circuit proposed in [8] ignores the impact of core leakage and iron losses and states that the relationship between the harmonic

and fundamental stay load loss is logarithmic. Alternatively, [7] proposes an equivalent circuit where stray load and core losses are represented in both the rotor and stator sides of the circuit. Additionally, the relationship between the harmonic and fundamental core and stray-load loss components are based on the eddy-to-hysteresis loss ratio of the machine.

Despite the introduction of VSD's in the late 20th century, there exists no international testing standard for induction machines under these conditions. It is only recently that the IEC modified its IEC 60034-2 standard and suggested the IEC 60034-2-3 ([22]) for harmonic power supply. However this standard was still in the draft phase at the time of this research.

1.3 Research Objectives

The main objective of this research is to develop a non-intrusive efficiency estimation technique for induction machines for both a sinusoidal powered induction machine as well as a VSD powered induction machine. Two electrical equivalent circuits are to be adapted and utilized in determining the efficiency of induction machines under sinusoidal and VSD harmonic power supply. The proposed technique is to be implemented and compared against the most accurate (and intrusive) international motor efficiency testing standards. Based on experimental results, a comprehensive analysis will be carried out on the performance of the proposed efficiency estimation technique. Conclusions will be drawn based on the analysis of results associated with tests and recommendations will be made for work to be done that could contribute to improvements and extensions of the proposed technique.

1.4 Scope and Limitations

Due to time and equipment limitations the scope of this research is to compare the proposed technique for sinusoidal power supplied machines against two

international efficiency estimation benchmarks; the IEEE 112-B and IEC 60034-2-1 methods. Although realistic supply conditions include a degree of unbalance, tests on 4 machines will be conducted whereby the power supplied is balanced as defined by the IEEE and IEC standards.

Whilst there are various VSD implementations that exist, harmonic testing in this research will be limited to pulse-width modulated voltage source inverters (PWM-VSI). A single machine will be tested under two PWM-VSI switching frequencies. However, due to the absence of international harmonic motor testing standards (at the time of testing), the proposed method will be compared against the direct method.

1.5 Outline of Research Report

The structure of this research report is as follows:

Chapter 2 provides a brief overview of the construction and operation of an induction machine. Three modes of operation of an induction motor and their respective power flows are discussed as they have relevance in validating the proposed concept. In addition, losses that occur during the operation of an induction motor are identified and defined with relation to the machine's equivalent circuit model.

Chapter 3 outlines the effects of harmonics in the power supply on induction machines and builds on the standard sinusoidal equivalent circuit to develop the harmonic equivalent circuit. A brief summary on PWM generation in voltage source inverters is given in addition to performance tests that can be used to determine machine efficiency.

Chapter 4 begins by giving a brief overview of non-intrusive speed estimation methods before detailing the proposed speed estimation method, speed estimation via vibration analysis using signal processing techniques.

Based on the theory development from Chapters 2 and 3, and given that the speed of an induction machine can be determined (as described in Chapter 4), Chapter 5 summarizes various non-intrusive efficiency estimation methods and outlines the proposed NIEE-PBIL technique.

Chapter 6 reviews the experimental equipment used to collect test data from an induction machine as well as the tools used to analyze the data to produce an efficiency estimate.

Chapters 7-9 presents the results and analysis of the tests conducted in determining speed and efficiency of induction motors compared against industry benchmarks. Chapter 7 presents the speed estimation analysis. The efficiency estimation of induction machines under sinusoidal and harmonic power supply are discussed in Chapters 8 and 9 respectively.

Based on analysis of the test results, Chapter 10 contains the concluding remarks and proposes recommendations for future work.

Chapter 2

Review of Induction Machines: Operation and Performance Characteristics

This chapter gives a brief overview on the construction and operation of an induction machine. Three modes of operation of an induction motor and their respective power flows are discussed as they have relevance in validating the proposed concept. In addition, losses that occur during the operation of an induction motor are identified and defined with relation to the machine's equivalent circuit model and power flow in its various modes of operation.

2.1 Construction of Induction Machines

The basic structure of an induction machine can be divided into three distinguishable parts; the stator, rotor and air-gap as seen in Figure 2.1.

The stator, which is composed of a frame of stacked laminations of high-grade steel, forms the magnetic core of the machine. In the case of a 3-phase machine, evenly distributed stator windings (distributed at 120 electrical degrees) are inserted into slots in the inner perimeter of the aforementioned laminations. The windings are connected to a 3-phase power supply in either a star or delta configuration [4].

The rotor of an induction machine, which is also comprised of laminated ferromagnetic material, is separated from the stator by a uniform air-gap [4]. Whilst there are various configurations of rotor windings attached to the rotor slots, for the purposes of this research, the squirrel-cage configuration will only be considered. The squirrel-cage configuration has aluminum/copper rings at the end of shortened aluminum/copper bars embedded in the rotor slots [4].

2.2 Operation of an Induction Machine

If the stator windings of an induction motor were supplied by a balanced, sinusoidal 3-phase power supply; each of the phase currents in the windings would produce a sinusoidal *magnetomotive force* (MMF). The sum of the phase MMF's produce a rotating magnetic field in the air-gap [4]. The speed at which

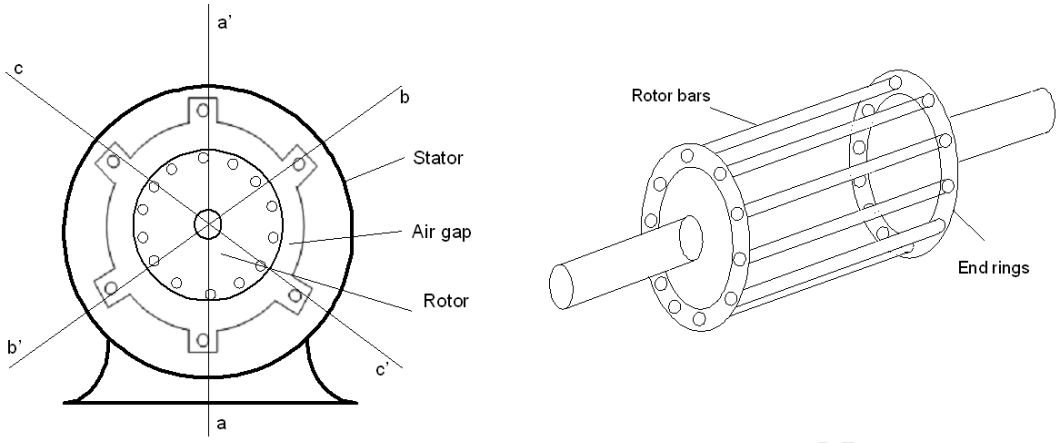

Figure 2.1: Construction of Induction Machine [3]

the rotating magnetic field rotates is referred to as the synchronous speed and is dependent upon the number of poles in the induction machine and the supply frequency as defined in Equation 2.1.

$$n_s = \frac{120 f_{supply}}{P} \tag{2.1}$$

Where:

- n_s is the synchronous speed in RPM.
- P is the number of poles in the induction machine.
- f_{supply} is the fundamental frequency of the supply source.

The rotating magnetic field in the air-gap induces a voltage across (and thus a current through) the rotor bars. This leads to an MMF produced by the rotor, which due to Faraday's law, attempts to align itself with the rotating MMF in the air-gap. This interaction leads to the rotor turning and producing a torque on the rotor shaft [4], [3]. The relation between the speed of the rotor shaft and the synchronous speed is defined in Equation 2.2.

$$s = \frac{n_s - n}{n_s} \tag{2.2}$$

Where:

- s is slip of the machine.
- n is speed of the rotor shaft.

Modes of Operation of an Induction Machine

The operation, and thus slip limits, of an induction machine are determined by the relationship between the rotor's and air-gap's MMF direction and speed. The modes of operation are plugging, motoring and generating, as seen in Figure 2.2.

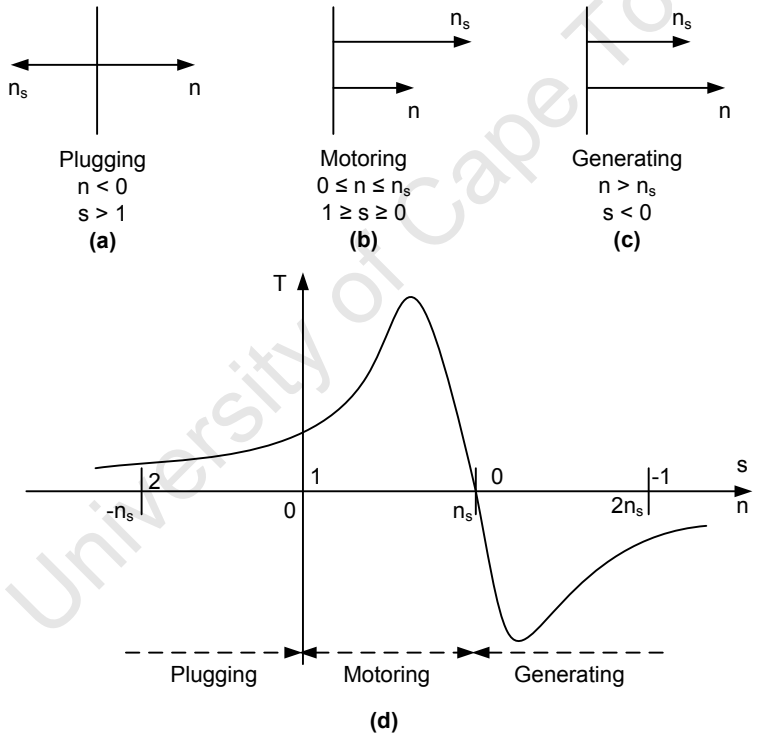

Figure 2.2: Modes of Operation of an Induction Machine [4]

Plugging Mode of Operation

If the direction of the rotor is in the opposite direction of the rotating air-gap magnetic field (as shown in Figure 2.2a), the resultant torque is said to be a

breaking torque. This operation is mainly utilized in drive applications to control motor speeds [4]. However, in the scope of this research as will be discussed in later chapters, this theory can also be applied to 'negative' harmonics in the power supply where the breaking torque is less than the main torque supplied during the motoring mode of operation.

Motoring Mode of Operation

When the speed of the rotor is less than that of the rotating magnetic field in the air-gap, an induction machine is said to be in motoring mode (as depicted in Figure 2.2b). This is the natural mode of operation of an induction machine [4].

Generating Mode of Operation

In the generating mode of operation, an induction machine rotor speed is greater than that of the rotating air-gap/synchronous speed as seen in Figure 2.2c. This results in the machine producing a torque acting in the opposite direction of the air-gap rotating field where the kinetic energy of the rotor is fed back into the stator supply [4].

2.3 Performance and Power Flow of Induction Machines

Efficiency of an induction machine is the ratio of the mechanical power delivered at the shaft of the machine divided by the electrical input power to the machine [23], and using the IEEE Std 112-2004, is calculated as shown in Equation 2.3.

$$\eta_{IM} = \frac{P_{mech}}{P_{elec}} = \frac{P_{out}}{P_{in}} \tag{2.3}$$

A commonly used form for induction machines in motoring mode is [1]:

$$\eta_{IM} = \frac{P_{in} - \sum P_{losses}}{P_{in}} \tag{2.4}$$

The power flow in an induction motor can be better understood using its electrical equivalent circuit seen in Figure 2.3.

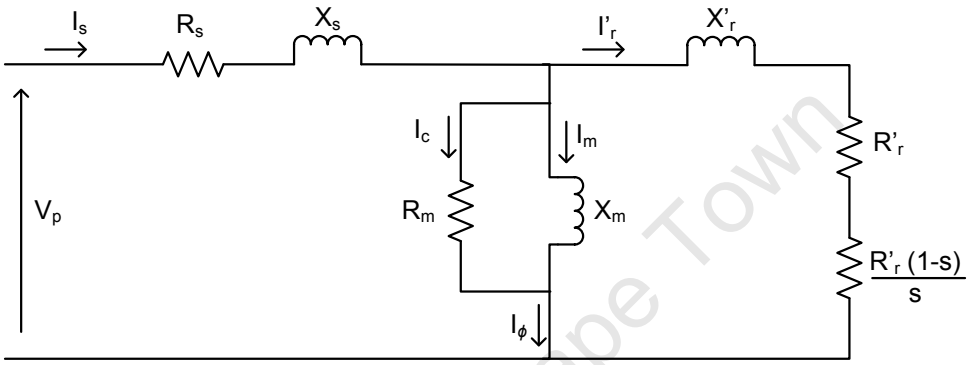

Figure 2.3: Induction Machine Equivalent Circuit

Where:

- V_p is the phase voltage.
- I_s is the stator current (or input line current).
- $I_\phi = I_c + I_m$ is the magnetic core current.
- I'_r is the rotor current referred to the stator side.
- R_s is the stator resistance.
- X_s is the stator leakage reactance.
- R_m is the electrical equivalent resistance representing core losses.
- X_m is the core magnetizing reactance .
- R'_r is the rotor resistance referred to the stator side.
- X'_r is the rotor leakage reactance referred to the stator side.
- s is the operating slip (as defined in Equation 2.2).

2.3.1 Losses in an Induction Machine

From Equations 2.3 and 2.4, the sum of the losses in an induction machine is the difference between the input and output power. Individual losses in the machine fall under two general categories: load dependent and load independent.

Stator Copper Loss

The stator copper (or stator winding) loss is dependent on the current passing through the stator resistance R_s. The losses include the heat loss due to current flow through the winding as well as the skin effect due to the frequency of current through the winding [4], [23]. The stator copper loss accounts for 25-40% of total losses in the machine and are considered load dependent [23].

Referring to Figure 2.3, in a balanced 3-phase power supplied induction machine the stator copper loss, P_{Rs-Cu}, can be expressed as:

$$P_{Rs-Cu} = 3{I_s}^2 R_s \tag{2.5}$$

Rotor Copper Loss

The rotor copper loss is the power lost in the form of heat due to the flow of current in the rotor bars. The losses account for 15-25% of total losses in the machine and are considered load dependent [23].

Referring to Figure 2.3, in a balanced 3-phase power supplied induction machine the rotor copper loss, P_{Rr-Cu}, can be expressed as:

$$P_{Rr-Cu} = 3{I'_r}^2 R'_s \tag{2.6}$$

Core Loss

The core losses comprise of the hysteresis and eddy current losses in the iron laminations of the machine as a result of the energy required to magnetize the core [4], [23]. The core losses account for 15% of total losses in the machine and are considered to be load independent [23].

Referring to Figure 2.3, in a balanced 3-phase power supplied induction machine the core loss, P_{core}, can be expressed as:

$$P_{core} = 3I_c^2 R_m \tag{2.7}$$

Where R_m is the electrical equivalent resistance of the core losses of the iron laminations in an induction machine that allows for hysteresis and eddy current losses to be accounted for in an electrical circuit [24].

Friction and Windage Losses

The friction and windage losses, P_{FW}, comprise of the heat loss due to bearing friction in the machine as well as the loss from air friction in cooling the machine from the cooling fan. These losses can account for 5-15% of total losses in the machine [23]. Whilst the loss is considered to load independent as stated in [23], according to [7], friction and windage losses vary with the square of the speed of the machine.

Stray Load Losses

The stray load losses are considered to be additional load losses not accounted for in the losses listed above and account for 10-20% of total machine losses [23]. The losses occur due to leakage fluxes of the windings and space harmonics associated with the stator and rotor [23].

The magnitude of these losses, P_{SLL}, are calculated from the difference between

the total losses in a machine and the sum of the conventional losses as seen in Equation 2.8 [23].

$$P_{SLL} = P_{in} - P_{out} - (P_{Rs-Cu} + P_{Rr-Cu} + P_{core} + P_{FW}) \tag{2.8}$$

2.3.2 Power Flow in an Induction Machine

In a balanced 3-phase power supplied induction machine, the mechanical developed power can be expressed as [4]:

$$P_{mech} = 3I_r^{'2}\frac{R_r'}{s}(1-s) \tag{2.9}$$

Due to the nature of the electro-mechanical energy conversion process, the output power of an induction machine (P_{out}) can be defined in electrical or mechanical terms. The output power can be calculated as a function of rotor current and resistance or as a function of the torque and speed generated as seen in Equation 2.10 [4].

$$\begin{aligned} P_{out} &= P_{mech} - P_{FW} = 3I_r^{'2}\tfrac{R_r'}{s}(1-s) - P_{FW} \\ &= \omega_{shaft}T_{shaft} \end{aligned} \tag{2.10}$$

Where:
- T_{shaft} is the torque at the shaft.
- ω_{shaft} is the shaft speed in radians per second $\left(\frac{2\pi n}{60}\right)$.

The power flow in the three modes of operation of an induction machine (listed in Chapter 2.2) can be illustrated as seen in Figure 2.4 [4], [25].

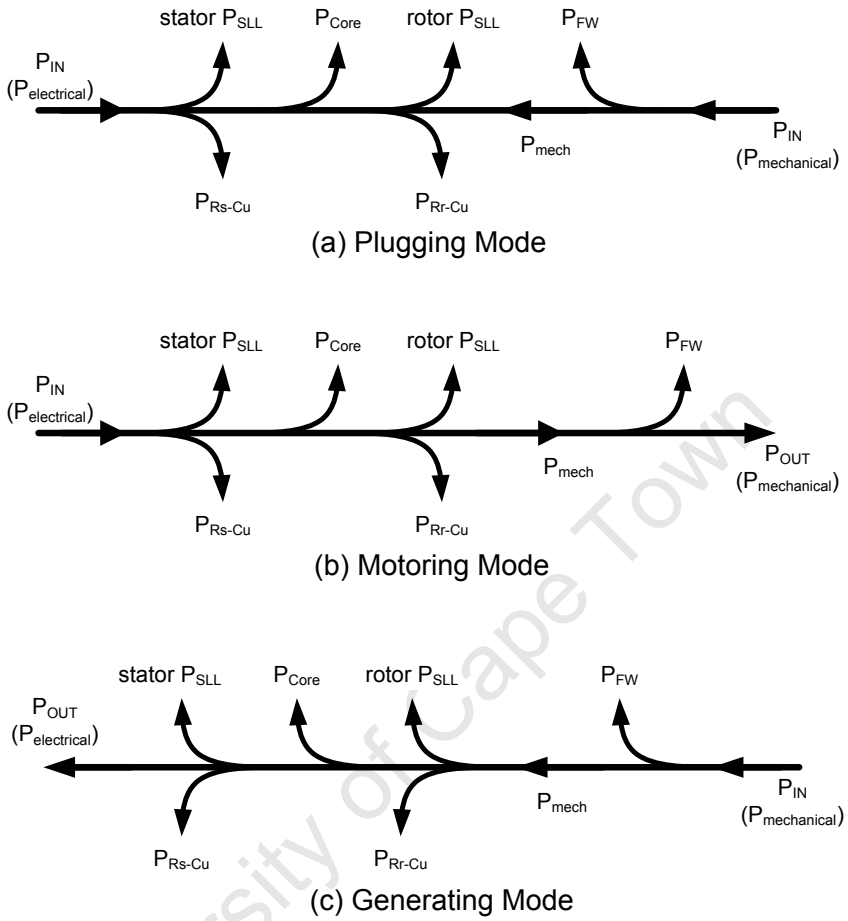

Figure 2.4: Power Flow of Induction Machine in Various Modes of Operation

2.4 Review of International Efficiency Estimation Standards

Whilst there are several standards worldwide that exist for testing an induction machine's efficiency, the two that are often referenced are the IEEE 112 and the IEC 60034-2-1.

2.4.1 IEEE 112 [1]

There are five methods described in the IEEE 112 standard: A, B, C, E and F. Method A is a *Direct Method* where the efficiency is derived from the ratio of the measured output and input powers. Method C is used in instances where two identical machines are available and coupled together using two independent power sources and each machine operates as a generator and motor alternatively. Method E adjusts the stator and rotor losses to a specified temperature so that their sum accounts for the total losses in the machine. Method F utilizes the equivalent circuit to determine efficiency after stray load losses have been measured.

Prior to the publication of the IEC 60034-2-1 standard, the IEEE 112-B loss segregation method was considered the most suitable procedure for determining a motor's efficiency with a high degree of accuracy [14], [13]. The IEEE 112-B segregates each of the losses that occur in an induction machine. Whilst a machine is connected to a dynamometer a rated load temperature test is conducted after the winding resistances have been measured at ambient temperature. A variable load test is performed whereby the stator winding temperatures cannot deviate by more than $10°C$ from the temperature at the hottest load point. A no-load test is also performed.

From the tests the stray load losses can be determined by subtracting the other temperature corrected losses (copper, friction, windage, core) from the difference between measured output power and measured input power at each load point. The stray load losses are then smoothed using linear regression analysis based on a linear function of the variation of stray load loss with measured torque until a correlation factor of 0.9 or greater is achieved.

2.4.2 IEC 60034-2-1 [2]

The IEC 60034-2-1 standard is similar to the IEEE 112-B method in that efficiency of a machine is determined by loss segregation that are based on

defined tests. Apart from not requiring temperature sensors to be embedded in the machine during testing, the IEC 60034-2-1 also derives the core and stray load losses differently when compared to the IEEE 112-B. According to the IEC 60034-2-1 standard, core losses vary with load which is accounted for by the voltage drop across the stator winding resistance. The difference between the IEC60034-2-1 and IEEE 112 standards with respect to determining stray load losses is that former standard determines the stray load loss as a function of input power whilst the latter determines the loss from output power.

2.4.3 Instrumentation Requirements [1],[2]

In order to ensure that the efficiency estimates of a machine are given to the highest degree of accuracy possible, the IEEE and IEC standards require that the test equipment implemented meet stringent specifications.

- Instrument transformers used should have an error of less than $\pm 0.3\%$.
- The voltage supply shall conform to the following:
  - The frequency shall be within $\pm 0,1\%$ of the rated frequency during measurements.
  - The harmonic distortion coefficient,(THD), shall not exceed 0.05 per phase.
  - The voltage unbalance ratio should not exceed 0.5%.
- Speed measurement shall provide a reading with an error of less that $\pm 1rpm$.
- Torque measurement shall have an accuracy less than $\pm 0.2\%$ of the full scale of the instrumentation.
- Temperature readings shall have an accuracy of $\pm 1°C$.

Chapter 3

Impact of Voltage Source VSDs on Induction Motor Performance

This chapter outlines the effects of harmonics in the power supply on induction machines with reference to standard equivalent circuit that was described in the previous chapter. However, before the effects of harmonics on an induction machine are reviewed, a brief summary on PWM generation in voltage source inverters is given. The chapter concludes with the development of the harmonic equivalent circuit and performance tests that can be used to determine the harmonic equivalent circuit parameters.

3.1 Overview of Voltage Source VSDs

In induction motor applications, a VSD is used to vary the speed of the machine by varying the supply frequency. This is achieved through the fact that the synchronous speed of the machine is dependent upon the supply frequency as noted in Equation 2.1 [6]. The block diagram of a VSD is shown in Figure 3.1. The numerous types of VSDs available are categorized according to the types of rectifiers and inverters implemented. However, due to the limitations in the scope of this research, an overview of only the PWM-VSI type of VSD will be outlined.

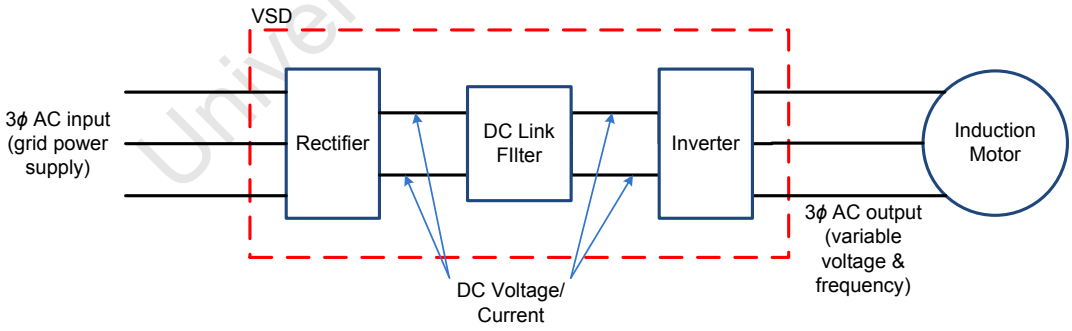

Figure 3.1: Block Diagram of VSD [5], [6]

3.1.1 Generation of PWM Voltage Signals

A PWM-VSI inverter uses a diode rectifier to convert the 3-phase AC power supply input into a DC voltage. This DC voltage is filtered with a capacitor in the DC link stage, thus the DC input in the inverter stage appears as a voltage source with no internal impedance. The inverter stage converts its DC input into a 3-phase PWM voltage output whose amplitude and frequency is independent of the induction motor [5]. An electrical schematic of the PWM-VSI drive can be seen in Figure 3.2.

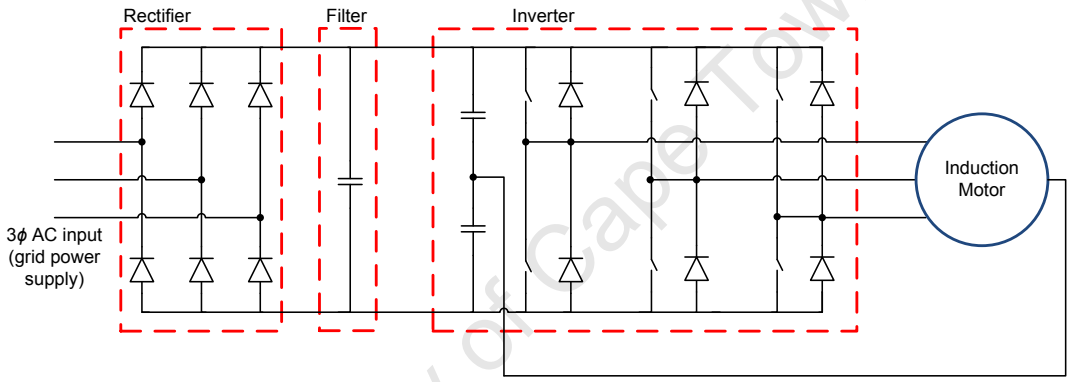

Figure 3.2: PWM-VSI Schematic [5], [6]

In a 3-phase voltage source PWM inverter, the output voltage is determined by the interaction between a carrier and modulation signal. Referring to Figure 3.3, [5] and [6], the operation of a PWM-VSI can be summarized as follows. The carrier signal v_{tri} operates at a frequency $f_{carrier}$ which determines the frequency at which the inverter switches are switched. The control signal for each phase ($v_{control,a}$, $v_{control,b}$, $v_{control,b}$) which operate at a frequency f_{mod} is used to control the switch duty ratio and is also the desired fundamental frequency of the output voltage. The modulating and carrier waves can be seen in Figure 3.3-a.

In order to create a PWM oscillating at a sinusoidal frequency, the voltage pulse duration's are determined by the relationship between v_{tri} and each $v_{control}$. Referring to 3.3-b, the phase PWM's of phase A, v_{AN}, and B, v_{BN}, are:

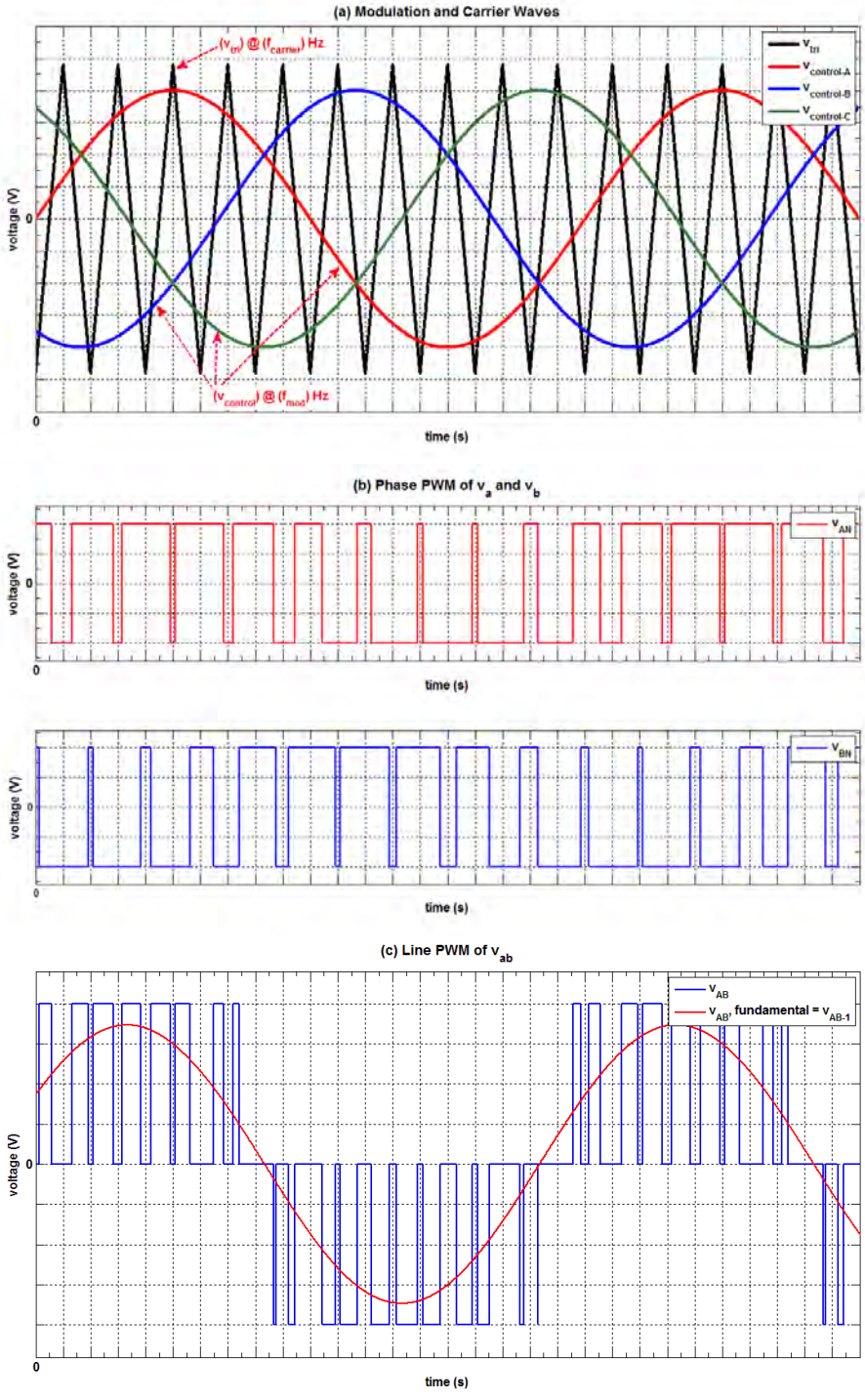

Figure 3.3: PWM-VSI Waveform Generation

$$v_{AN} = \begin{cases} \frac{-V_{DC}}{2} & if: \ v_{control,a} < v_{tri} \\ \frac{V_{DC}}{2} & if: \ v_{control,a} > v_{tri} \end{cases} \tag{3.1}$$

and

$$v_{BN} = \begin{cases} \frac{-V_{DC}}{2} & if: \ v_{control,b} < v_{tri} \\ \frac{V_{DC}}{2} & if: \ v_{control,b} > v_{tri} \end{cases} \tag{3.2}$$

Where V_{DC} is the output DC voltage from the *DC link stage* as seen in Figure 3.1.

The PWM line voltage delivered to the induction motor, as seen in Figure 3.3-c, is the difference between the PWM phase voltages:

$$v_{AB} = v_{AN} - v_{BN} \tag{3.3}$$

The phase of the fundamental harmonic, v_{AB-1}, is equal to the phase of the difference between v_{AN} and v_{BN} as defined in Equation 3.4.

$$\angle v_{AB-1} = \angle(v_{AN} - v_{BN}) \tag{3.4}$$

This theory holds true respectively for the PWM line voltages v_{BC} and v_{CA} which are also received by the induction motor. These line PWM voltages have a fundamental frequency equal to that of the control signals $v_{control,a}$, $v_{control,b}$ and $v_{control,c}$ which are all equal.

3.1.2 Harmonics in a PWM-VSI

The amplitude modulation ratio, m_a, and frequency modulation ratio, m_f, are defined as:

$$m_a = \frac{\hat{v}_{control}}{\hat{v}_{tri}} \tag{3.5}$$

$$m_f = \frac{f_{carrier}}{f_{mod}} \tag{3.6}$$

Where:

- $\hat{v}_{control}$ is the peak amplitude of the modulation signals $v_{control,a}$, $v_{control,b}$, $v_{control,c}$.
- $\hat{v}_{tri}$ is the peak amplitude of the carrier signal v_{tri}.
- f_{mod} is the frequency of the modulation signals $v_{control}$.
- $f_{carrier}$ is the frequency of the carrier signal v_{tri}.

The harmonics in the line PWM exist as sidebands centered around multiples of m_f. As the fundamental harmonic of each of the 3-phase PWM line voltages are 120° out of phase, the phase difference between each m_f harmonic of each PWM line voltage is $(120m_f)°$ out of phase which will equal zero if m_f is a multiple of 3 [5]. The harmonic spectrum of the voltage source PWM can be seen in Figure 3.4.

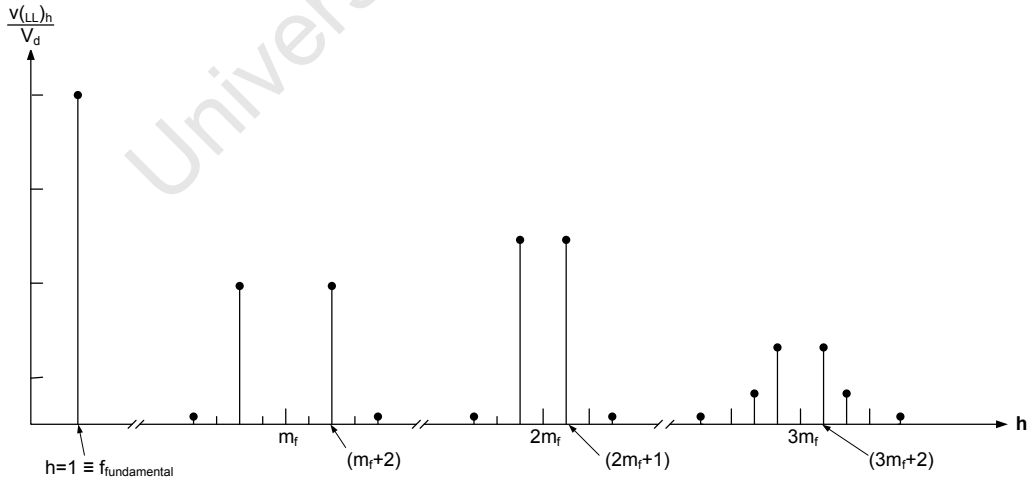

Figure 3.4: Harmonic Spectrum of Line PWM [5]

If the amplitude modulation increases to a sufficiently large value, the PWM

will degenerate into a square wave voltage [5]. In this instance, the line voltage can be expressed as a trigonometric function whose harmonic order is determined by the number of pulses in the inverter. Given that there are six pulses (derived from Figure 3.2), the square-wave trigonometric function, v_{AB}, and harmonic order, h, are defined in Equations 3.7 and 3.8 [5], [7].

$$v_{AB} = V_{m,1}sin(\omega_1 t) + \begin{cases} -\frac{V_{m,1}}{h}sin(h\omega_1 t) & when\ k\ is\ a\ odd\ number \\ \frac{V_{m,1}}{h}sin(h\omega_1 t) & when\ k\ is\ an\ even\ number \end{cases} \tag{3.7}$$

Where:

$$h = 6k \pm 1 \tag{3.8}$$

and

- $k = 1, 2, 3, 4, ...$
- $V_{m,1} = \frac{2\sqrt{3}}{\pi}V_{DC}$, where V_{DC} is the output of the inverter DC link stage.

The magnitudes of each harmonic h is equal to $\frac{V_{m,1}}{h}$ as seen in Figure 3.5.

3.2 Development of the IM Harmonic Equivalent Circuit

Harmonics exist in an induction machine regardless of the power supply due to constructional constraints that occur in the manufacturing process. These harmonics are classified as *Space Harmonics*. The harmonics that occur as a result of the power supply quality are called *Time Harmonics*. The IEEE 112 Standard defines a power supply to be sinusoidal if the harmonics distortion

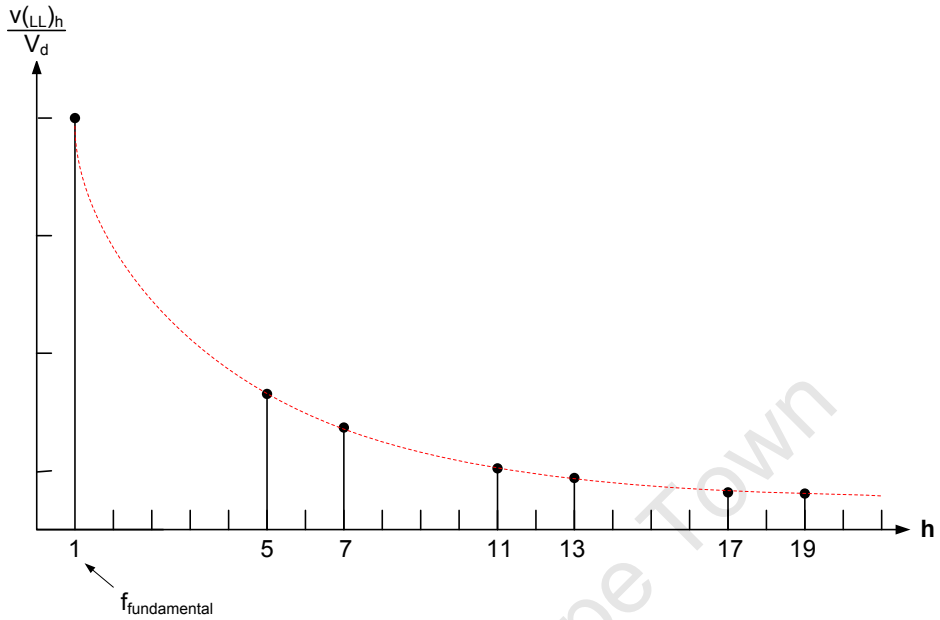

Figure 3.5: Harmonics when m_a is large (square-wave inverter)

coefficient THD (defined in Equation 3.9) does not exceed 0.05 [1].

$$THD = \frac{\sqrt{E^2 - E_1^2}}{E} \tag{3.9}$$

Where:

- E_1 is the RMS of the fundamental voltage.
- E is the RMS of the voltage wave.

According to the IEC 60034-17 standard, the harmonic voltage factor HVF is defined as [26]:

$$HVF = \sqrt{\sum_{h>1} \frac{(V_h)^2}{h}} \tag{3.10}$$

Forward harmonics are defined as the harmonics that add towards the

fundamental harmonic of the machine as both rotating MMF's are in the same direction. Backward harmonics refer to harmonics that oppose the fundamental torque generated by the machine as their MMF's that are generated rotate in the opposite direction to that of the fundamental [4], [27].

Space Harmonics

Time harmonics refer to the harmonics generated from the power supply and were discussed in Chapters 3.1.1 and 3.1.2.

Space Harmonics are caused by the impracticality of having an induction machine with an infinitely large number of slots whose windings are sinusoidally distributed resulting in a sinusoidal MMF in the air-gap [4]. The practical result of the interaction of an induction machine with a finite number of slots and the power supply is a rotating MMF in the air-gap with harmonics [4], [27].

Given that the fundamental synchronous speed is n_1 (from Equation 2.1 for the fundamental frequency of the power supply) and the fundamental slip is s_1 (from Equation 2.2), the synchronous speed of the h'th space harmonic is:

$$n_h = \frac{n_1}{h} \tag{3.11}$$

The forward and backward rotating harmonic synchronous slips are defined in Equation 3.12 [4], [27]:

$$s_h = \begin{cases} (1+h) - hs_1 & when\ k\ is\ a\ odd\ number\ for\ backward\ rotating\ harmonics \\ (1-h) + hs_1 & when\ k\ is\ an\ even\ number\ for\ forward\ rotating\ harmonics \end{cases} \tag{3.12}$$

Where h and k are defined as in Equation 3.8.

3.2.1 Harmonic Losses in a VSI Supplied IM

The influence of harmonics in the power supply affects an induction machine's running temperature, noise and vibration levels which increases losses and thus decreases efficiency [28]. Harmonic losses account for 10-20% of the total power losses which are incurred when a machine operates at rated load with a harmonic power supply [5].

Harmonic Copper Losses

The copper loss at fundamental frequency is defined in Equations 2.5 and 2.6. From [29] and [30], the copper losses due to harmonics in the power supply, $P_{Cu,h-total}$ is defined as:

$$P_{Cu,h-total} = \sum_{h\neq 1}(I_h)^2 R_h = \sum_{h\neq 1}\left(I_{s,h}^2 R_{s,h} + I_{r,h}^2 R_{r,h}\right) \tag{3.13}$$

Where:

- I_h is the h'th harmonic current in the IM.
- R_h is the total resistance of the motor to the h'th harmonic.
- $I_{s,h}$ is the h'th harmonic stator current.
- $R_{s,h}$ is the resistance of the stator to the h'th harmonic.
- $I_{r,h}$ is the h'th harmonic rotor current.
- $R_{r,h}$ is the resistance of the rotor to the h'th harmonic.

Whilst [29] states that the resistance's are unaffected by frequency thus presumed constant, [8] states that since the rotor frequency equals $hf_{fundamental}s_h$, the rotor resistance varies. At high frequencies the current through the rotor crowds at the outer edge of the rotor bars decreasing the effective area of the rotor bars thus increasing rotor resistance. This phenomenon is commonly referred to as the *skin effect* resulting in an increase in the rotor resistance along increasing harmonic orders, of which the exact relationship is dependent upon the rotor slot

configuration [8].

Core Losses

As stated in Chapter 2.3.1, the core loss is the sum of the eddy current and hysteresis losses. Since these are dependent on frequency, the harmonic core loss $P_{core,h-total}$ is defined as [30]:

$$P_{core,h-total} = \sum_{h \neq 1} \left(k_{hyst} h f_{fundamental} B_{max,h}^2 + k_{eddy} (h f_{fundamental})^2 B_{max,h}^2 \right) m \tag{3.14}$$

Where:
- k_{hyst} and k_{eddy} are the lamination hysteresis and eddy current loss coefficients.
- $B_{max,h}$ is the maximum flux density at the respective harmonic frequency.
- m is the total mass of the laminations.

The stator core loss is modeled with a resistor, $R_{ms,h}$. Although several publications have assumed the rotor core loss to be negligible; as the rotor core losses are dependent upon frequency and a slip of near unity at $h \gg 1$, a rotor core loss resistor $R_{mr,h}$ is introduced [31]. The standstill value of the rotor core loss resistor ($R_{mr,base}$) is assumed to be equal to the stator core loss resistor ($R_{ms,base}$) where the stator core loss is known from no-load tests at base frequency f_{base} (usually 50/60 Hz). The harmonic values of the core loss resistors can be determined at each harmonic order as defined in Equations 3.15 and 3.16 [7].

$$R_{ms,h} = R_{ms,base} \frac{h f_{fundamental} (1 + k_{e/h} f_{base})}{f_{base} (1 + k_{e/h} h f_{fundamental})} \tag{3.15}$$

$$R_{mr,h} = R_{mr,base}\frac{s_h h f_{fundamental}(1 + k_{e/h} s_{base} f_{base})}{s_{base} f_{base}(1 + k_{e/h} s_h h f_{fundamental})} \tag{3.16}$$

Where $k_{e/h}$ is the ratio of eddy-current to hysteresis loss coefficient.

Stray Load Losses

The stray load losses incurred under harmonic power supply include rotor copper loss induced by the stator slot MMF and permeance harmonics and iron loss in the stator and rotor teeth due to high frequency flux pulsations [7], [30]. In addition, iron loss from end leakage flux and zig-zag leakage flux in the stator and rotor also contribute towards stray load losses. From [29], an approximation of the amount of power associated to stray load loss due to harmonic supply ($P_{SSL,h-total}$) is:

$$P_{SSL,h-total} \approx \sum_{h \neq 1} I_h^2 (h f_{fundamental})^2 \tag{3.17}$$

Various models have been developed in order to account for stray load losses. In [7], the stator and rotor stray load losses are represented as resistors $R_{SLL-s,h}$ and $R_{SLL-r,h}$ in parallel with their respective inductance's. If the stator and rotor leakage reactances are assumed to be equal (as seen in cage motors), then the stator and rotor standstill stray-load loss resistance values can be assumed to be equal at base frequency [7]. Since the stray-load loss resistances are equal at standstill, their values can be derived using the machines measured total stray load loss (using the IEEE or IEC standard at base frequency) at a known slip/speed. Given that their values at base frequency are known, the stray load loss resistance for each harmonic can be defined:

$$R_{SLL-s,h} = R_{SLL-s,base}\frac{h f_{fundamental}(1 + k_{e/h} f_{base})}{f_{base}(1 + k_{e/h} h f_{fundamental})} \tag{3.18}$$

$$R_{SLL-r,h} = R_{SLL-r,base} \frac{s_h h f_{fundamental}(1 + k_{e/h} s_{base} f_{base})}{s_{base} f_{base}(1 + k_{e/h} s_h h f_{fundamental})} \tag{3.19}$$

3.2.2 Harmonic Equivalent Circuit

Given that inductive reactance is a function of frequency and assuming that inductance is independent of supply frequency, harmonic reactance can be defined as seen in Equation 3.20. Therefore, using the information from Chapter 3.2.1, a harmonic equivalent circuit can be derived as seen in Figure 3.6.

$$X_h = h X_{fundamental} \tag{3.20}$$

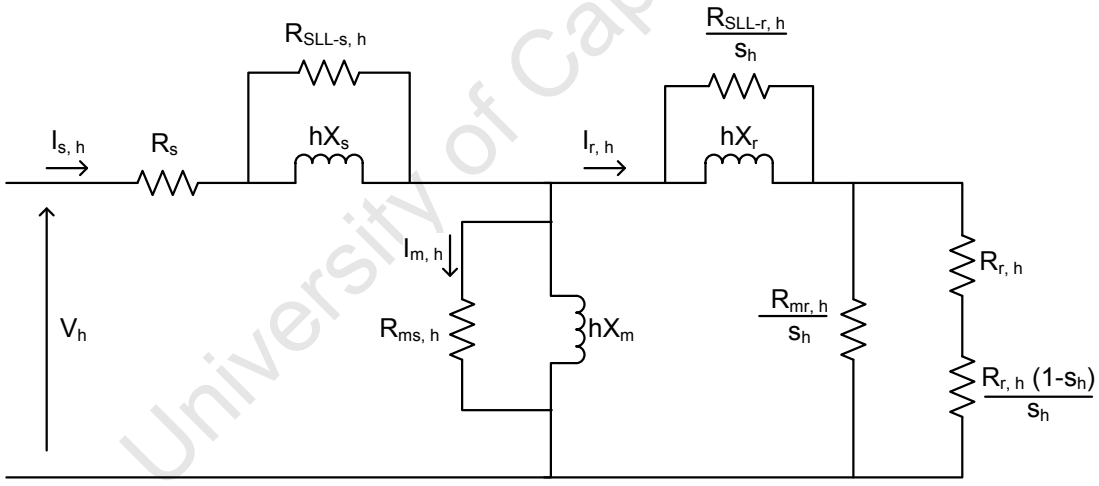

Figure 3.6: Harmonic Equivalent Circuit [7]

In [8] a simplified harmonic equivalent circuit-model is suggested where the core losses are discounted for every harmonic order except the fundamental as seen in Figure 3.7. The total stray load loss is represented with one resistor $R_{SLL,h}$ defined in terms of its base-frequency value as [8]:

$$R_{SLL,h} = h^{0.8} R_{SLL,base} \tag{3.21}$$

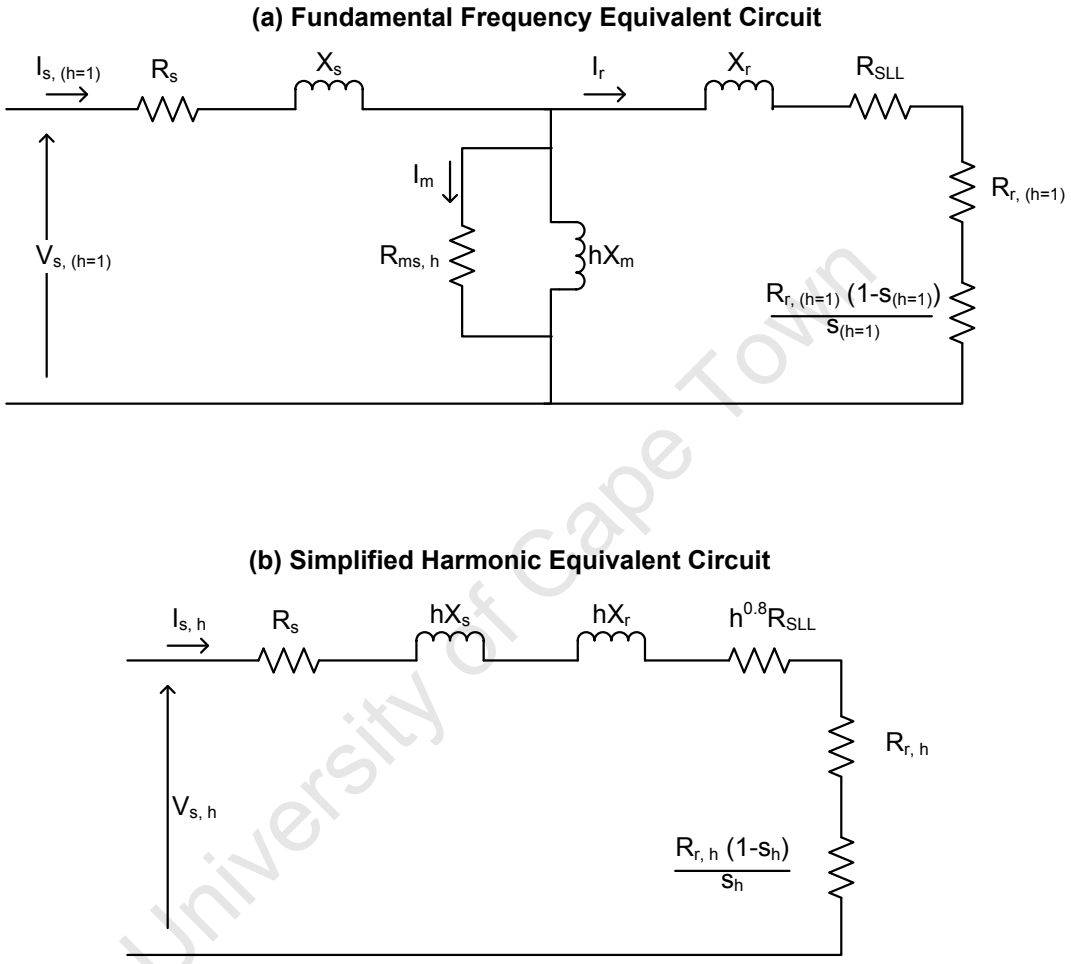

Figure 3.7: Simplified Harmonic IM Model [8]

3.3 PWM Supplied IM Efficiency Test

The most common method of determining an induction machines efficiency is the Shaft-Torque Method otherwise known as the *Direct Method*. The method

Table 3.1: Specified Temperature for Machine at Rated Load [1], [2]

Thermal Class of Insulation System	Reference Temperature $°C$ (including $25°C$ ambient temperature)
A	75
B	95
F	115
H	135

involves measuring the machines torque and speed at the shaft in order to determine the shaft output power [16]. However, the IEEE 112-B advises against the use of costly dynamometers to measure torque in field conditions, thus alternative methods of efficiency estimation are required [1], [16].

An alternative field test method is suggested based on the IEEE 112, IEC 60034-2-1 and IEC 60034-2-3 standards [25].

3.3.1 Thermal Test

In cases where the winding resistance cannot be measured directly at rated load, the temperature of the windings can be used to determine resistance if the resistance at ambient temperature (*Cold Winding Resistance*) is known. However, in cases where the temperature cannot be measured, the winding reference temperature at rated load is based on the machines thermal class as shown in Table 3.1 [1], [2].

However, as stated earlier, harmonics in the power supply affect an induction machines temperature, thus a thermal test is carried out. The thermal test involves running the machine at rated load until the temperature rise is less than $1°C$ over a 30 minute period (as specified in the IEEE Std-112). The power supply to the machine is then switched off and resistance and temperature of the windings are measured when the shaft stops rotating. This test is conducted with both a balanced sinusoidal power supply and a PWM-VSI power supply for

comparison [25].

3.3.2 No-Load Test

In order to ascertain the harmonic core losses associated with the PWM-VSI, a no-load test is carried out. Two tests are performed (with/without PWM-VSI) where the machine's voltage is varied from 125% of the rated voltage downwards until a voltage that causes a rise in current is reached[25].

The power absorbed by an induction machine during a balanced sinusoidal supply no load test ($P_{NL-(SINE)}$) is the sum of the friction and windage, core and stator copper losses as defined in Equation 3.22 [32]. Given that the voltage, current, power and winding temperatures are measured and using information from the thermal test, the equivalent core loss resistance R_m can be deduced similar to the IEC-60034-2-1 method.

$$P_{NL-(SINE)} = P_{FW} + P_{core(SINE)} + P_{Rs-Cu} \tag{3.22}$$

Due to the nature of high order harmonics present at synchronous speed and harmonics being transferred to the rotor cage, the power absorbed by an induction machine during a PWM-VSI supplied no load test ($P_{NL-(PWM)}$) includes additional rotor copper losses as shown in Equation 3.23 [32]. However, if these rotor losses are assumed to be negligible then the difference between $P_{NL-(PWM)}$ and $P_{NL-(SINE)}$ can be attributed to harmonic core losses as the magnetizing RMS current is assumed to be equal [32].

$$\begin{aligned} P_{NL-(PWM)} &= P_{FW} + P_{core(PWM)} + P_{Rs-Cu} + P_{Rr-Cu} \\ &\approx P_{FW} + P_{core(PWM)} + P_{Rs-Cu} \end{aligned} \tag{3.23}$$

$$\sum_{h>1} P_{core,h} = P_{NL-(PWM)} - P_{NL-(SINE)} \tag{3.24}$$

3.3.3 Locked Rotor Test

The locked rotor test involves clamping the motor shaft whilst powering the machine at 25% of its rated frequency and increasing the voltage until the machines rated current is reached. This test is also performed once for each type of power supply. In addition to being able to determine the rotor resistance and leakage reactance of the machine, the additional copper losses due to skin effect can be determined from this test [25], [32].

$$\begin{aligned} P_{LR(SINE)} &= P_{Rs-Cu} + P_{Rr-Cu} \\ P_{LR(PWM)} &= P_{Rs-Cu} + P_{Rr-Cu} \end{aligned} \tag{3.25}$$

$$\sum_{h>1} P_{Cu,h} = P_{LR(PWM)} - P_{LR(SINE)} \tag{3.26}$$

Chapter 4

Non-Intrusive Rotor Speed Estimation

The following chapter gives a brief overview of non-intrusive speed estimation methods before detailing the proposed method, speed estimation via vibration analysis using signal processing techniques.

4.1 Review of Non-Intrusive Speed Detection Techniques

As described in Chapter 2.3, the output power of an induction machine can be defined in terms of its input power and losses or in terms of its developed torque:

$$\begin{aligned} P_{out} &= P_{IN} - \sum P_{losses} = P_{IN} - \left(3I_r'^2 R_r' + \sum P_{other\ losses}\right) \\ &= 3I_r'^2 \frac{R_r'}{s}(1-s) - P_{FW} \end{aligned} \tag{4.1}$$

As seen in Equation 4.1, both definitions of output power require the rotor current I_r' which is dependent upon the operating slip and thus the rotor speed. The various methods of determining the speed of the machine without access to the shaft are summarized.

4.1.1 Model Reference Adaptive System (MRAS)

In MRAS, the motor speed is estimated from measurements of the machine's instantaneous stator voltages and currents thus deriving a mathematical model for the machine. The rotor speed and stator resistance are simultaneously identified in order to overcome the difficulty of using the rotor flux to determine the slip at low speed ranges. This is achieved by developing a set of observers that improves the machines model accuracy [10], [33].

However, the disadvantage of the MRAS is that machine parameters have to be known beforehand and the accuracy of speed estimation is decreased at low speed operations [3].

4.1.2 Machine Current Signature Analysis (MCSA)

Due to rotor shape eccentricity, the rotation of the rotor creates speed dependent harmonics that can be found in the stator current [20]. The frequency of the largest speed-current harmonic is a function of the machines supply frequency f_{supply}, operating slip s and number of poles P as defined in Equation 4.2 [20].

$$f_{speed-current} = \left(1 \pm \frac{2(1-s)}{P}\right) f_{supply} \tag{4.2}$$

As the speed-current harmonic is much smaller than the current harmonic of the power supply, methods have been developed to extract the speed-current harmonic using a non-linear adaptive algorithms thus solving Equation 4.2 for slip [20]. The disadvantage of such methods is the requirement of having the machine operating in steady state mode.

4.2 Proposed Rotor Speed Estimation Technique

In order to determine the shaft speed non-intrusively an extension of mechanical vibration analysis described in [3] is utilized.

4.2.1 Overview of Vibration Analysis

Due to an induction machines manufacturing and assembly imperfections, an induction motor rotates at a speed proportional to the vibrations generated as a result of the inherent imbalance of rotating parts [10], [34].

Given that the shaft speed of an induction machine is n, creating a mechanical vibration once per revolution, the rotational frequency f_{rot} is [35]:

$$f_{rot} = \frac{n}{60} \tag{4.3}$$

If the induction machine is operating in motoring mode (where $1 \geq s \geq 0$) the synchronous speed of the machine will be greater than the shaft speed. Therefore, a limit on the shaft speed can be defined in terms of supply frequency (f_{supply}) and the number of poles (P) of the machine as seen in Equation 4.4.

$$n \leq \frac{120 f_{supply}}{P} \tag{4.4}$$

Combining Equations 4.3 and 4.4, the rotational frequency of an induction machine operating in motoring mode has an upper limit defined by the supply frequency as:

$$f_{rot} \leq \frac{2 f_{supply}}{P} \tag{4.5}$$

Given that the scope of this research is limited to analyzing 4-pole induction machines at a fundamental supply frequency of less than 50 Hz, the largest rotating frequency harmonic to be considered is 25 Hz.

The vibration data is collected through an accelerometer attached to an ADC where the data is then transformed into the frequency domain (via a FFT algorithm) and analyzed. As the rotational frequency is a fraction of the supply frequency, the vibration harmonics caused by power supply harmonics will not fall in the defined threshold as the fundamental power supply frequency is a fraction of the harmonics in a PWM power supply. Therefore, the largest vibration harmonic below $\frac{2 f_{supply}}{P}$ (25 Hz) will correspond to the speed of the machine [3]. Figure 4.1 shows an example of data collection and spectral analysis.

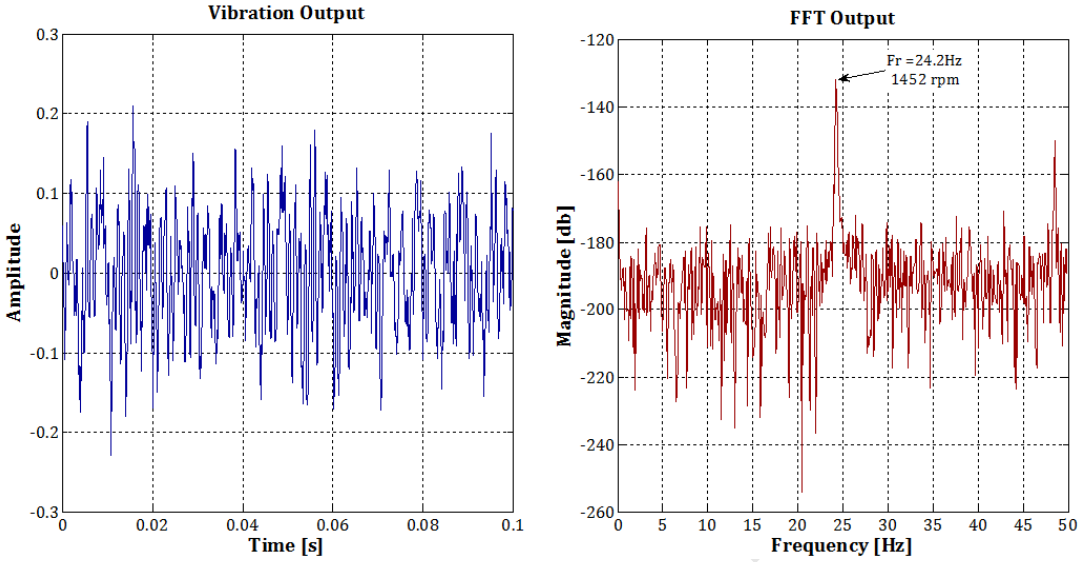

Figure 4.1: Example of Speed Estimation Through Vibration Analysis [3]

4.2.2 Vibration Signal Analysis

If the vibration data is sampled for a period of t seconds at a frequency of $f_{sample,n}$, the total number of data points collected would equal $N = f_{sample,n}t$. When analyzing the frequency spectrum, the highest resolution at which the rotational frequency (hence speed) could be estimated is [36]:

$$f_{resolution} = \frac{f_{sample,n}}{N} \tag{4.6}$$

$$n_{resolution} = 60 f_{resolution} \tag{4.7}$$

In order to increase the speed estimation accuracy without increasing the sampling time or frequency the signal processing techniques such as windowing, zero padding and interpolation should be employed on the data [10]. However, as the speed estimation process is only suitable for steady state speed estimation, it is assumed that machine is in steady state with respect to speed

during vibration analysis and the vibration data collection period.

Windowing

Widowing refers to transforming a data set before a FFT is applied by multiplying the data with a window function. The reason behind winding lies in the nature of real data signals not being perfectly periodic resulting in an approximation of the true spectra of signal. This loss in accuracy is called leakage thus windowing attempt to make a data signal more periodic by transforming the ends of a data set towards zero [36], [10].

Whilst windowing reduces the spectral resolution in the frequency domain, it also reduces the influence of noise in the signal [9], [37]. The effect of a window transformation is shown in Figure 4.2-b.

Zero Padding

Initially FFT algorithms could only transform data sets that contained 2^x sample points where x was an integer. If a data set did not have a *two-to-the-power* length, a number of zero's would be appended to the data set (see Figure 4.2-c) so that it would conform with the algorithm requirements, hence the name *Zero Padding* [38], [10].

However, whilst modern FFT algorithms no longer have such constraints, there are further benefits to zero padding. Appending zeros to a data set does not affect the sampling frequency yet the increased number of samples (from N to $N + N_{zeros}$) results in the frequency resolution being increased from $\frac{f_{sample,n}}{N}$ to $\frac{f_{sample,n}}{N+N_{zeros}}$ thus increasing the frequency estimation of the speed of the induction machine [38], [10]. Thus, zero padding can be interpreted as interpolation in the frequency domain.

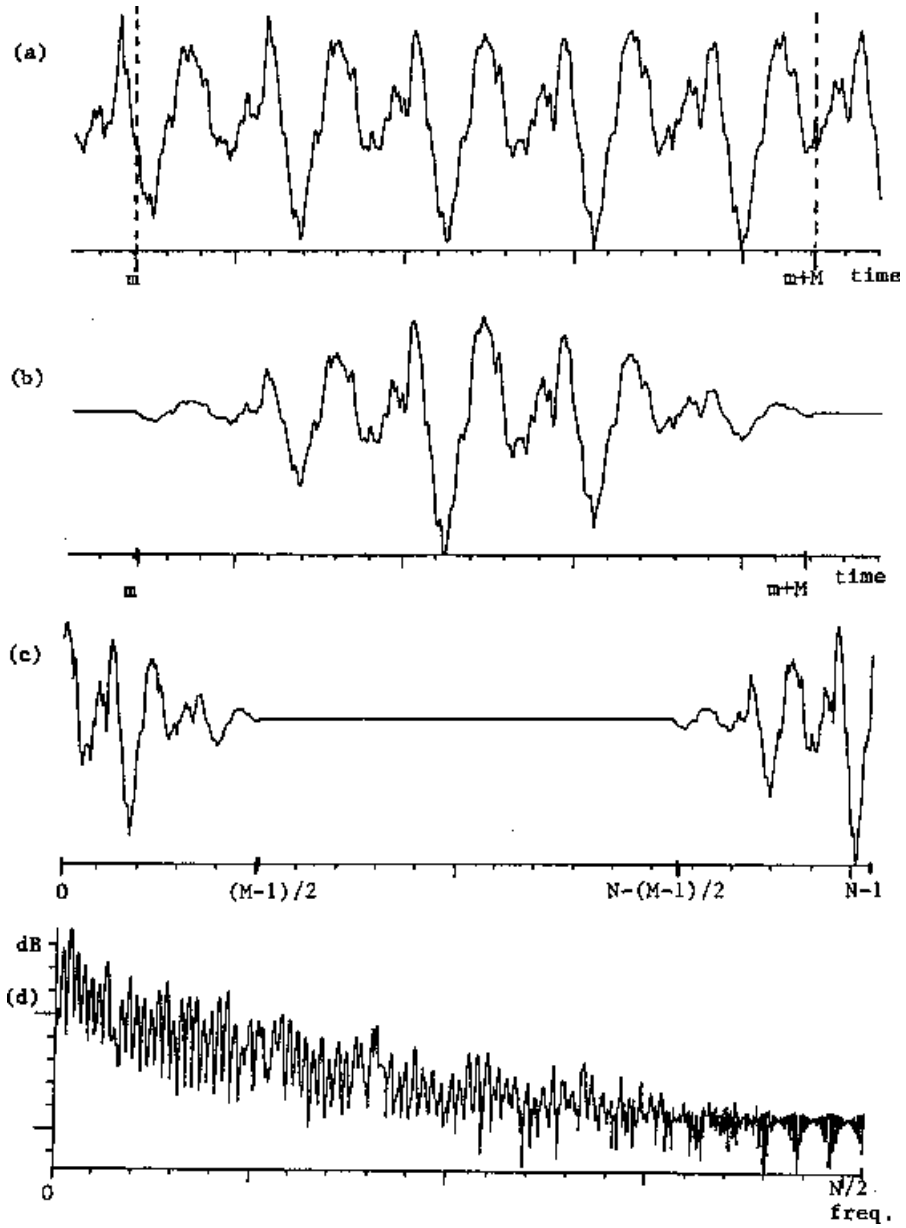

Figure 4.2: Signal Processing Steps. (a) Sampled Data, (b) After windowing, (c) After Zero Padding, (d) PSD Waveform [9]

Parabolic Interpolation

After zero padding is applied the signal can then be Fourier transformed in terms of its Power Spectral Density (PSD) where the peak harmonic below the $\frac{2f_{supply}}{P}$

frequency limit signifies the machine speed. The PSD of the harmonic response is used as it is more accurate than the linear response when determining the rotating frequency [9].

Since the frequency response at the speed harmonic represent a *sinc* function and the frequency at which it response occurs rather than its amplitude is of importance, parabolic interpolation can be used to increase accuracy of the estimated speed [10].

Referring to Figure 4.3, the parabolic interpolation algorithm performs the following steps [10]:

1. Find the largest rotational harmonic PSD_1 and its corresponding frequency f_1 within the bounds $0 < PSD_1 < \frac{2f_{supply}}{P}$.
2. Gather (f_1, PSD_1)'s two adjacent points (f_2, PSD_2) and (f_3, PSD_3).
3. Calculate the parabolic-interpolated speed-vibration frequency $f_{interpolated}$ using the three points found in Step 2 as in shown in Equation 4.8:

$$f_{interpolated} = f_1 + \frac{(f_1 - f_2)(PSD_2 - PSD_3)}{2(PSD_2 - 2PSD_1 + PSD_3)} \tag{4.8}$$

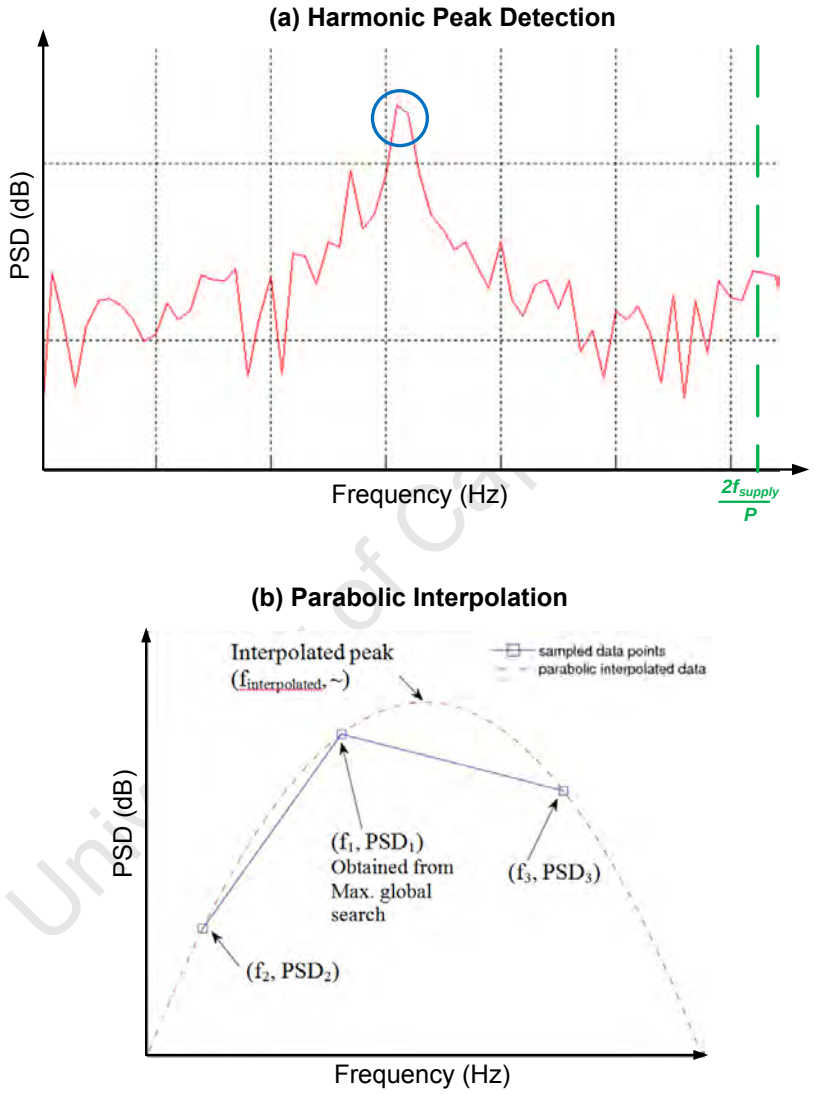

Figure 4.3: Parabolic Interpolation in Speed Estimation [10]

Chapter 5

Development of NIEE-PBIL Technique for Various Power Supplied IMs

Based on the theory development from Chapters 2 and 3, and given that the speed of an induction machine can be accurately determined (as described in Chapter 4), the need for a non-intrusive efficiency estimation is discussed. A non-intrusive efficiency estimation method is proposed and outlined whereby an induction machines efficiency can be determined in the presence of sinusoidal or harmonic power supply.

5.1 Motivation for Non-Intrusive Efficiency Estimation (NIEE) Method

Increasing demand of energy combined with rising energy costs has led to a desire to increase the efficiency of energy utilization. According to a report published by the International Energy Agency (IEA), electric motors account for $43-46\%$ of global electrical energy consumption [12]. Thus one of the main reasons for monitoring an induction machine's efficiency is to ensure that utilization occurs with least amount of energy supply. Additional reasons for monitoring motor efficiency include instances where machines are rewound and replacing worn-out, inefficient machines with newer ones [39].

5.1.1 In-Situ Efficiency Estimation

The IEEE and IEC efficiency determination procedures outlined in Chapters 2.4 and 3.3 require the motor under consideration to undergo intrusive laboratory based tests (such as no-load test, blocked rotor test, rated load thermal test) which affect the machine's productivity, thus the need for in-situ tests [15].

Whilst numerous in-situ efficiency estimation methods already exist, they have certain drawbacks which include being unable to determine the efficiency of PWM-VSI supplied induction machines. Several such methods are summarized below.

Slip Method

The slip method utilizes the nameplate slip data and assumes that the ratio of machines operating output power and rated output power is equal to ratio of the operating slip and rated nameplate slip as seen in Equation 5.1 [17].

$$\frac{P_{output,load}}{P_{output,rated}} = \frac{s_{load}}{s_{rated}} \tag{5.1}$$

Thus, if the speed and input power of the loaded machine is non-intrusively measured, the efficiency of machine can be determined by:

$$\eta = \frac{s_{load}}{s_{rated}} \times \frac{P_{output,rated}}{P_{input,load}} \tag{5.2}$$

Despite improvements on the slip method to account for voltage variations as in the *Ontario Hydro Modified Slip Method*, since the nameplate rated slip value can deviate by 20% from the actual rated slip value and that the assumption of the output power to slip ratio (linear proportional) is inaccurate; the slip method does not provide an accurate assessment of efficiency [16], [17].

Current Method

The current method is similar to the slip method in that it operates under the assumption that the efficiency of the machine is proportional to the ratio of the load and nameplate rated current as seen in Equation 5.3. However, this relationship is inaccurate thus the resulting efficiency estimate is incorrect [16], [17]. Additionally, if the machine has been rewound, the nameplate rated current may no longer be accurate [40].

$$\eta = \frac{I_{load}}{I_{rated}} \times \frac{P_{output,rated}}{P_{input,load}} \tag{5.3}$$

Equivalent Circuit Method - ORNEL96

The Oak Ridge National Laboratory method (ORNEL96) is a variation of the equivalent circuit method that does not require intrusive load tests to be performed. An equivalent circuit of the machine is derived from the motor's nameplate data which, as mentioned earlier, has inaccuracies in their stated values more-so when considering rewound machines [16], [17], [40].

Air-Gap Torque Method - NAGT

The non-intrusive air gap torque method (NAGT) outlined in [18] estimates the torque in the motor air-gap using empirical data relating to each segregated loss as suggested in the IEEE Std-112 where applicable. The drawback to this method is that it relies on an intrusive electrical circuit injecting DC current into the machine in order to ascertain the online stator resistance [18]. Apart from the intrusiveness of installing the circuit (which requires the machine to be decoupled from the power source), the effect of the DC signal injection from the circuit affect the running operation of the machine by creating unbalanced voltages and currents in the stator as well as causing 'additional power dissipation and torque distortion' [18].

Optimization-based methods

Optimization-based methods use genetic algorithms to determine a machines electrical equivalent circuit parameters from limited, non-intrusive test data as described in [41], [42], [43] and more recently [19]. However, these implementations have not yet been adapted for PWM-VSI powered induction machines (which is included in as one of the scopes of this research).

5.2 Model Simplification and Assumptions

The proposed efficiency estimation technique is an extension of the optimization-based methods described in [20], [19] and [42] where the induction machine equivalent circuit parameters are solved using an adaptive search algorithm in conjunction with a speed estimator and the measured stator voltage and current. Whilst numerous equivalent circuits have been developed for analyzing induction motor performance under balanced and VSI-PWM sources, this research will only implement 2 common versions. A modification of the circuit proposed by [31] in Figure 5.1(b) and the standard equivalent circuit seen in Figure 5.1(a) will be implemented in the proposed the efficiency estimation method.

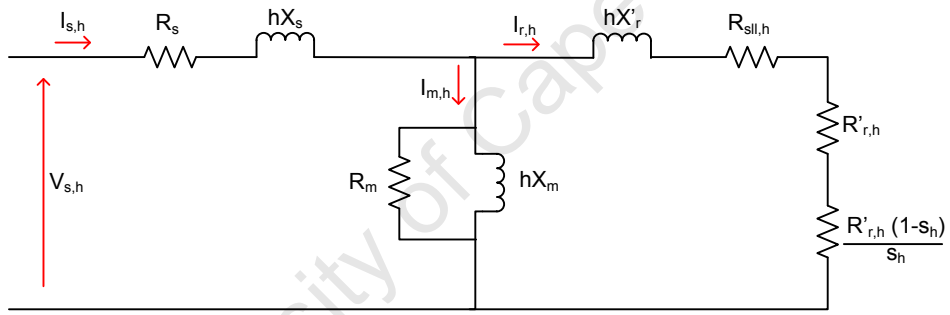

(a) Standard Equivalent Circuit

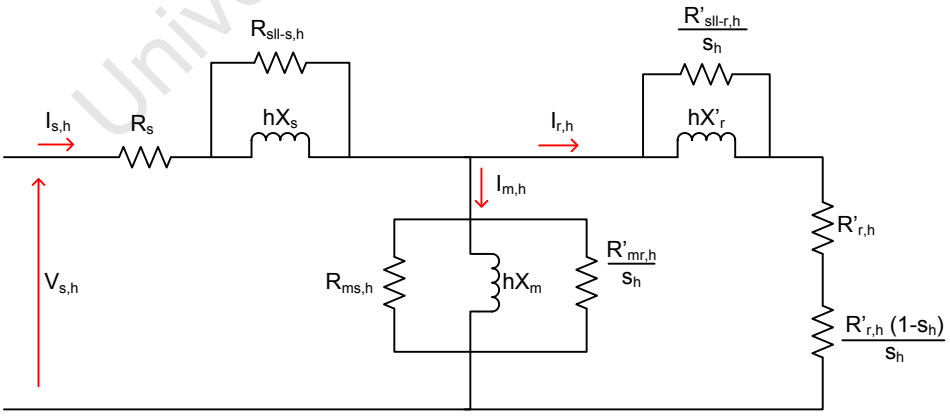

(b) Iron-Loss Equivalent Circuit

Figure 5.1: Equivalent Circuit Implementations used in the NIEE-PBIL Method

Balanced Sinusoidal Power Supply Model

Referring to Figure 5.1, when considering an induction machine with a balanced sinusoidal power supply ($THD < 0.05$ as defined in the IEEE 112 Std), the equivalent circuits only exist for the harmonic component $h = 1$.

Balanced PWM-VSI Power Supply Model

Given that each harmonic in the power supply can be treated as independent sources as suggested in [44] (demonstrated in Figure 5.2), an infinite number of parameters would be required to be known as there are an infinite number of harmonics in a PWM-VSI (as seen in Equation 5.4).

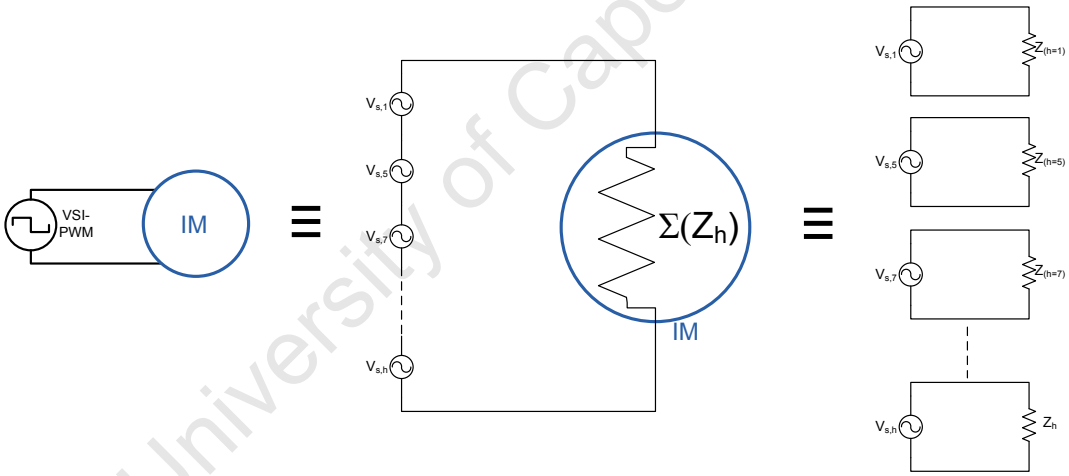

Figure 5.2: Superposition of Harmonics in IM Circuit

$$h = 6k \pm 1 \quad where\, k = 1, 2, 3, 4, ..., \infty \tag{5.4}$$

In order to reduce the number of unknown parameters simplifying assumptions can be made to the model in relation to harmonic parameters. As the eddy-to-hysteresis loss ratio ($k_{e/h}$) cannot be measured non-intrusively (referred

in Equations 3.15, 3.16, 3.18 and 3.19), the relationship between the core and stray-load harmonic resistances can be simplified using the harmonic relationship suggested in [8] where:

$$R_{sll-s,h} = h^{0.8} \cdot R_{sll-s,base} \tag{5.5}$$

$$R_{sll-r,h} = \frac{s_h}{s_{base}} \cdot h^{0.8} \cdot R_{sll-r,base} \tag{5.6}$$

and

$$R_{ms,h} = h^{0.8} \cdot R_{ms,base} \tag{5.7}$$

$$R_{mr,h} = \frac{s_h}{s_{base}} \cdot h^{0.8} \cdot R_{mr,base} \tag{5.8}$$

Additionally, skin effect is assumed to be negligible as the rotor configuration is assumed to be unknown.

5.2.1 Current/Voltage Sample Rate

From Figure 5.1, the equivalent circuit for each harmonic can be deduced given that parameters at the base frequency and the harmonic order h is known. Additionally, to solve for power loss, this also requires at least the harmonic current or voltage to be known. However, as the harmonic order increases, the influence of harmonics on machine performance decreases resulting in the need for a limited number of front order harmonics (harmonics closest to the fundamental) to accurately determine machine performance [45], [46].

Therefore, given that the fundamental frequency is less than or equal to $50Hz$, sampling voltage and current at a frequency of $16kHz$ is sufficient as it allows for analysis of up to the $160th$ harmonic (as defined in the scope and limitations

of this research). A Fourier analysis of the stator's instantaneous current and voltage can be used to determine the harmonic magnitudes $I_{s,h}$ and $V_{s,h}$ at each harmonic h.

5.2.2 Thermal Model

The steady-state full load temperature of the machine at rated frequency is assumed to be known from either the nameplate data, previous rated frequency tests or based on the IEEE 112/IEC 60034-2-1 standards regarding the machine's insulation class listed on its nameplate [1], [2].

The thermal coefficient of the machine k_{TH} (SI Unit: $^{\circ}C/W$) is assumed to be independent of the fundamental and harmonic frequencies as well as the machine's base frequency. This assumption is based on each harmonic being considered as a separate power source and compensating for frequency differences through adjustments in core and stray load loss resistor values. Therefore, given that a machine's operating temperature is known, the total losses (including harmonic losses) incurred in a machine can be deduced and vice-versa [44], [19].

The stator resistance at ambient temperature is assumed to be known based on measurements taken during the machine's shutdown/maintenance period. In addition, the stator and rotor windings are the only parameters assumed to be affected by the machines operating temperature. The temperature for each winding (stator and rotor) is assumed to equal to the operating temperature and the winding materials are assumed to be comprised of copper and aluminum respectively [41]. Thus for a given load temperature, the stator and rotor resistor values at a previously measured temperature can be adjusted as follows:

$$R_{s,T-load} = R_{s,T-base}\frac{T - load + k_{Cu}}{T - base + k_{Cu}} \tag{5.9}$$

$$R_{r,T-load} = R_{r,T-base}\frac{T - load + k_{Al}}{T - base + k_{Al}} \tag{5.10}$$

5.2.3 Iron and Stray Load Loss Model

For the Standard Equivalent Circuit (Figure 5.1(a)), the stator and rotor leakage reactances are related to each other based on the ratio specified by the IEEE 112 standard and the design class of the machine as seen in Table 5.1.

Table 5.1: Stator to Rotor Reactance Ratio [1]

Machine Design Class (NEMA)	Ratio of $\frac{X_{stator}}{X_{rotor}}$
A, D and wound rotor motors	1.00
B	0.67
C	0.43

The full load stray load losses of an induction machine at base frequency are assumed to be based on the rated output power as specified by the IEEE 112 and shown in Table 5.2.

If the stator and rotor stray load losses are treated separately in the equivalent circuit model (as seen in Figure 5.1(b)), it is assumed that the stator resistance at base frequency $R_{SLL-s,base}$ is related to rated full-load stray load loss power $P_{SLL-rated}$ at rated stator phase current $I_{s-rated}$ by Equation 5.11 [7].

$$\frac{I_{s-rated}^2 R_{SLL-s,base} X_{s,base}^2}{R_{SLL-s,base}^2 + X_{s,base}^2} = \frac{P_{SLL-rated}}{3} \tag{5.11}$$

Where $\frac{P_{SLL-rated}}{3}$ is the rated stray load loss per phase. Solving for $R_{SLL-s,base}$ in the quadratic Equation 5.11, the larger value is chosen so that voltage drop across

Table 5.2: Stray-Load Loss Estimate [1]

Machine Full-Load Rating (kW)	Stray Load Loss (% of Full-Load Rating)
1-90	1.8
91-375	1.5
376-1850	1.2
$\geq$ 1851	0.9

the stator inductance at base frequency ($X_{s,base}$) remains unchanged [7]. The difference between the stator and rotor leakage reactances can be ignored as was found in [19] whereby experimental results proved that the overall efficiency of a machine is not dependent on the leakage reactance ratio. Therefore, neglecting the difference between the stator and rotor leakage reactances at base frequency, the standstill values of the rotor stray load loss resistor $R_{SLL-r,base}$ and core loss resistor $R_{mr,base}$ can be assumed to be equal to their stator counterparts (referred to in Equations 5.5 - 5.8) as seen in Equations 5.12 and 5.13 [7]. As stated earlier in Chapter 3.2.1, this assumption is based on the relationship of the stator and rotor leakage reactances being equal and simplifying model assumptions made in the electrical equivalent circuit as proposed in [7].

$$\frac{R_{SLL-r,base}}{s_{rated,base}} = R_{SLL-s,base} \tag{5.12}$$

$$\frac{R_{mr,base}}{s_{rated,base}} = R_{ms,base} \tag{5.13}$$

5.2.4 Mechanical Loss Model

As there is currently no method for non-intrusively determining a the friction and windage losses, the total power attributed to friction and windage at rated load is assumed to be 1.2% of input power at rated load as suggested in [47]. However, [7] suggests that the friction and windage losses should be varied according to square of operating speed for harmonic power supply. The friction and windage constant k_{FW} is based on the *Coulomb plus viscous friction* model in [48] where:

$$k_{FW} = \frac{P_{FW,rated}}{\omega^2_{mech,rated}} = \frac{1.2\%\ of\ P_{in,rated}}{\omega^2_{mech,rated}} \tag{5.14}$$

$$P_{FW} = k_{FW}\omega^2_{mech} \tag{5.15}$$

5.3 Parameter Identification via PBIL

Based on the aforementioned assumptions, the parameters that require identification in order to determine machine efficiency are X_s, X_m, $R_m s$, R'_r and k_{TH} whereas the slip can determined non-intrusively by speed estimation from vibration analysis. Whilst [19], [42] and [41] suggest using a genetic algorithm (*GA*) to solve for the unknown parameters, a population based incremental learning (*PBIL*) algorithm is proposed based on its simplicity and robustness as well as it being able to outperform a GA [49], [50].

5.3.1 Generating an Individual in the PBIL Algorithm

In order to solve for the unknown parameters, a group (*population*) of trial solutions is generated based on the random sampling of a probability vector (ρ). A trial solution (*individual*, $\ddot{I}$) is a set of concatenated binary-coded real numbers with each member of the set representing one of the unknown parameters [51], [50]. In this instance, each parameter is encoded with a 15-bit binary number. Thus, given that there are 5 unknown parameters each encoded as a 15-bit string, a trial *individual* consists of $5 \times 15 = 75 bits$ and the probability vector consists of a set of 75 real numbers each between the value of $0-1$. In order to randomly generate an *individual*, a vector of 75 random numbers between $0-1$ is generated and compared to the elements in the probability vector. If the value of an element in ρ is greater than the corresponding element in the random vector Ψ, the corresponding bit in $\ddot{I}$ is set to 1; otherwise it is set to 0 [51], [50].

$$\overset{75}{\underset{e=1}{\ddot{I}_e}} = \begin{cases} 1, & for\ \rho_e > \Psi_e \\ 0, & for\ \rho_e \leq \Psi_e \end{cases} \tag{5.16}$$

A *population* of *individuals* is generated where each *individual* is based on a newly computed random vector. The generation of an individual is illustrated in Figure 5.3 and Equation 5.16. The parameters in $\ddot{I}$ are decoded using a binary-to-decimal conversion where the parameter's real value in the $0-1$ range is the

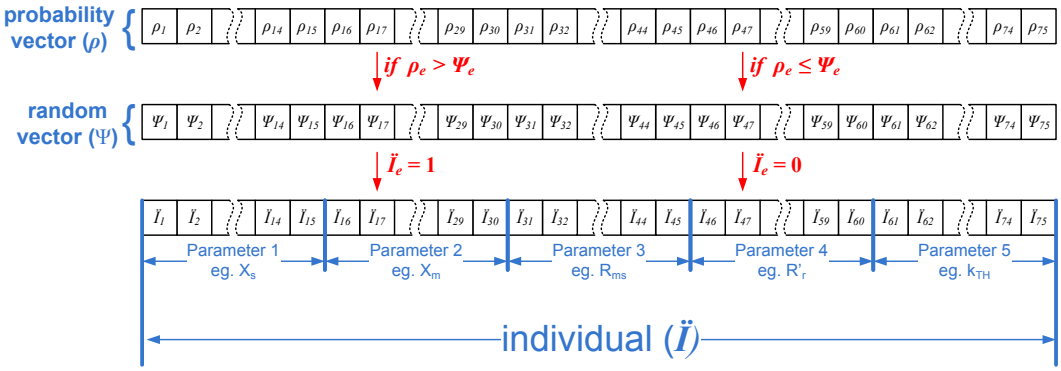

Figure 5.3: Generation of a PBIL *individual*

dot product of the 15-bit parameter array and the decoder array $\ddot{D}$ (where $\ddot{D}$ is defined in Equation 5.17). After decoding the bit representation, the unknown parameters are scaled according to boundary limits as displayed in Table 5.3.

$$\sum_{e=1}^{15} \ddot{D}_e = 2^{-e} \tag{5.17}$$

At the algorithm initialization, each element in ρ is set to 0.5 so that each bit in an *individual* (and thus each bit in the 1*st population* generation) has a 50% probability of being a 1 or a 0. This is equivalent to creating a generation of *individuals* unbiased towards an optimal parameter solution. Unlike the genetic algorithm, the order in which the parameters populate an *individual* does not matter as seen in Figure 5.3, [50], [52].

5.3.2 Evaluating a Population Individual

In order to assess whether or not each population individual's values represent the actual values of the induction motor under consideration, the trial parameters are used to estimate measured constants through the system model. The error between the population-based estimate and measured constants is used to quantify an individual's *fitness*.

Table 5.3: Equivalent Circuit Parameters to be Solved

Parameter	Binary Assignment	Real Boundary †	Real Resolution
$X_{s,base}(\Omega)$	$\ddot{I}_{1-15}$	$(0, 100]$	± 0.003
$X_{m,base}(\Omega)$	$\ddot{I}_{16-30}$	$(0, 500]$	± 0.015
$R_{ms,base}(\Omega)$	$\ddot{I}_{31-45}$	$(0, 5000]$	± 0.153
$R'_{r,Tamb}(\Omega)$	$\ddot{I}_{46-60}$	$(0, 100]$	± 0.003
$k_{TH}(^\circ C/W)$	$\ddot{I}_{61-75}$	$(0, 1]$	$\pm 2^{-15}$

† $(a, b] \equiv a <$ Parameter $\leq b$

The measured constants are instantaneous 3-phase line voltages and currents supplied to the induction machine at a loading point. Using Fourier analysis the harmonic phase voltage $\vec{V}_{p,h}$ and harmonic stator (line) current $\vec{I}_{s,h}$ can be deduced, thus the power supplied to the machine can be defined as a function of the harmonics:

$$\begin{aligned} P_{in,h} &= 3|\vec{V}_{p,h}||\vec{I}_{s,h}|\cos(\angle\vec{V}_{p,h} - \angle\vec{I}_{s,h}) \\ P_{in,total} &= \sum_{h=1}^{\infty} P_{in,h} \end{aligned} \tag{5.18}$$

Given that the stator resistance $R_{s,Tamb}$ at ambient temperature ($T_{ambient}$), the rotor resistance $R'_{r,Tamb}$ from the PBIL parameter and the operating temperature (T_{load}) of a machine is known, the motor resistances at the operating point can be determined from [1]:

$$R_{s,load} = \frac{R_{s,Tamb}(T_{load} + k_{Cu})}{T_{ambient} + k_{Cu}} \tag{5.19}$$

$$R'_{r,load} = \frac{R_{r,Tamb}(T_{load} + k_{Al})}{T_{ambient} + k_{Al}} \tag{5.20}$$

Where $k_{Cu} = 234.5$ and $k_{Al} = 225$ is the temperature coefficient for copper and aluminum respectively.

Table 5.4: Source of Equivalent Circuit Parameters for Efficiency Estimation

Parameter	Source
$R_{s,load}$	from Equation 5.19
X_s	PBIL parameter
X_m	PBIL parameter
$R_{SSL-s,base}$	from Table 5.2 and Equation 5.11
$R_{ms,base}$	PBIL parameter
X_r	from Table 5.1
$R_{SSL-r,base}$	from Equation 5.12
$R_{mr,base}$	from Equation 5.13
$R'_{r,load}$	PBIL parameter and Equation 5.20
s	from speed estimate described in Chapter 4

If the operating temperature is known and hence, the winding resistances are adjusted accordingly, the remaining equivalent circuit parameters can be deduced by utilizing nameplate data as shown in Table 5.4.

Based on the equivalent circuit in Figure 5.1 and the parameters, the following equations can be defined.

The conductance of the stator, rotor and magnetizing branches are:

$$\begin{array}{lcll} & & \textbf{Standard Equivalent Circuit} & \textbf{Iron-Loss Equivalent Circuit} \\ \vec{Z}_{stator} & = & R_{s,load} + jX_s & R_{s,load} + \frac{jX_sR_{SSL-s}}{jX_s+R_{SSL-s}} \\ \vec{Z}_{rotor} & = & R_{r,load} + \frac{R_{r,load}(1-s)}{s} + jX_s & R_{r,load} + \frac{R_{r,load}(1-s)}{s} + \frac{jX_sR_{SSL-r}}{jsX_s+R_{SSL-r}} \\ \vec{Y}_{core} & = & \frac{1}{R_{ms}} + \frac{1}{jX_m} & \frac{1}{R_{ms}} + \frac{1}{jX_m} + \frac{s}{R_{mr}} \end{array} \tag{5.21}$$

$$\vec{Y}_{stator} = \frac{1}{\vec{Z}_{stator}} \tag{5.22}$$

$$\vec{Y}_{rotor} = \frac{1}{\vec{Z}_{rotor}} \tag{5.23}$$

$$\vec{Z}_{core} = \frac{1}{\vec{Y}_{core}} \tag{5.24}$$

From the conductance equations, an estimate of stator, rotor and core currents can be made:

$$\vec{I}_{s,Est} = \frac{\vec{V}_s \cdot \vec{Y}_{stator}\left(\vec{Y}_{rotor} + \vec{Y}_{core}\right)}{\vec{Y}_{stator} + \vec{Y}_{rotor} + \vec{Y}_{core}} \tag{5.25}$$

$$\vec{I}_{m,Est} = \frac{\vec{V}_s \cdot \vec{Y}_{stator} \cdot \vec{Y}_{core}}{\vec{Y}_{stator} + \vec{Y}_{rotor} + \vec{Y}_{core}} \tag{5.26}$$

$$\vec{I}_{r,Est} = \frac{V_s \cdot \vec{Y_{stator}} \cdot \vec{Y_{rotor}}}{\vec{Y}_{stator} + \vec{Y}_{rotor} + \vec{Y}_{core}} \tag{5.27}$$

As seen in Equation 5.26, the magnetizing current is defined by the magnetizing leakage reactance and the stator and rotor core loss resistors. Whilst segregating the magnetizing current into its stator and rotor components will not affect the analysis on the system of equations (i.e. $\vec{I}_{m,Est} = \vec{I}_{Rms,Est} + \vec{I}_{Xm,Est} + \vec{I}_{Rmr,Est}$), in [41] it was found that compounding the magnetizing components into one branch gives a better approximation of individual parameters as well as overall machine efficiency estimation in machine parameter optimization.

From Equations 5.25 - 5.27 the estimated input and output power of the induction machine can be determined:

$$P_{in,Est} = 3\left(\Re(\vec{Z}_{stator})|\vec{I}_{s,Est}|^2 + \Re(\vec{Z}_{rotor})|\vec{I}_{r,Est}|^2 + \Re(\vec{Z}_{core})|\vec{I}_{m,Est}|^2\right) \quad (5.28)$$

$$P_{out,Est} = 3\left(\frac{\Re(Z_{rotor})(1-s)}{s} \cdot |\vec{I}_{r,Est}|^2\right) - k_{FW}\left(\frac{2\pi n}{60}\right)^2 \quad (5.29)$$

Therefore, from Equations 5.28 and 5.29, the estimated power loss can be defined as:

$$P_{loss,Est} = P_{in,Est} - P_{out,Est} \quad (5.30)$$

5.3.3 Temperature Estimation

Referring to Chapter 5.3.2), the temperature of a machine at the loading condition was required to adjust the stator and rotor winding resistances. Under laboratory conditions, in order to accurately determine the winding temperature and hence the actual stator resistance, thermocouples would be attached to the machine windings. However, the presence of thermocouples embedded in the machine is considered too invasive for field testing, thus a temperature estimation technique implemented.

As power loss in an induction machine is related with its temperature rise, a thermal coefficient k_{TH} is introduced to define the relationship between power loss and operating temperature [19]:

$$T_{load} = k_{TH}P_{loss} + T_{ambient} \quad (5.31)$$

As seen in Equation 5.31, in order to estimate the operating temperature at a specific load (T_{load}), the total power loss in the machine (P_{loss}) must be estimated. However, without an initial temperature that allows for deriving the operating resistance, the estimated value of P_{loss} would be unobtainable [19]. To overcome

this problem, [19] suggested that an initial temperature be determined from the effective input current in the application of unbalanced power conditions. However, as a PWM power source is being considered, the initial temperature should be based on a factor of the harmonic current. Therefore, it is proposed that the initial temperature estimation is a ratio between the total harmonic current, I_H, and the rated current at base frequency. $I_{rated,base}$. From [8] I_H is defined as:

$$I_H = \sqrt{\sum_{h=1}^{\infty} I_h^2} \tag{5.32}$$

Where:
– I_h is the RMS current at harmonic order h

Therefore,

$$T_{load,Est} = \frac{I_H}{I_{rated,base}}(T_{rated,base} - T_{ambient}) + T_{ambient} \tag{5.33}$$

Where:
– $I_{rated,base}$ is the rated full load current stated on the machine's name plate data.
– $T_{rated,base}$ is the rated full load temperature based on the machine's name plate insulation class as suggested in the IEEE 112-B and IEC-60034-2-1 standards.

Using $T_{load,Est}$ as an initial temperature, the estimated power loss of the machine can now be derived based on each of the PBIL trial *individuals*. The estimated temperature is determined in an iterative manner as seen in Figure 5.4 until a value of convergence is attained [19].

Once the estimated load temperature has converged to a value, the stator

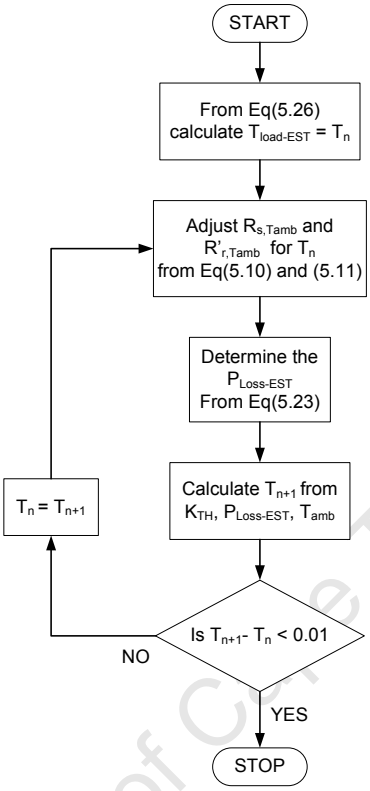

Figure 5.4: Temperature Estimation Flowchart

current estimate $\vec{I}_{s,Est}$ and input power estimate $P_{in,Est}$ can be re-evaluated from Equations 5.25 and 5.28. These values may then be used to improve future parameter populations in the PBIL by aiming to reduce the error between the estimated and measured values.

$$err_P = \frac{P_{in,total} - P_{in,Est}}{P_{in,total}} \times 100\% \tag{5.34}$$

In comparing the currents, [42] suggests that the current's amplitude and phase should both be optimized for improved parameter identification.

$$err_{I-mag} = \frac{|\vec{I}_s| - |\vec{I}_{s,Est}|}{|\vec{I}_s|} \times 100\% \tag{5.35}$$

$$err_{I-ang} = \frac{\angle\left(\vec{I}_s\right) - \angle\left(\vec{I}_{s,Est}\right)}{\angle\left(\vec{I}_s\right)} \times 100\% \tag{5.36}$$

In order to accurately estimate the operating temperature, the value of k_{TH} must accurately reflect the machine thermal model defined in Equation 5.31. This is achieved by adding the coefficient to the list of unknown parameters and comparing its effectiveness in determining the rated full load temperature at base frequency. Given that the rated voltage and speed at base frequency is obtainable from the machine's nameplate data, the estimated full load currents (Equations 5.37-5.39) can be derived using the conventional balanced-power equivalent circuit (refer to Figure 2.3). The stator resistance at ambient temperature is adjusted to the IEEE 112 recommended rated load temperature as well as the PBIL trial rotor resistance parameter [19].

The estimated power loss at rated load can now be defined in terms of the estimated rated currents:

$$R_{s,Trated} = \frac{R_{s,Tamb}(T_{nameplate} + k_{Cu})}{T_{ambient} + k_{Cu}}$$

$$R'_{r,Trated} = \frac{R_{r,PBIL}(T_{nameplate} + k_{Al})}{T_{ambient} + k_{Al}}$$

$$\vec{Y}_{s,rated} = \frac{1}{R_{s,Trated} + jX_s} \qquad \vec{Y}_{r,rated} = \frac{1}{\frac{R_{r,Trated}}{s} + jX_s + R_{SLL}}$$
$$\vec{Y}_{m,rated} = \frac{1}{R_m} + \frac{1}{X_m}$$

$$\vec{I}_{s-rated,Est} = V_{s,nameplate} \times \frac{\vec{Y}_{s,rated} \cdot (\vec{Y}_{r,rated} + \vec{Y}_{m,rated})}{\vec{Y}_{s,rated} + \vec{Y}_{r,rated} + \vec{Y}_{m,rated}} \tag{5.37}$$

$$\vec{I}_{r-rated,Est} = V_{s,nameplate} \times \frac{\vec{Y}_{s,rated} \cdot \vec{Y}_{m,rated}}{\vec{Y}_{s,rated} + \vec{Y}_{r,rated} + \vec{Y}_{m,rated}} \tag{5.38}$$

$$\vec{I}_{m-rated,Est} = V_{s,nameplate} \times \frac{\vec{Y}_{s,rated} \cdot \frac{1}{R_m}}{\vec{Y}_{s,rated} + \vec{Y}_{r,rated} + \vec{Y}_{m,rated}} \tag{5.39}$$

$$P_{rated-loss,Est} = 3\left(R_{s,Trated}|\vec{I}_{s-rated,Est}|^2 + R_m|\vec{I}_{m-rated,Est}|^2 + R_{r,Trated}|\vec{I}_{r-rated,Est}|^2\right) + P_{SLL,rated} + P_{FW,rated} \tag{5.40}$$

Where $P_{SLL,rated}$ and $P_{FW,rated}$ can be deduced using the nameplate data and the IEEE 112 standard.

The thermal coefficient value can now be improved after every population iteration by aiming for the smallest error between the estimated rated full load temperate $T_{rated,Est}$ and the actual full load temperature $T_{rated,base}$ where [19]:

$$T_{rated,Est} = P_{rated-loss,est} \cdot k_{TH} + T_{ambient} \tag{5.41}$$

$$err_{k-TH} = \frac{T_{rated,base} - T_{rated,Est}}{T_{rated,base}} \times 100\% \tag{5.42}$$

5.3.4 Multi-Load Based Parameter Optimization

Since there are 5 unknown parameters, in order to attain a unique solution from the optimization algorithm, 5 operating points should be used whereby the loads points shall consist of having the machine operate under 1 stable load point and then briefly varying the load to 4 other points so that a complete data set is available for the efficiency estimation process. Due to the brief time at which the differing loads are kept, the operating temperature at these incidental load points are assumed to be equal to the stable load point. The result of having varying load points at the same thermal condition results in a a non-singular set of data available in order for the optimization algorithm to converge to a unique solution [20].

When considering optimization based on multiple load points, a fitness function can be derived based least squares nonlinear optimization model [20]. Based on the error functions in Equations 5.34 - 5.42, the multi-load fitness function F can be defined as seen in Equation 5.43 where $err_{,i}$ refers to the fitness error of a stable or incidental load point i.

$$F = \frac{1}{1 + err_{k-TH}^2 + \sum_{i=1}^{N} \left(err_{P,i}^2 + err_{I-mag,i}^2 + err_{I-ang,i}^2 \right)} \tag{5.43}$$

The current angle is included as a fitness test as it was observed in [42] that implicitly including it improves the consistency of attaining the core loss equivalent circuit components (R_m and X_m).

5.3.5 Parallel-PBIL (pPBIL) Optimization For Enhanced Termination Criteria

As can be seen in Equation 5.43, the PBIL aims to converge at a global maximum solution for F. The optimal solution has been found when the probability vector ρ converges on a single solution after multiple successive generation evaluations. An overview of the PBIL algorithm can be seen in Figure 5.5.

For each bit with a value of 1 in the best population *individual* $\ddot{I}_{BEST}$, the corresponding element in the probability vector is increased by a learning rate k_{LR} as seen in Equation 5.44. Increasing the learning rate increases the chances of premature convergence on a local rather than global optimal solution, thus a rate of $0.1 \leq k_{LR} \leq 0.4$ is suggested [50], [52].

$$\rho_e = (1 - k_{LR})\rho_e + k_{LR}\ddot{I}_{BEST} \tag{5.44}$$

In order to increase the probability of finding the global optimal solution, [50] suggests that each of probability vector's elements is moved by 0.5% towards a neutral 0.5 probability after every generation thus maintaining diversity in

successive *population* generations.

$$\rho_e = \rho_e - 0.005(\rho_e - 0.5) \tag{5.45}$$

In order to ensure that a global optimum solution has been reached, GA parameter optimization methods described in [19] and [42] set a generational run-time limit of 20,000 and 10,000 generations respectively. The disadvantage of arbitrarily setting a generational limit is wasted/redundant computational time spent if a optimal solution has been found before the generational limit. Alternatively, if the generational limit is set too low, an global optimal solution may not be found.

In order to ensure that a global optimal solution has been found, the proposed NIEE-PBIL algorithm implements two PBIL probability vectors that are updated in parallel and compared against each other as a test for convergence. In order to ensure that the optimal solution is not a result of premature convergence the proposed algorithm continues running until the two probability vectors equal each other for a proposed number of successive iterations. Apart from using parallel probability vectors for search-algorithm termination, the NIEE-PBIL algorithm allows for partial information interchange between vectors which not only results in improved search-time performance but additionally ensures that global optimum solutions rather than than local optimums are reached when compared to a traditional GA [53], [49], [50]. The NIEE-PBIL parallel implementation algorithm is shown in Figure 5.6.

The advantage of implementing parallel populations and probability vectors in the pPBIL compared against implementing multiple runs in a standard PBIL lies in the pPBIL using crossover in the probability vector to combine dissimilar solutions [54]. As reported in [54], when comparing the pPBIL to a simple PBIL, GA and parallel GA, the pPBIL performs better that all the other algorithms it was compared against in a number of tested problems.

5.3.6 Summary of Proposed NIEE-PBIL Method

A summary of the proposed NIEE-PBIL efficiency estimation method and it's associated algorithm parameters is outlined in Table 5.5.

Table 5.5: Summary of Proposed NIEE-PBIL Method

Speed Estimation Method	Vibration Analysis
Equivalent Circuit Parameters to be Identified	5 (X_s, X_m, R_r, R_m, k_{TH})
Binary Precision of Parameters to be Identified	15 bits per parameter
No. of parallel probability vectors	2
No. of parallel populations	10
No. of individuals per population	10
No. of successive generations before probability vector information interchange	20
No. of successive generations of probability vectors equaling each other for algorithm termination	10

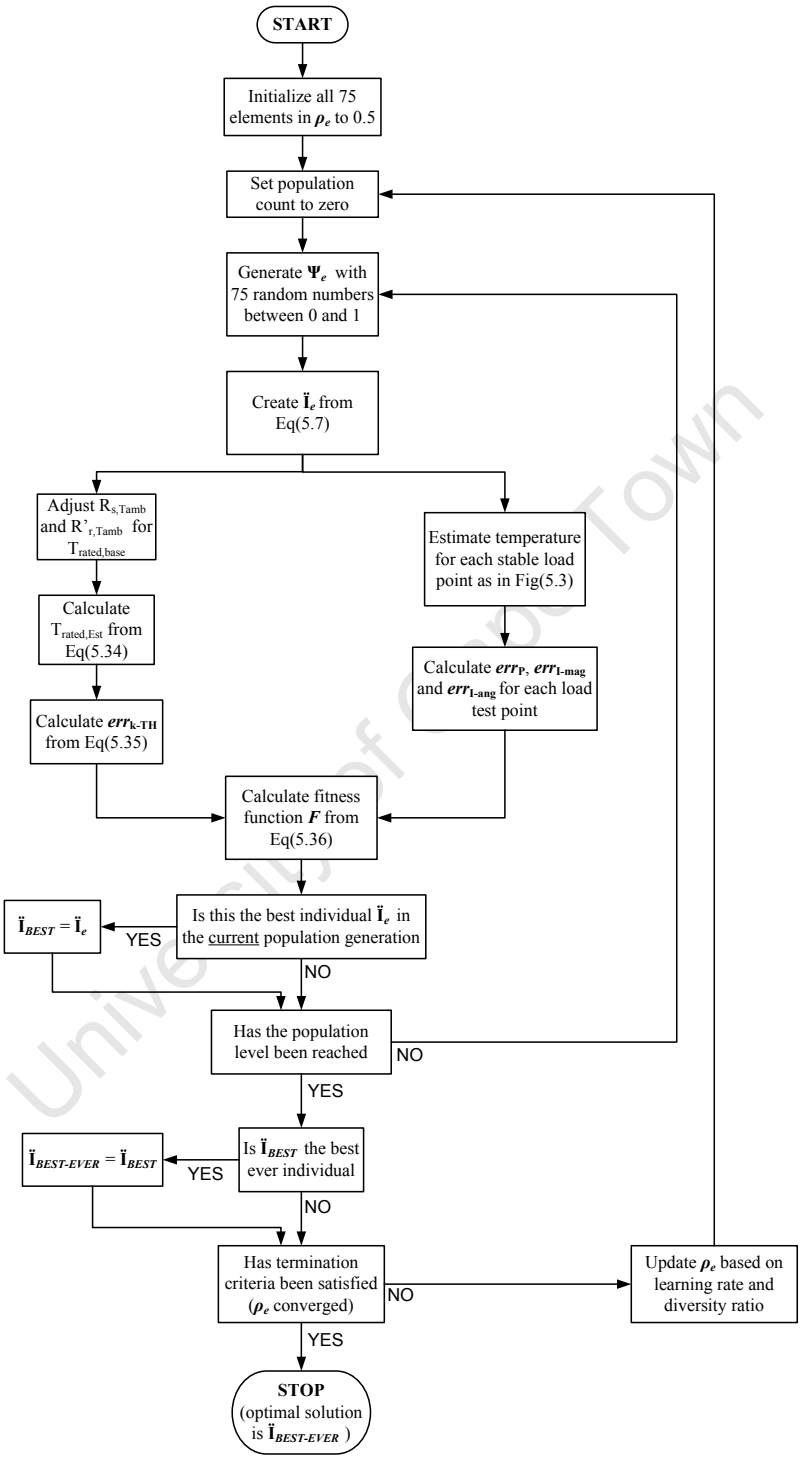

Figure 5.5: PBIL Parameter Optimization Overview

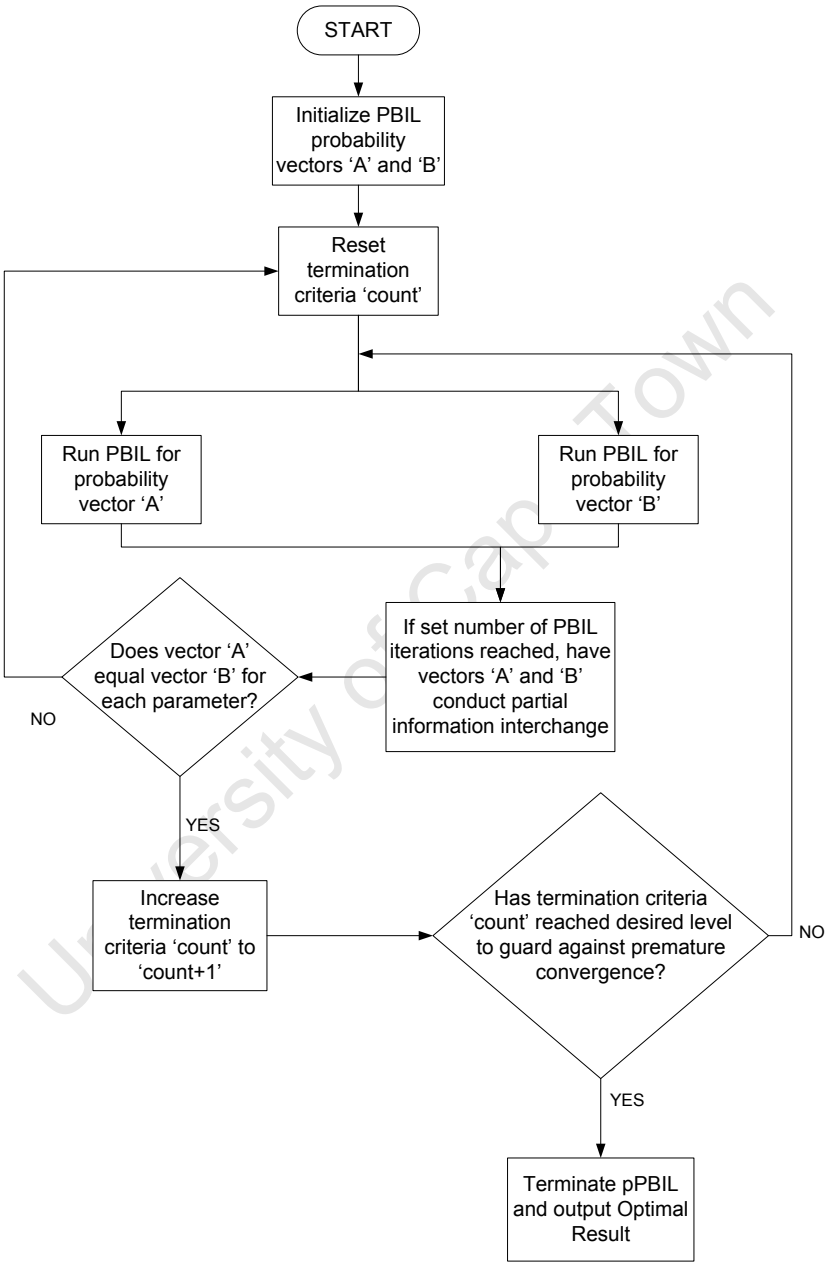

Figure 5.6: Parallel PBIL (pPBIL) Parameter Optimization

Chapter 6

Experimental Setup and Procedures

The following chapter outlines the experimental equipment used to collect test data from an induction machine as well as the tools used to analyze the data to produce an efficiency estimate from the method described in the previous chapter.

6.1 Overview of Experimental Procedure for Efficiency Estimation

Based on the proposed technique outlined in Chapter 5 a method for determining machine efficiency has been developed ensuring consistent results between independent tests. The procedure for determining the efficiency of an induction machine under sinusoidal and PWM-VSI power supply is shown in Figure 6.1.

In order to determine the accuracy of the proposed efficiency estimation procedure, the efficiency of the machine is compared to that determined by the IEEE 112-B and IEC 60034-2-1 standards in cases under sinusoidal power supply. When considering harmonic power supply, the IEC 60034-2-3 standard was still in draft form (at the time of this publication). Therefore, the efficiency estimate of a PWM-VSI supplied induction machine is compared to the Direct-Method where shaft torque and speed are used to calculate output power. Thus, given the benchmarks in use, the actual torque and speed of the machine under the operational load is required in addition to the measured electrical input power. The experimental setup is illustrated in Figure 6.2 where 6 line measurements are taken on the inputs of the induction machine and, during harmonic testing, the inverter.

6.2 Loading of the Induction Machine

Four different induction machines were used to test the proposed efficiency estimation technique under sinusoidal supply conditions and only the $7.5kW$

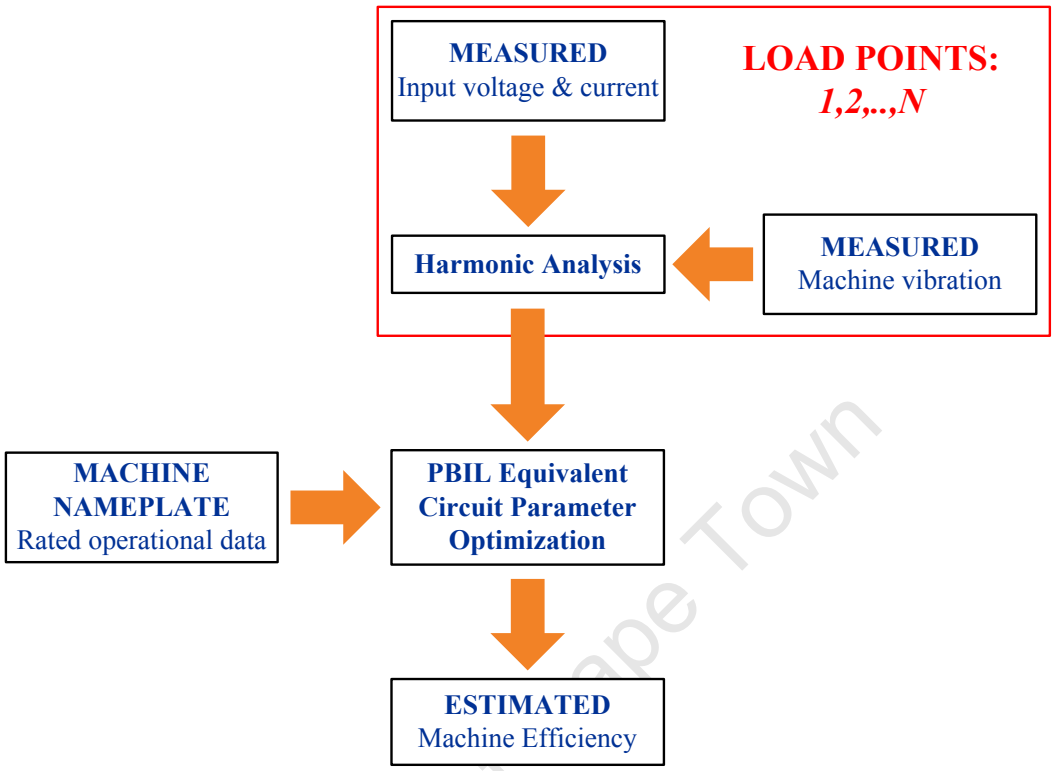

Figure 6.1: Efficiency Estimation Block Diagram

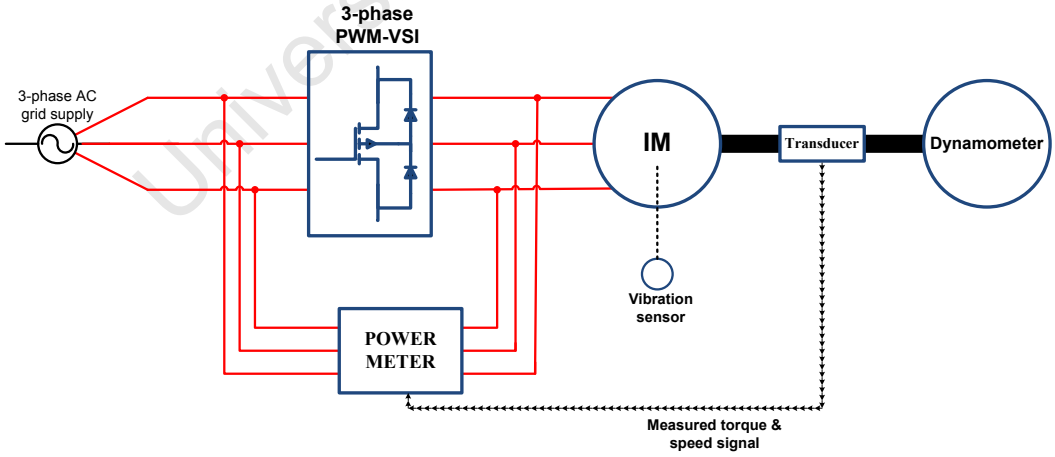

Figure 6.2: Laboratory Test Setup

Standard Efficiency induction machine was used in the case of PWM-VSI supply experimental tests. A summary of the information found in the data sheets for each of the induction motors used for efficiency estimation testing is shown in Table 6.1.

Table 6.1: Nameplate Data of Induction Motors Under Consideration

	Standard Efficiency		Premium Efficiency	
Rated Output (kW)	7.5	11	7.5	11
Rated Frequency (Hz)	50 Hz	50 Hz	50 Hz	50 Hz
Poles	4	4	4	4
Rated Line Voltage (V)	380	380	380	380
Rated Line Current (A)	15.2	23.9	14.9	22.9
Rated Speed (rpm)	1450	1455	1460	1460
Rated P.F.	0.87	0.837	0.89	0.83
Design Class	N	N	N	N
Insulation Class	F	F	H	H
R_{stator} @ $T_{ambient}$	1.897	0.990	1.575	0.796

The induction machine is loaded with a separately excited DC machine, rated at 15kW, which acts as a dynamometer. The load torque of the induction machine is controlled by varying the armature current of the dynamometer. The dynamometer is coupled to the induction machine through an inline torque transducer. The shafts of the induction and DC machines are aligned with a dial gauge alignment clock to ensure that the horizontal and vertical displacements of the two machines do not exceed $0.4mm$ and the shaft angular displacement is less than $1°$.

The inline torque transducer, a *Magtrol TM 312*, measures the torque and speed on the shaft of the induction machine. The torque is measured to an accuracy of $< 0.2Nm$ for any load under its maximum rating of $200Nm$ [55]. The value of the measured torque is output as an analog DC signal with a $\pm 5V$ full scale deflect. The speed of the shaft is measured using an optical sensor which outputs a square wave PWM signal through a conditioning circuit with an accuracy of $< 1rpm$ [55].

The induction machine test rig is shown in Figure 6.3.

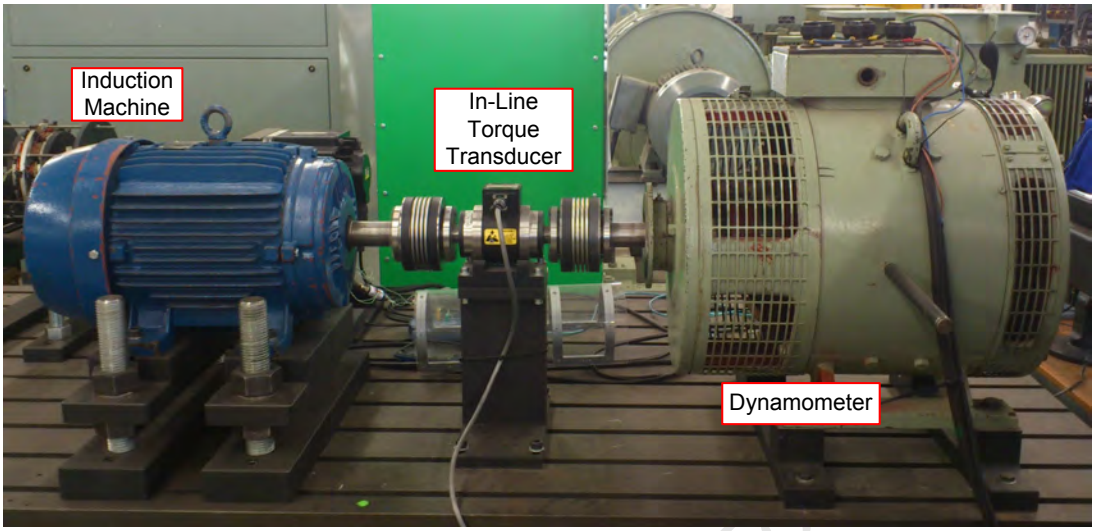

Figure 6.3: Induction Machine Test Rig

6.3 Power Supply and Measurement

A 15kW Telemecanique Altivar 5 variable speed drive is used to supply the induction machine with a PWM voltage, connected as shown in Figure 6.2. The switching frequency of the PWM supply can be adjusted by means of an analog dial. The power meter used in the system is a Yokogawa WT1800 Precision Power Analyzer with six power input channels. Three channels are used to measure the PWM-VSI supply's line voltage and line current to the induction motor. In addition, the torque and speed signals from the inline transducer are read by the analyzer which enable it to determine the running efficiency of an induction machine by the Direct Method.

The power analyzer is also capable of capturing the instantaneous line currents and voltages fed to the induction machine. These values can then be processed by the Non-Intrusive Efficiency Estimation method to determine motor efficiency. The power analyzer is capable of sampling the input power at a frequency of $16 - 32\ kHz$ for a sample period of 100 milliseconds.

6.4 Vibration Data Acquisition

A dual axis accelerometer is used to detect the vibration in the machine. However, as the speed related vibrations are centered around the horizontal axis of an induction machine (the vibrations are radial), only 1 axis is utilized which provides sufficient data for speed estimation. The ADXL202E IC chip was used where the analog output pin (X_{FILT}) is sampled rather than the PWM duty cycle output. This can be accomplished due to the fact that the analog output is proportional to the magnitude of the vibration. This allows for analog sampling where the entire bandwidth of half of the sampling rate is available for analysis [3]. A National Instruments NI-cDAQ samples the analog data at sampling frequency of $10kHz$, thus, a $5kHz$ bandwidth of vibration data is available for analysis. The circuit is encased in a box that has magnets to attach it to an induction machine's casing. The circuit diagram and accelerometer setup is shown in Figure 6.4.

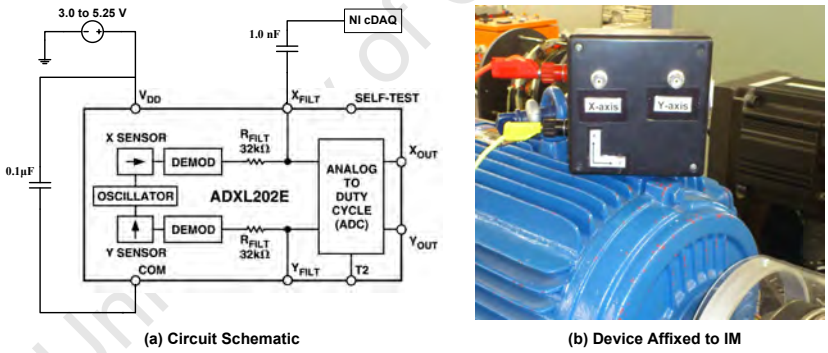

Figure 6.4: Vibration Data Acquisition

6.5 Instrumentation Accuracy

The experimental setup is based on the instrumentation requirements stated in the IEEE 112 and IEC 60034-2-1 standards as summarized in Table 6.2.

Table 6.2: Variable Measurement Accuracy Implemented

Variable Measurement Error	IEC 60034-2-1/ IEEE 112-B	Experimental Setup
Voltage	±0.2%	✓
Current	±0.2%	✓
Power	±0.2%	✓
Resistance	±0.2%	✓
Frequency	±0.1%	✓
Temperature	$\pm 1^{\circ}C$	✓
Torque	±0.2%	✓
Speed	$\pm 1rpm$	✓
Instrument Transformers	±0.3%	✓

Chapter 7

Speed Estimation Using Vibration Analysis

7.1 Test Results

As stated in Chapter 5.3.4, a proposed option of determining a machines efficiency is to measure inputs at temporal load points. In [20] the temporal load points are defined by the *MCSA* speed estimation technique whereby one minute is required to estimate speed, thus 1 minute for each temporal load point. The assumption made is that the temporal load points have the same operating temperature as the stable load points, though in reality this does not hold true.

In order to decrease the impact of temperature variations in temporal load changes, the duration of each load change needs to be as small as possible. Therefore, in addition to analyzing the accuracy of speed estimation using vibration analysis, the estimation at varying sample times is also considered.

As found in [10], reducing the influence of noise using *windowing* does not compensate for the cost in spectral leakage. Therefore, only the effect of the degree of zero padding and sample time is investigated. The **MATLAB** function source-code for analyzing vibration data is shown in Appendix A.1.

The accuracy of the speed estimation algorithm applied for a PWM-VSI supplied 7.5 kW induction machine (see Table 6.1) operating at various stable load conditions. The test was conducted three separate times for each load point to ensure that the estimation technique is valid through repeatability. The results for rated load are shown in Figure 7.1 and the results for the various loads tested are shown in Appendix B.1, Figures B.2, B.3 and B.4.

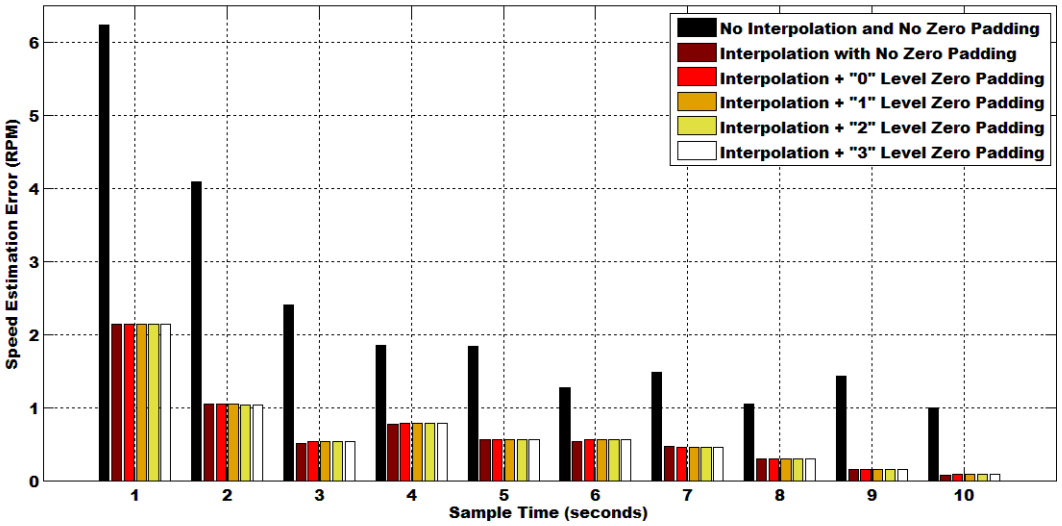

Figure 7.1: 7.5 kW IM Speed Estimation Error Analysis @ 100% of Rated Load

Based on the results tabulated in Table 7.1 and Appendix Tables B.2, B.3, B.4; the best speed estimation condition occurs when sampling vibration data for 5 seconds and applying parabolic interpolation and zero padding with a zero-pad factor of 1. Applying this condition leads to a speed estimation error of less than $1rpm$ which falls within the measurement error of the benchmark (torque transducer). The estimation condition applied to a single test at various loads can be seen in Table 7.2.

Table 7.1: 7.5kW IM Speed Estimation Repeatability Analysis @ 100% of Rated Load

		Sample Time of Vibration Data (seconds)									
		1	2	3	4	5	6	7	8	9	10
No Interpolation	$\overline{n_{err}}$	6.2463	4.0973	2.4041	1.8526	1.8457	1.2665	1.4797	1.0544	1.4354	0.9959
with No Z_{PF}	σ	3.0730	2.7465	1.2736	0.9175	0.3334	0.4155	0.5297	0.4533	0.6094	0.4847
Interpolation	$\overline{n_{err}}$	2.1418	1.0460	0.5141	0.7734	0.5548	0.5282	0.4664	0.2980	0.1560	0.0763
with No Z_{PF}	σ	1.7898	0.3175	0.3724	0.2028	0.3552	0.2458	0.1225	0.0493	0.0648	0.0792
Interpolation	$\overline{n_{err}}$	2.1411	1.0454	0.5333	0.7846	0.5609	0.5592	0.4604	0.2918	0.1556	0.0855
with $Z_{PF} = 0$	σ	1.7875	0.3444	0.2527	0.2293	0.3861	0.2707	0.1162	0.0468	0.0569	0.0689
Interpolation	$\overline{n_{err}}$	2.1386	1.0431	0.5358	0.7832	0.5555	0.5564	0.4607	0.2906	0.1543	0.0849
with $Z_{PF} = 1$	σ	1.7813	0.3374	0.2503	0.2320	0.3882	0.2662	0.1165	0.0467	0.0577	0.0685
Interpolation	$\overline{n_{err}}$	2.1387	1.0415	0.5339	0.7835	0.5545	0.5571	0.4608	0.2904	0.1541	0.0852
with $Z_{PF} = 2$	σ	1.7773	0.3369	0.2493	0.2335	0.3897	0.2663	0.1165	0.0471	0.0581	0.0684
Interpolation	$\overline{n_{err}}$	2.1380	1.0410	0.5334	0.7834	0.5542	0.5573	0.4608	0.2904	0.1541	0.0853
with $Z_{PF} = 3$	σ	1.7758	0.3362	0.2486	0.2342	0.3901	0.2661	0.1165	0.0474	0.0584	0.0684

$\overline{n_{err}}$ represents the average error between actual and estimated speeds (in rpm)

σ is the standard deviation for the repeatability tests

Table 7.2: Speed Estimation of 7.5kW IM Using Parabolic Interpolation, Zero Padding Factor of 1 and a 5 Second Vibration Sample Time

% of Rated Load	Estimated Speed (rpm)	Measured Speed (rpm)	Absolute Error (rpm)
150	1421.38	1420.98	-0.4001
125	1436.82	1436.93	0.1095
100	1451.74	1451.73	-0.0126
75	1465.9	1465.56	-0.3444
50	1478.22	1477.53	-0.6870
25	1489.45	1490.14	0.6913

Using a similar analysis to that performed on the 7.5kW induction machine, the results for tests on the 11kW induction machine are shown in Figure 7.2 and Table 7.3. In Figure 7.2, 'N' refers to the log_2 value of the number of samples rounded up to the next integer. The results of analyzing vibration data collected from a 7.5kW induction machine supplied from a PWM-VSI inverter with a switching frequency of 1250Hz is shown in Table 7.4.

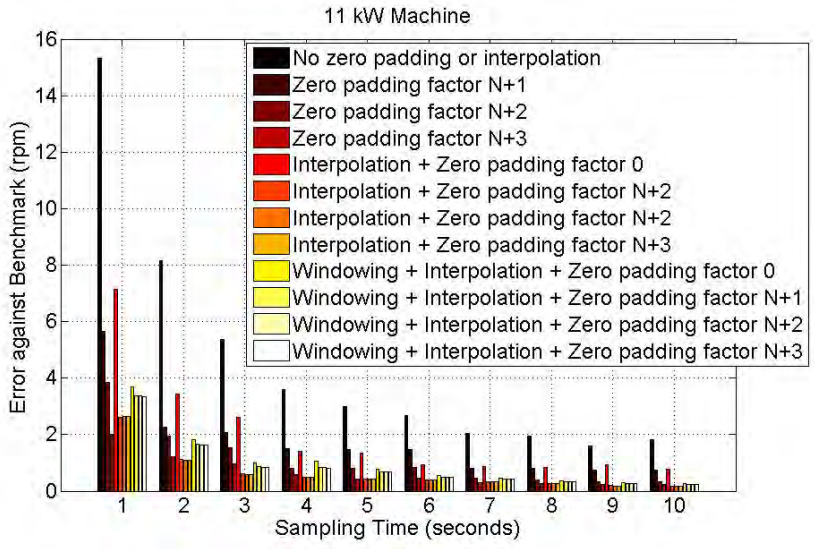

Figure 7.2: 11 kW IM Speed Estimation Error Analysis @ 100% of Rated Load [10]

Table 7.3: Speed Estimation of 11kW IM Using Parabolic Interpolation, Zero Padding Factor of 1 and a 5 Second Vibration Sample Time

% of Rated Load	Estimated Speed (rpm)	Measured Speed (rpm)	Absolute Error (rpm)
150	1412.8	1412.85	0.0456
125	1432.68	1433.08	0.3956
100	1449.54	1448.61	-0.9304
75	1464.46	1463.97	-0.4886
50	1477.52	1477.23	-0.2888
25	1489.26	1488.58	-0.6825

Table 7.4: Speed Estimation of 7.5kW PWM-VSI Supplied IM with Switching Frequency of 1250Hz

% of Rated Load	Estimated Speed (rpm)	Measured Speed (rpm)	Absolute Error (rpm)
100	1490.13	1489.68	-0.4468
85	1492.67	1492.77	0.1048
75	1495.60	1496.51	0.9144
60	1500.50	1500.45	-0.0497
50	1508.85	1508.03	-0.8205
40	1513.28	1512.84	-0.4380
30	1514.25	1514.53	0.2761

Based on the results the proposed vibration analysis technique delivers a high degree of accuracy in determining the rotor speed at various loads of an induction machine. Given that the sampling rate is $10kHz$ and the sample time is 5 seconds, the theoretical rotational frequency resolution is $0.2Hz$ or $12rpm$. Therefore, as seen from the results, zero-padding and parabolic interpolation provides a great influence in overcoming the deficient spectral resolution in attaining a speed estimation within $1rpm$ or $0.017Hz$.

As a sampling time of only 5 seconds is required to attain an accurate rotor speed estimation; temporal load changes in the efficiency estimation method proposed in Chapter 5.3.4 would allow for the assumption that the temperatures of the load changes are equal to the stable load temperature.

Chapter 8

NIEE-PBIL Technique Applied to Sinusoidal Power Supplied Motors

The method of determining the efficiency of an induction motor through PBIL parameter identification is verified by using the technique on balanced-power supplied induction machines and by comparing the results against international efficiency testing standards. The proposed algorithm's accuracy is compared against the IEEE and IEC international motor testing standards.

8.1 Methodology of NIEE-PBIL with IM Rated Power Supply

A power supply is considered balanced when the voltage unbalance factor is less than 0.5% and the harmonic distortion coefficient (THD) is below 0.05 (in terms of harmonics) [1]. Thus, when considering sinusoidal power supply, the harmonic aspects mentioned in the method proposed in Chapter 5 are ignored and will only be investigated during harmonic power supply tests.

As seen in Figure 5.1, the two IM electrical equivalent circuit configurations that are implemented in the sinusoidal supply efficiency estimation technique are used with the harmonic order $h = 1$, essentially using only the fundamental equivalent circuits of the proposed harmonic efficiency estimation method.

The same assumptions that were made in the harmonic efficiency estimation technique proposed in Chapter 5 apply, albeit only for the fundamental frequency of the harmonic equivalent circuits. Referring to Figure 5.1, the following assumptions are made with respect to the balanced power supply PBIL efficiency estimation technique:

- Data (voltage, current, vibration) from at least five different load points are able to be collected for each machine under consideration.
- The slip, s, is determined from speed vibration analysis as described in Chapter 4 and [10].
- The stator resistance at ambient temperature is known beforehand for each machine tested.

- Whilst the leakage reactance ratio X_s/X_r can be derived from the IEEE 112 Standard and machine's design class found on the nameplate (see Table 5.1), the ratio implemented in both NIEE-PBIL circuit implementations is $X_s/X_r = 1$.
- The friction and windage loss coefficient, k_{FW}, is derived from the machines rated speed and efficiency found on the nameplate.
- The friction and windage losses for each load point are determined by the operating speed and k_{FW}.
- The rated stray load loss determined from the nameplate and Table 5.2 determines the stray load loss resistance value(s) as defined in the IEEE 112 Standard.
- The five unknown machine parameters to be identified by the PBIL (regardless of the equivalent circuit model being utilized) are: X_s, X_m, R'_r, k_{TH} and (R_{m-1b} or R_m).

As summarized in Chapter 2.4, the IEEE 112-B and IEC 60034-2-1 test methods determine a machine's efficiency at various load points from tests at a specified operating temperature. Therefore, in order to derive meaningful results, the NIEE-PBIL algorithm will consider that for a given machine, all variable load tests operate at the same temperature.

8.2 Test Results

The motors tested under rated balanced power conditions were the 7.5kW and 11kw standard and premium induction machines. The testing of the machines using the two international standards was conducted by A. vanWyk and published in [11]. Three separate tests were conducted for each machine in order to convey a consistency in the results. Due to the manual nature in which loading of a machine is controlled, a repeatability test being performed at the exact same loading condition for each test is challenging as there are minor

variations in user desired torque and thus output power. Therefore in order to ensure accuracy in averaging data from the repeatability tests, the efficiency estimation data for each test is regressed to fit a n-order polynomial curve where n equals the number of load points minus 1 and the percentage load is defined by the rated torque rather than the rated output power.

Whilst no-load and blocked-rotor tests were carried out in accordance with the IEEE and IEC standards to ascertain motor efficiency, these results were not used by the NIEE-PBIL method in determining efficiency. The average test data collected over three tests used by the NIEE-PBIL algorithm for each machine is shown in Table 8.1. The NIEE-PBIL results for each repeatability test on each machine before polynomial regression is shown in Figures 8.1 - 8.4.

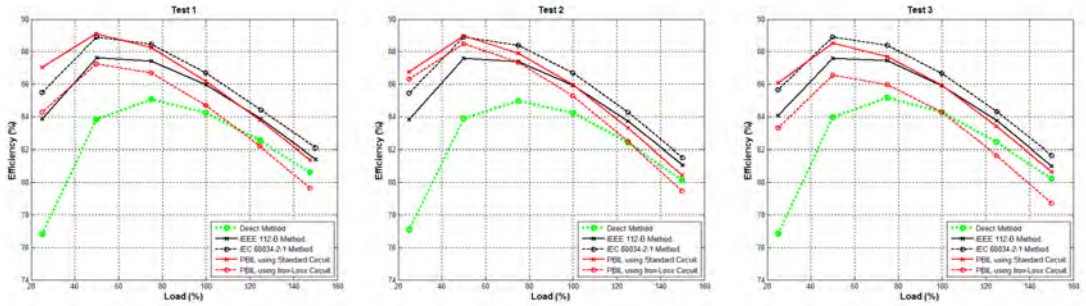

Figure 8.1: Efficiency Estimation Repeatability Results for 7.5kW Standard Efficiency IM Under Balanced Power Supply

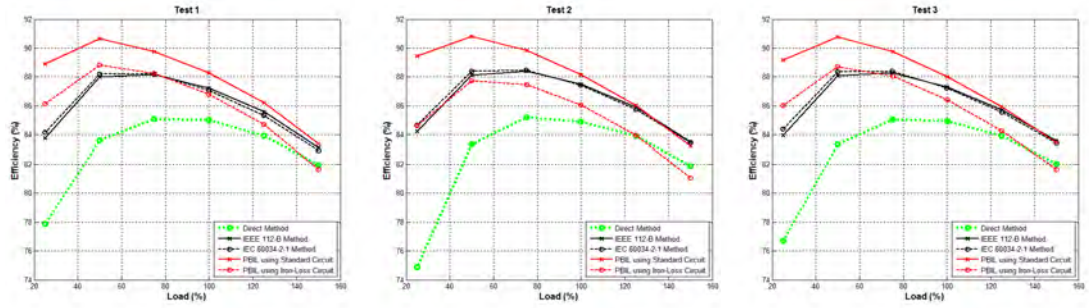

Figure 8.2: Efficiency Estimation Repeatability Results for 7.5kW Premium Efficiency IM Under Balanced Power Supply

Table 8.1: Test Data of Induction Machines Under Balanced Supply at Critical Load Points [11]

(a) 7.5kW Standard Efficiency IM

% of rated load	V_s (V)	I_s (A)	P_{in} (W)	Freq (Hz)	*Speed* (rpm)
150	382.6	22.94	13628.52	50.03	1419.31
125	383.04	18.97	11244.57	50.03	1436.26
100	383.75	15.23	8901.23	50.03	1451.93
75	382.57	11.9	6679.22	50.03	1465.35
50	384.29	8.96	4550.19	50.04	1478.06
25	385.18	6.69	2505.52	50.04	1489.4

(b) 7.5kW Premium Efficiency IM

% of rated load	V_s (V)	I_s (A)	P_{in} (W)	Freq (Hz)	*Speed* (rpm)
150	378.18	22.71	13448.82	49.99	1429.3
125	383.49	18.52	11067.1	50	1445.8
100	384.29	14.96	8824.46	50.02	1458.67
75	383.3	11.71	6663.38	50.03	1470.01
50	384.31	8.74	4564.02	50.04	1480.88
25	384.78	6.28	2513.18	50.05	1490.87

(c) 11kW Standard Efficiency IM

% of rated load	V_s (V)	I_s (A)	P_{in} (W)	Freq (Hz)	*Speed* (rpm)
150	378.78	36.35	20234.91	50.03	1409.33
125	379.4	29.72	16620.91	50.02	1429.52
100	379.93	23.88	13171.74	50.02	1447.46
75	381.68	18.77	9912.65	50.03	1463.08
50	382.81	14.46	6786.45	50.03	1476.54
25	384.5	11.22	3754.67	50.03	1488.69

(d) 11kW Premium Efficiency IM

% of rated load	V_s (V)	I_s (A)	P_{in} (W)	Freq (Hz)	*Speed* (rpm)
150	380.82	34.28	19240.24	49.97	1429.5
125	384.55	28.17	15903.1	49.99	1445.99
100	385.97	22.91	12709.76	50	1459.1
75	387.35	18.23	9623.17	50.01	1470.61
50	388.71	14.16	6608.61	50.02	1481.24
25	388.71	10.97	3652	50.03	1490.87

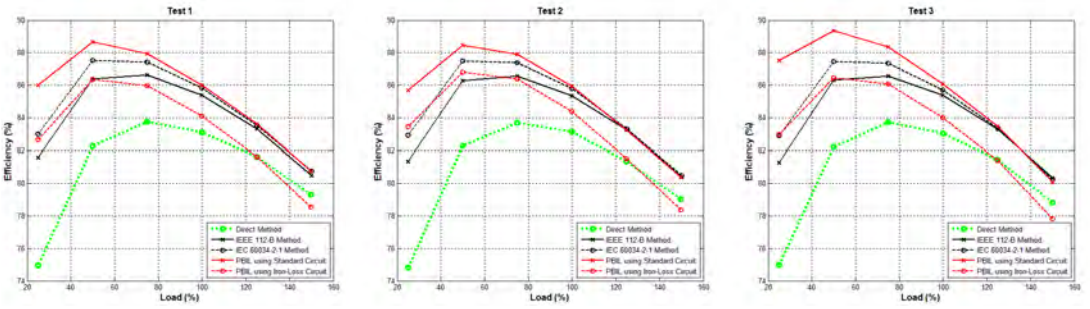

Figure 8.3: Efficiency Estimation Repeatability Results for 11kW Standard Efficiency IM Under Balanced Power Supply

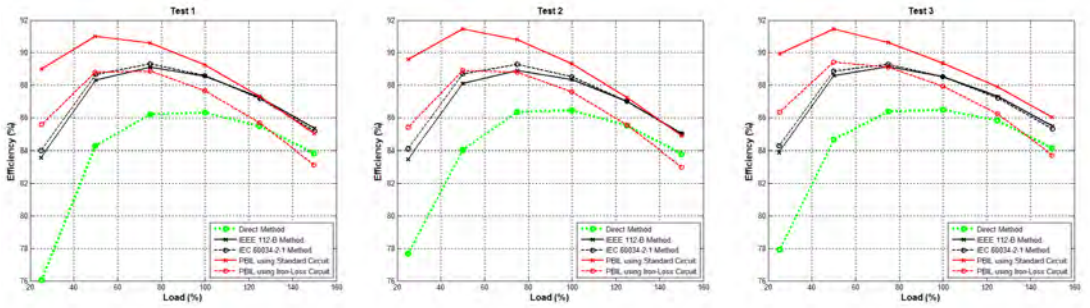

Figure 8.4: Efficiency Estimation Repeatability Results for 11kW Premium Efficiency IM Under Balanced Power Supply

8.3 Balanced Power Efficiency Estimation Analysis

After polynomial regression and then averaging, the efficiency estimation results for each machine are shown in Figures 8.5-8.8. The efficiency estimation variations at critical load points are detailed in Table 8.2.

Upon inspection of the results in Figures 8.5-8.8 and Table 8.2 it can be seen that the NIEE-PBIL efficiency estimation algorithm at various loads follows the trend of the IEEE 112-B and IEC 60034-2-1 efficiency testing standards rather than the direct method. This correlation can be seen in all machines tested thus allowing for the conclusion that the NIEE-PBIL algorithm, regardless of the equivalent circuit implemented, adjusts for load losses in a similar manner as the IEEE and IEC standards. This is not true for the direct efficiency estimation which only

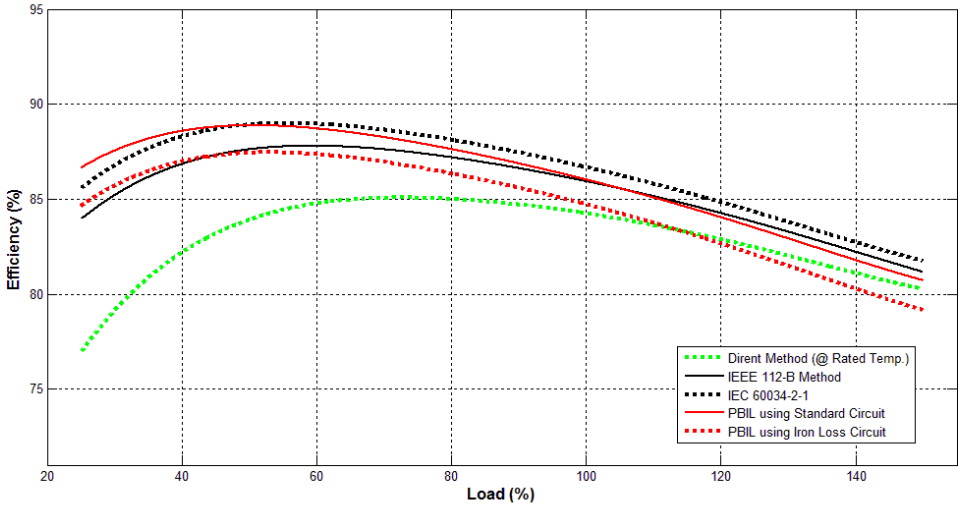

Figure 8.5: Efficiency Estimation of 7.5kW Standard Eff. Motor

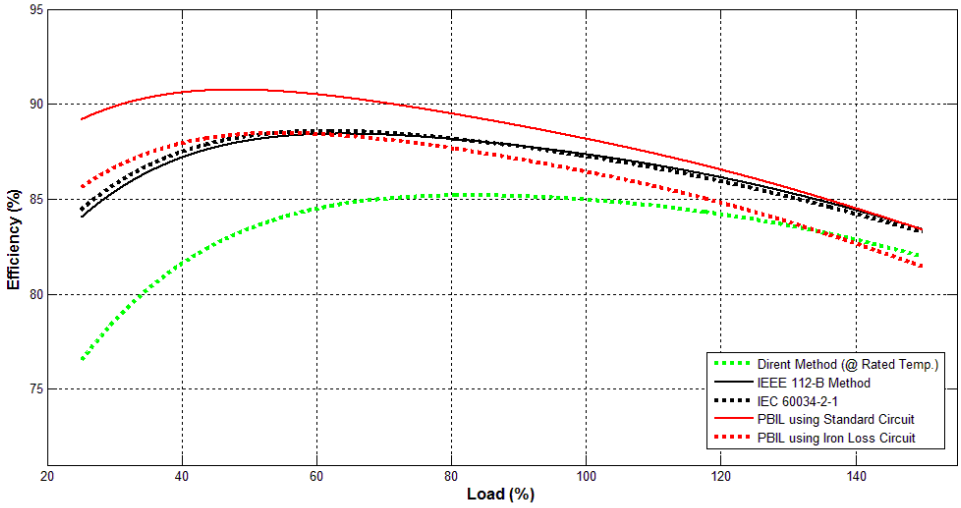

Figure 8.6: Efficiency Estimation of 7.5kW Premium Eff. Motor

measures operating speed and torque. As the tests are conducted at each of the machine's full-load rated temperatures, the direct method in this instance cannot compensate for assumed temperature changes at differing load points thus are neglected when conducting an error investigation into the effectiveness of the NIEE-PBIL method.

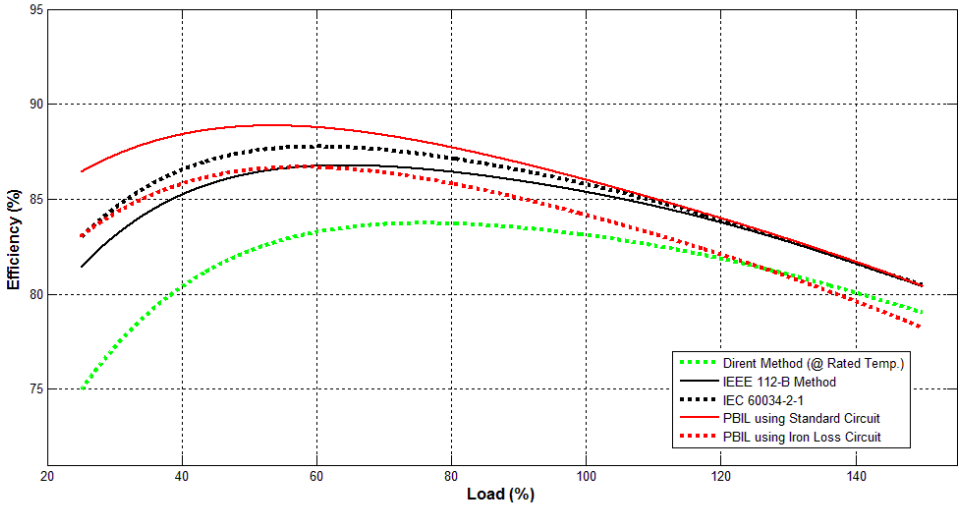

Figure 8.7: Efficiency Estimation of 11kW Standard Eff. Motor

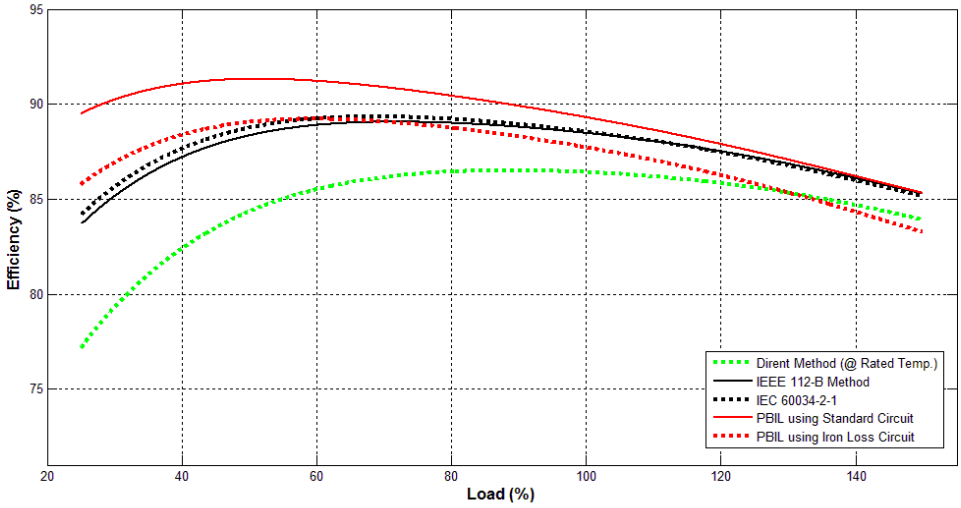

Figure 8.8: Efficiency Estimation of 11kW Premium Eff. Motor

With all the machines that were tested, the Iron-Loss implementation of the NIEE-PBIL gives a lower efficiency estimation compared to that of the Standard Circuit NIEE-PBIL implementation. When the machines are overloaded (125-150% of rated load), the Standard Circuit implementation gives a better approximation of efficiency than the Iron-Loss Circuit implementation. The variation of error in this instance for the Standard Circuit

Table 8.2: Efficiency Estimation of Induction Machines Under Balanced Supply at Critical Load Points

(a) 7.5kW Standard Eff. Motor

Measured Efficiency	% of Rated Load					
and Estimation Error (%)	25	50	75	100	125	150
Direct Method	76.91	83.90	85.07	84.24	82.47	80.26
Error of Standard Circuit	-9.73	-4.97	-2.89	-1.78	-1.02	-0.46
Error of Iron-Loss Circuit	-7.72	-3.53	-1.61	-0.49	0.37	1.10
IEEE 122-B	83.92	87.61	87.43	85.93	83.78	81.16
Error of Standard Circuit	-2.71	-1.27	-0.53	-0.09	0.29	0.44
Error of Iron-Loss Circuit	-0.71	0.18	0.75	1.20	1.68	2.00
IEC 60034-2-1	85.53	88.91	88.41	86.69	84.34	81.76
Error of Standard Circuit	-1.11	0.04	0.45	0.66	0.85	1.04
Error of Iron-Loss Circuit	0.90	1.48	1.73	1.95	2.24	2.59

(b) 7.5kW Premium Eff. Motor

Measured Efficiency	% of Rated Load					
and Estimation Error (%)	25	50	75	100	125	150
Direct Method	76.45	83.43	85.13	84.96	83.93	81.97
Error of Standard Circuit	-12.72	-7.31	-4.67	-3.21	-2.15	-1.41
Error of Iron-Loss Circuit	-9.13	-4.99	-2.79	-1.48	-0.40	0.52
IEEE 122-B	84.01	88.08	88.29	87.35	85.76	83.40
Error of Standard Circuit	-5.16	-2.66	-1.50	-0.82	-0.32	0.02
Error of Iron-Loss Circuit	-1.57	-0.34	0.37	0.90	1.43	1.95
IEC 60034-2-1	84.41	88.32	88.36	87.25	85.55	83.27
Error of Standard Circuit	-4.76	-2.43	-1.44	-0.92	-0.52	-0.11
Error of Iron-Loss Circuit	-1.17	-0.11	0.44	0.81	1.22	1.82

(c) 11kW Standard Eff. Motor

Measured Efficiency	% of Rated Load					
and Estimation Error (%)	25	50	75	100	125	150
Direct Method	74.91	82.25	83.73	83.11	81.47	79.03
Error of Standard Circuit	-11.50	-6.58	-4.34	-2.90	-1.98	-1.38
Error of Iron-Loss Circuit	-8.11	-4.28	-2.41	-1.06	-0.05	0.80
IEEE 122-B	81.40	86.33	86.60	85.37	83.28	80.40
Error of Standard Circuit	-5.01	-2.51	-1.47	-0.64	-0.17	-0.01
Error of Iron-Loss Circuit	-1.63	-0.20	0.46	1.20	1.76	2.17
IEC 60034-2-1	82.94	87.49	87.40	85.79	83.39	80.48
Error of Standard Circuit	-3.48	-1.35	-0.67	-0.22	-0.06	0.07
Error of Iron-Loss Circuit	-0.09	0.96	1.26	1.62	1.87	2.25

(d) 11kW Premium Eff. Motor

Measured Efficiency	% of Rated Load					
and Estimation Error (%)	25	50	75	100	125	150
Direct Method	77.16	84.34	86.32	86.41	85.60	83.91
Error of Standard Circuit	-12.34	-6.98	-4.35	-2.89	-1.89	-1.41
Error of Iron-Loss Circuit	-8.61	-4.71	-2.61	-1.31	-0.22	0.64
IEEE 122-B	83.65	88.34	89.05	88.47	87.20	85.28
Error of Standard Circuit	-5.85	-2.98	-1.62	-0.83	-0.30	-0.03
Error of Iron-Loss Circuit	-2.12	-0.70	0.13	0.75	1.37	2.01
IEC 60034-2-1	84.13	88.75	89.30	88.55	87.14	85.17
Error of Standard Circuit	-5.37	-2.57	-1.37	-0.75	-0.35	-0.15
Error of Iron-Loss Circuit	-1.64	-0.30	0.37	0.83	1.31	1.90

NIEE-PBIL is 0.01-0.44% measured against the IEEE 112-B method at 150% of rated load when considering all machines. Alternatively, the Iron-Loss NIEE-PBIL underestimates the efficiency by 1.95-2.17% when compared against the IEEE 112-B method. Given that the IEEE and the IEC efficiency estimates are approximately equal, the same phenomenon is observed where the Standard Circuit NIEE-PBIL efficiency estimate variation is 0.06-1.04% and the Iron-Loss Circuit NIEE-PBIL efficiency estimate variation is 1.31-2.59%.

At lower loading conditions for all machines, the Iron-Loss NIEE-PBIL implementation gives a better efficiency estimation than the Standard Circuit implementation. In this instance the Iron-Loss Circuit implementation has an error variation of 0.09-1.64% when compared to the IEC 60034-2-1 method at 25% of rated load. Alternatively, the Standard Circuit implementation overestimates the efficiency by 1.11-5.37% when compared to the IEC 60034-2-1 method at 25% of rated load. When comparing the efficiency estimates at lower loading conditions to the IEEE 112-B standard, the Standard Circuit

NIEE-PBIL efficiency estimate variation is 1.27-5.85% and the Iron-Loss Circuit NIEE-PBIL efficiency estimate variation is 0.18-2.12%.

8.3.1 Parameter Identification

An investigation of repeatedly executing the NIEE-PBIL algorithm until termination was carried out for the same set of input measurements for each machine. An assessment of the repeated *runs* for both implementations of the algorithm is shown in Tables 8.3-8.6 and the mean ($\bar{x}$) and standard deviations (σ^2) of each parameter identified is summarized in Table 8.7.

Table 8.3: $7.5kW$ Standard Motor with Repeated PBIL Parameter Identification

(a) Standard Circuit

	X_s (Ω)	X_m (Ω)	R'_r (Ω)	R_m (Ω)	k_{TH} ($^\circ C/W$)	PBIL Eff. @ Full Load (%)
Run 1	1.263	37.35	0.9247	3547	0.05344	86.3
Run 2	1.170	37.02	0.9338	4372	0.05350	86.4
Run 3	1.219	37.09	0.9338	4498	0.05371	86.5
Run 4	1.170	37.11	0.9338	4656	0.05350	86.4
Run 5	1.563	39.60	0.9064	4913	0.05362	86.4

(b) Iron-Loss Circuit

	X_s (Ω)	X_m (Ω)	R'_r (Ω)	R_m (Ω)	k_{TH} ($^\circ C/W$)	PBIL Eff. @ Full Load (%)
Run 1	1.563	39.03	0.9155	2449	0.05075	85.6
Run 2	1.347	37.73	0.9293	2516	0.05072	85.6
Run 3	1.564	39.06	0.9109	3026	0.05112	85.7
Run 4	1.193	36.67	0.9338	3643	0.05191	85.9
Run 5	1.317	37.51	0.9247	4419	0.05231	86.0

Table 8.4: $7.5kW$ Premium Motor with Repeated PBIL Parameter Identification

(a) Standard Circuit

	X_s (Ω)	X_m (Ω)	R'_r (Ω)	R_m (Ω)	k_{TH} ($^\circ C/W$)	PBIL Eff. @ Full Load (%)
Run 1	1.3672	41.73	0.7324	1250	0.07028	87.3
Run 2	1.2894	41.14	0.7233	5000	0.07385	88.1
Run 3	1.2436	41.02	0.7324	3301	0.07312	88.0
Run 4	1.2985	42.01	0.7370	2362	0.07327	88.0
Run 5	1.1673	40.34	0.7324	4389	0.07349	88.1

(b) Iron-Loss Circuit

	X_s (Ω)	X_m (Ω)	R'_r (Ω)	R_m (Ω)	k_{TH} ($^\circ C/W$)	PBIL Eff. @ Full Load (%)
Run 1	1.5625	42.83	0.7095	3682	0.07028	87.4
Run 2	1.1108	38.09	0.7324	3542	0.07074	87.5
Run 3	1.2665	40.44	0.7324	2500	0.06934	87.2
Run 4	1.1719	39.06	0.7645	894	0.06235	85.4
Run 5	1.2680	40.70	0.7233	4912	0.07129	87.7

Table 8.5: $11kW$ Standard Motor with Repeated PBIL Parameter Identification

(a) Standard Circuit

	X_s (Ω)	X_m (Ω)	R'_r (Ω)	R_m (Ω)	k_{TH} ($^\circ C/W$)	PBIL Eff. @ Full Load (%)
Run 1	0.5829	19.35	0.5859	629	0.04883	85.8
Run 2	1.0727	21.27	0.5310	896	0.05026	85.8
Run 3	1.0925	21.39	0.5219	1767	0.05154	86.1
Run 4	0.7797	19.94	0.5859	330	0.04688	84.6
Run 5	0.7797	19.97	0.5859	313	0.04590	84.4

(b) Iron-Loss Circuit

	X_s (Ω)	X_m (Ω)	R'_r (Ω)	R_m (Ω)	k_{TH} ($^\circ C/W$)	PBIL Eff. @ Full Load (%)
Run 1	1.1230	21.33	0.5127	4477	0.05124	86.0
Run 2	1.1093	21.29	0.5127	4985	0.05151	86.1
Run 3	1.1719	21.58	0.5127	2497	0.05054	85.7
Run 4	1.5625	24.29	0.4898	1905	0.05078	85.5
Run 5	1.0544	20.49	0.5219	2422	0.05042	85.7

Table 8.6: $11kW$ Premium Motor with Repeated PBIL Parameter Identification

(a) Standard Circuit

	X_s (Ω)	X_m (Ω)	R'_r (Ω)	R_m (Ω)	k_{TH} ($^\circ C/W$)	PBIL Eff. @ Full Load (%)
Run 1	1.0849	21.96	0.4807	4922	0.05713	89.3
Run 2	1.5625	24.86	0.4532	5000	0.05823	89.3
Run 3	1.0910	21.96	0.4807	3809	0.05661	89.2
Run 4	1.0208	21.56	0.5127	455	0.05099	87.7
Run 5	1.1719	22.35	0.4807	1875	0.05612	89.0

(b) Iron-Loss Circuit

	X_s (Ω)	X_m (Ω)	R'_r (Ω)	R_m (Ω)	k_{TH} ($^\circ C/W$)	PBIL Eff. @ Full Load (%)
Run 1	1.1719	22.08	0.4761	3750	0.05524	88.9
Run 2	1.0803	21.73	0.4807	4756	0.05560	89.1
Run 3	1.1536	21.04	0.4761	4172	0.05435	88.9
Run 4	1.0712	21.65	0.4852	2511	0.05444	88.7
Run 5	1.0727	21.47	0.5127	547	0.04666	86.2

Table 8.7: Summary of Repeated PBIL Parameter Identification

	$X_s\,(\Omega)$	$X_m\,(\Omega)$	$R'_r\,(\Omega)$	$R_m\,(\Omega)$	$k_{TH}(^\circ C/W)$	PBIL Eff. @ Full Load (%)
						$7.5kW$ **Standard Efficiency Motor**
Standard Circuit						
$\bar{x}$	1.2772	37.63	0.9265	4397	0.0536	86.42
σ^2	$2.69(10^{-2})$	1.22	$1.42(10^{-4})$	$2.67(10^{+5})$	$1.23(10^{-8})$	$5.96(10^{-3})$
Iron-Loss Circuit						
$\bar{x}$	1.3968	38.00	0.9229	3211	0.0514	85.78
σ^2	$2.64(10^{-2})$	1.07	$9.01(10^{-5})$	$6.86(10^{+5})$	$5.10(10^{-7})$	$4.70(10^{-2})$
						$7.5kW$ **Premium Efficiency Motor**
Standard Circuit						
$\bar{x}$	1.2732	41.25	0.7315	3260	0.0728	87.92
σ^2	$5.46(10^{-3})$	$4.24(10^{-1})$	$2.51(10^{-5})$	$2.29(10^{+6})$	$2.06(10^{-6})$	$1.18(10^{-1})$
Iron-Loss Circuit						
$\bar{x}$	1.2759	40.22	0.7324	3106	0.0688	87.04
σ^2	$3.01(10^{-2})$	3.25	$4.09(10^{-4})$	$2.26(10^{+6})$	$1.35(10^{-5})$	$9.20(10^{-1})$
						$11kW$ **Standard Efficiency Motor**
Standard Circuit						
$\bar{x}$	0.8615	20.39	0.5621	787	0.0487	85.32
σ^2	$4.72(10^{-2})$	$8.10(10^{-1})$	$1.07(10^{-3})$	$3.58(10^{+5})$	$5.43(10^{-6})$	$6.41(10^{-1})$
Iron-Loss Circuit						
$\bar{x}$	1.2042	21.80	0.5099	3257	0.0509	85.82
σ^2	$4.19(10^{-2})$	2.11	$1.42(10^{-4})$	$1.89(10^{+6})$	$2.18(10^{-7})$	$6.28(10^{-2})$
						$11kW$ **Premium Efficiency Motor**
Standard Circuit						
$\bar{x}$	1.1862	22.54	0.4816	3212	0.0558	88.90
σ^2	$4.71(10^{-2})$	1.76	$4.44(10^{-4})$	$3.97(10^{+6})$	$7.88(10^{-6})$	$4.88(10^{-1})$
Iron-Loss Circuit						
$\bar{x}$	1.1099	21.59	0.4861	3147	0.0533	88.37
σ^2	$2.38(10^{-3})$	$1.44(10^{-1})$	$2.35(10^{-4})$	$2.79(10^{+6})$	$1.39(10^{-5})$	1.42

From Table 8.7, looking at the deviation σ^2 across the NIEE-PBIL runs for each parameter, it can be seen that all parameters except for the core loss resistor R_m and in some instances, the core leakage reactance X_m, have converged. The reason for such a deviation in the estimation of the machines core loss resistor can be explained through the temperature estimation technique implemented.

8.3.2 Loss Analysis of NIEE-PBIL Technique

As the NIEE-PBIL algorithm determines the equivalent circuit parameters of an induction motor, the losses that occur during loading can be determined and compared to the measured results from the standards. Moreover, this kind of comparison can be used to explain the differences between the efficiency estimate from the NIEE-PBIL method and that measured using the IEEE and IEC methods.

In order to account for the differences between the proposed method's efficiency estimations and the measured results, a closer inspection of the losses is required. This is presented in the subsequent sections.

Effect of Thermal Model on Losses

One of the key parameters identified in the NIEE-PBIL algorithm is the thermal coefficient k_{TH}. Through determining the operating temperature, losses for each load point are estimated. Therefore, whilst considering each of the losses that occur in the machine independently, the variation of these losses across the load range can be related to the thermal model utilized in the efficiency estimate algorithm.

Recalling the temperature estimation method from Chapter 5, the temperature rise and operating temperature of a machine at any given load is related to a constant thermal coefficient k_{TH}.

$$\Delta T_{load} = k_{TH}\, P_{load,loss} \tag{8.1}$$

$$T_{load} = \Delta T_{load} + T_{ambient} \tag{8.2}$$

Where k_{TH} is determined by optimizing for the rated full load temperature found on the nameplate. Figures 8.9 and 8.10 illustrate two ways in which the thermal

estimate at varying load points may lead to inconsistencies in loss estimation.

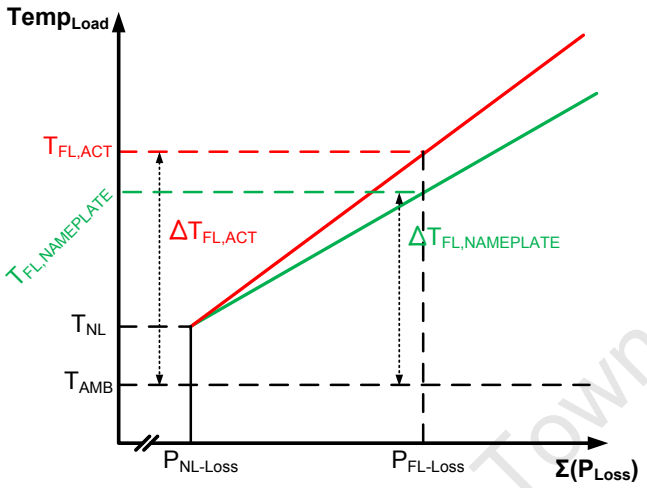

Figure 8.9: Effect of Incorrect Full Load Temp. Input

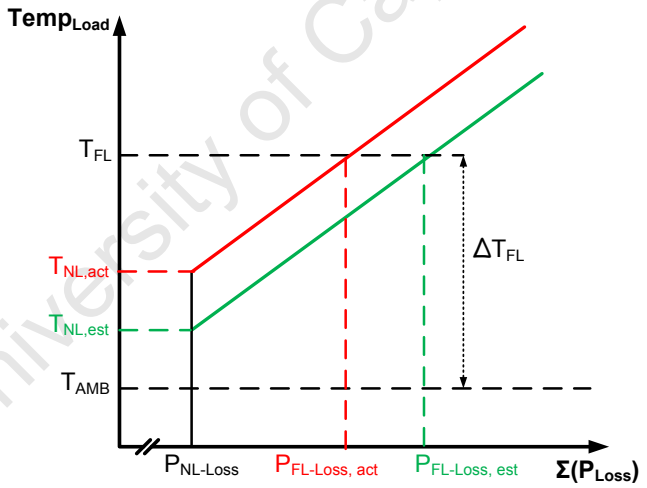

Figure 8.10: Effect of Incorrect No-Load Loss Estimation

In Figure 8.9, if the nameplate rated temperature $T_{FL,NAMEPLATE}$ differs from the machine's actual full load temperature $T_{FL,ACT}$, the result of the PBIL optimization algorithm will lead to an incorrect k_{TH} value. As k_{TH} acts as a linear transformation, temperature errors and thus machine loss errors will vary in a linear fashion. Given that using the rated values of the machine is the most prominent factor in which k_{TH} is optimized, this error will carry forward

to various load-point loss estimates. Whilst Figure 8.9 illustrates the full-load temperature being underestimated using the insulation class found on the nameplate data, the opposite may also be true in that the full-load temperature may be overestimated. In either scenario, an inaccurate temperature versus power loss ration will lead to inconsistent loss estimates over a load range.

If the PBIL algorithm incorrectly estimates the parameters in terms of the no load losses as illustrated in Figure 8.10, the temperature estimation varies in a scalar manner. This will cause create a fixed vertical offset in the efficiency estimation. This phenomenon occurs as a result of inaccurate assumptions made in the NIEE-PBIL model such as the incorrectly assuming the rated stray load loss is 1.8% of rated input power as well as the rated friction and windage losses equaling 1.2% of the rated input power. This can be seen when comparing the Standard and Iron-Loss implementations of the NIEE-PBIL (Figures 8.5-8.8) where the differences between the two are (mostly) constant.

The effect of the PBIL applying both an incorrect scalar and linear model in order to derive k_{TH} results in the effect seen in Figure 8.11 where the NIEE-PBIL over and underestimates temperature and thus losses based on the scalar and linear inaccuracies. This phenomenon is evident when comparing the NIEE-PBIL method to the IEEE and IEC standards. At higher load points the NIEE-PBIL method overestimates the losses/temperature resulting in a lower efficiency estimation when compared to the standards. At lower load points, the NIEE-PBIL algorithm underestimates the losses/temperature thus overestimating the efficiency.

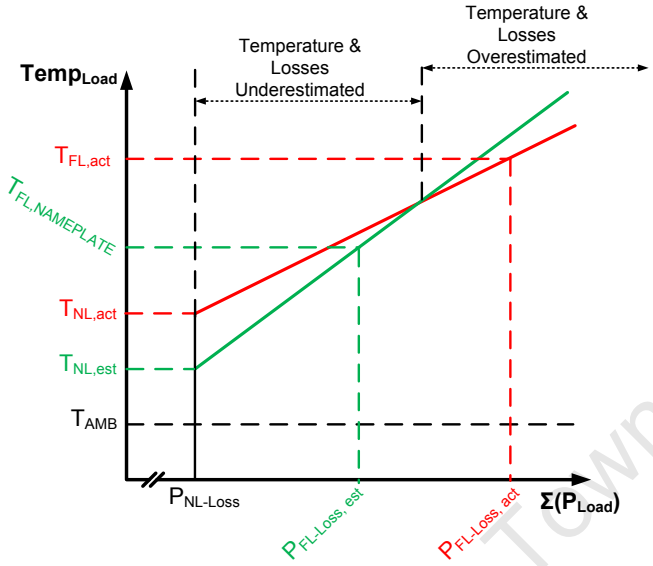

Figure 8.11: Temperature & Load-Loss Estimation Error

Load Independent Losses

Traditionally, no-load losses are referred to as the sum of the core and friction and windage losses. Both circuit implementations of the NIEE-PBIL use the same method to determine friction and windage losses as determined from the square of estimated speed. Since the same speed at each load point is used on both NIEE-PBIL implementations, the friction and windage losses accounted for in each implementation for each load point of a machine is equal. Therefore, if the friction & windage losses and the core losses for each circuit implementation are summed together, the differences will be a result of the estimated core losses.

In Figure 8.12, the NIEE-PBIL losses attributed to the core and friction and windage are shown referring to the repeated algorithms runs summarized in Table 8.3. As illustrated in the figure, due to the inconsistency in attaining a core loss resistor value (referring to Table 8.7), there is an inconsistency in determining the core losses. However, Figures 8.12(a) and 8.12(b) show that each core loss estimate is parallel for each PBIL run for the Standard and Iron-Loss circuit implementations respectively. Therefore, since the friction and windage losses

are the same for each PBIL run, the inconsistency in attaining a core loss resistor value can be attributed to the NIEE-PBIL incorrectly estimating no load loss temperature (and thus the actual no-load loss incurred) as illustrated in Figure 8.10.

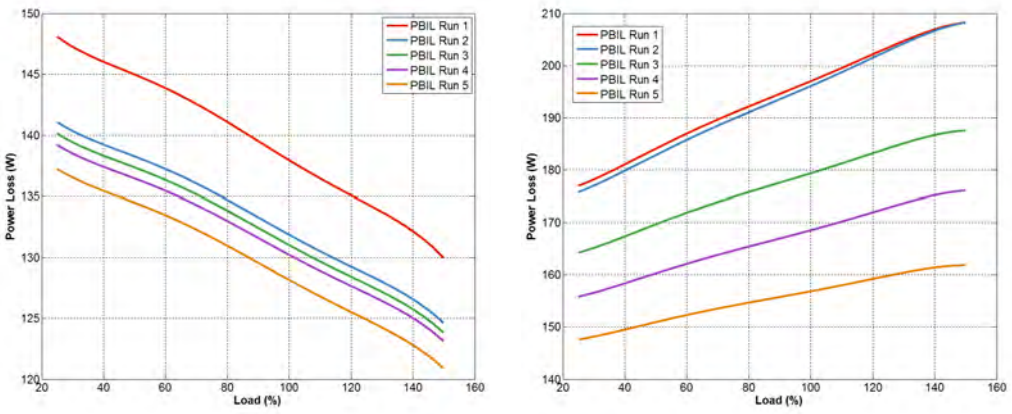

(a) Standard Circuit (b) Iron-Loss Circuit

Figure 8.12: Effect of NIEE-PBIL Repeatability Run on No-Load Losses in the $7.5kW$ Standard Efficiency IM

As the IEEE and IEC methods are used as benchmarks, the no-load loss analysis can be extended to include a comparison between the measured and estimated losses as shown in Figure 8.13. Whilst both standards assume the same load independent value of friction and windage losses, the IEEE 112-B standard assumes a constant core loss throughout all loading conditions whereas the IEC standard takes into account the voltage across the in determining core loss as shown in Equation 8.3.

$$V_{core} = \sqrt{(V_s - \sqrt{3}I_s R_s cos(\theta))^2 + (\sqrt{3}I_s R_s sin(\theta))^2} \tag{8.3}$$

From Figure 8.13 it can be seen that the NIEE-PBIL Iron-Loss circuit implementation for determining no-load losses gives a closer approximation to the IEEE standard when compared to the NIEE-PBIL Standard circuit implementation. Additionally, NIEE-PBIL Standard Circuit estimation of

no-load losses matches the trend of the IEC estimation albeit with an offset. This trend can be explained by the way the IEC standard and the NIEE-PBIL Standard Circuit similarly consider voltage across the core as a determining factor of loss. The difference in no-load loss trends between the two implementations of the NIEE-PBIL can be attributed to the inclusion of a slip-dependent rotor core resistor in the Iron-Loss circuit implementation where the slip at lower load points increases the core loss resistance thus reducing the proportional current flowing through the core loss model, and hence the core loss estimate.

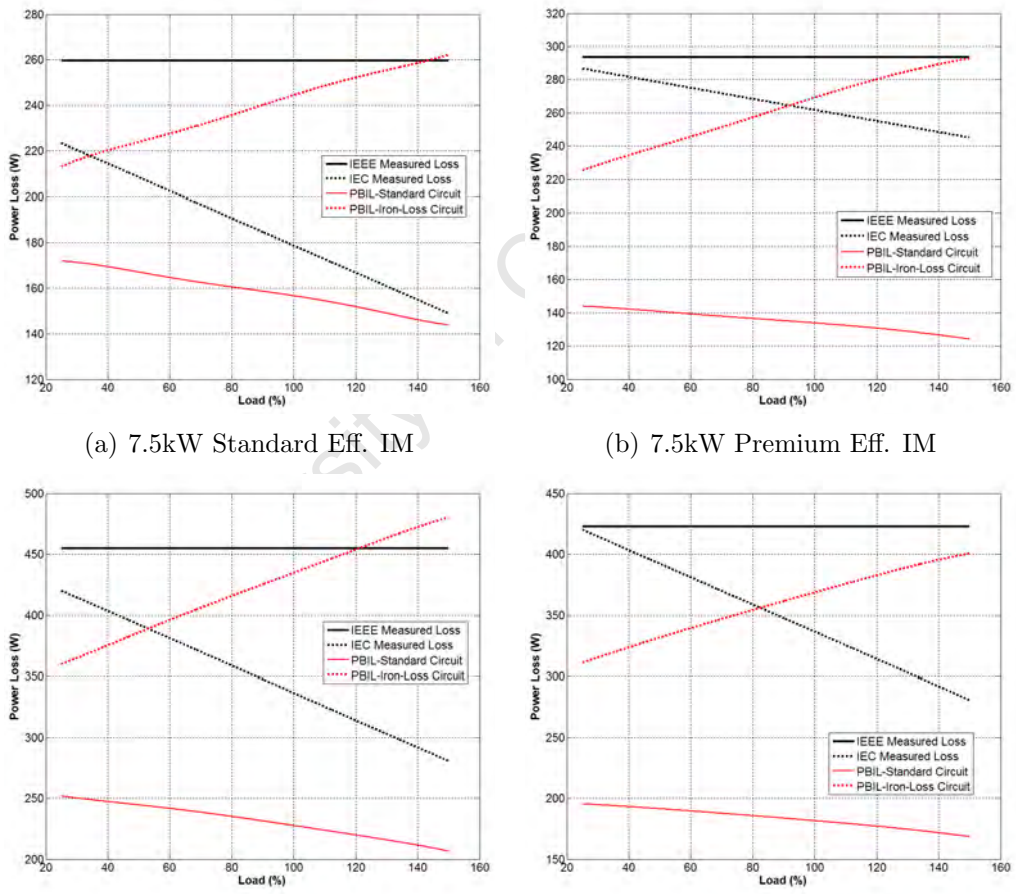

(a) 7.5kW Standard Eff. IM

(b) 7.5kW Premium Eff. IM

(c) 11kW Standard Eff. IM

(d) 11kW Premium Eff. IM

Figure 8.13: Comparison Between Measured and Estimated Load Independent Losses

Copper Losses

The copper losses in an induction machine can be separated into two categories: stator and rotor copper losses. The effect of repeated PBIL runs on rotor and stator copper losses can be seen in Figures 8.14 and 8.15. As shown in Figures 8.14 and 8.15, the copper losses estimated from repeated NIEE-PBIL runs, regardless of the circuit implemented, give consistent results through all machine loading conditions. Thus it can be conclude that, as the attained rotor resistance and k_{TH} values have a low standard deviation over repeated PBIL runs (from Table 8.7), the effect of high variations in the attained core loss values do not influence copper losses.

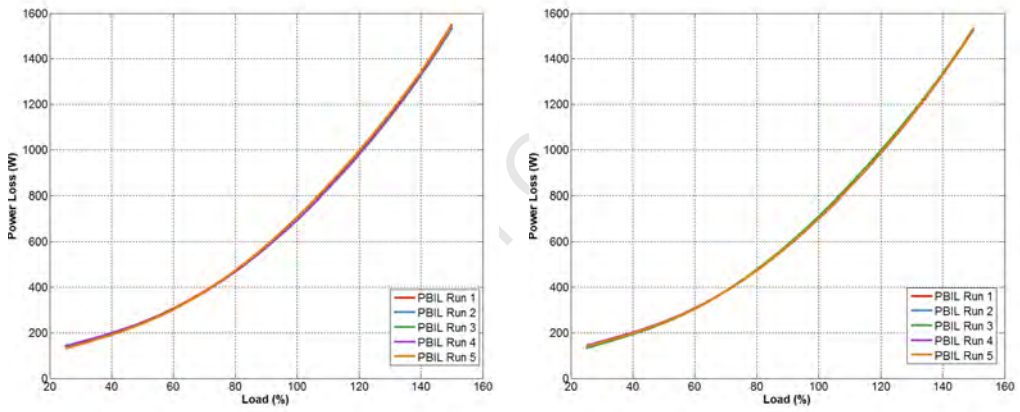

(a) Standard Circuit (b) Iron-Loss Circuit

Figure 8.14: Effect of NIEE-PBIL Repeatability Run on Stator Copper Losses in the $7.5kW$ Standard Efficiency IM

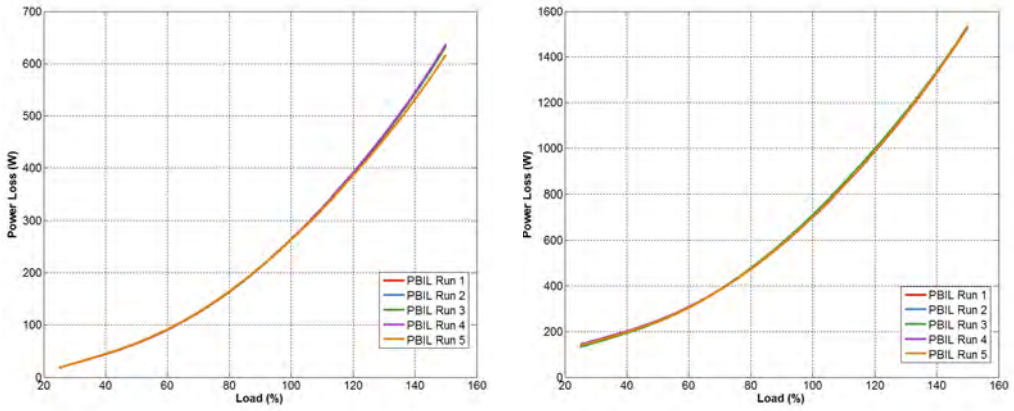

(a) Standard Circuit (b) Iron-Loss Circuit

Figure 8.15: Effect of NIEE-PBIL Repeatability Run on Rotor Copper Losses in the 7.5kW Standard Efficiency IM

The comparison between measured and estimated copper losses are shown in Figures 8.16 and 8.17. Referring to Figures 8.16 and 8.17 it can be seen that both implementations of the NIEE-PBIL algorithm (Standard/Iron-Loss circuit) determine the same stator and rotor losses regardless of machine size (7.5kW/11kW) and type (Standard/Premium Efficiency). Therefore, the differences between overall machine efficiency as well as inconsistent core loss resistance estimate of the two NIEE-PBIL circuit implementations are not attributed to copper loss estimation.

As the NIEE-PBIL algorithm solves for all equivalent circuit parameter simultaneously and given that the efficiency (and thus loss estimate) of the machine can be considered fairly accurate (from Figures 8.5-8.8); the higher estimated versus measured stator copper loss could be as a result of attempting to compensate for lower no-load (core) losses (see Figure 8.13). Alternatively, the opposite might be true where the no-load losses are underestimated as a result of overestimation of the stator copper losses.

Conversely, the rotor copper losses (as shown in Figure 8.17), whilst closer in approximation to the measured losses when compared to the stator loss estimation, are in fact underestimated. When considering the variation of rotor

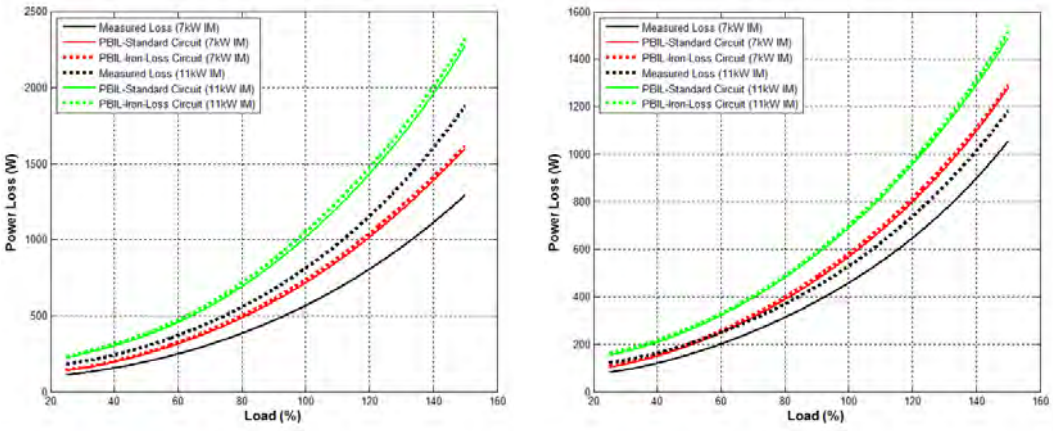

(a) Standard Efficiency IMs (b) Premium Efficiency IMs

Figure 8.16: Comparison Between Measured and Estimated Stator Copper Losses

losses against changes in machine load, the trend in the estimated copper losses follows that of the measured loss trend.

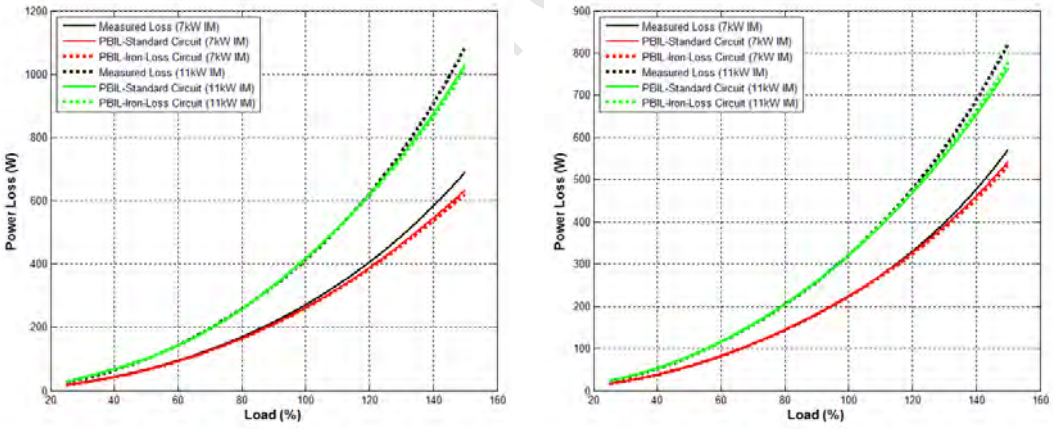

(a) Standard Efficiency IMs (b) Premium Efficiency IMs

Figure 8.17: Comparison Between Measured and Estimated Rotor Copper Losses

As seen in Figure 8.18, with the exception of the $7.5kW$ Premium Efficiency induction machine, the error variation between the measured and estimated rotor copper losses is between 3.5% from full-load towards no-load conditions. As loading of the machine varies, the variation between the NIEE-PBIL estimated rotor losses and the measured rotor losses increases towards full load

from both loading directions. This could be explained by the winding resistance-temperature ratio could be inaccurate and in reality the stator thermal coefficient could be lower thus at higher load points the effect of rotor resistance decreases as illustrated in Figure 8.9.

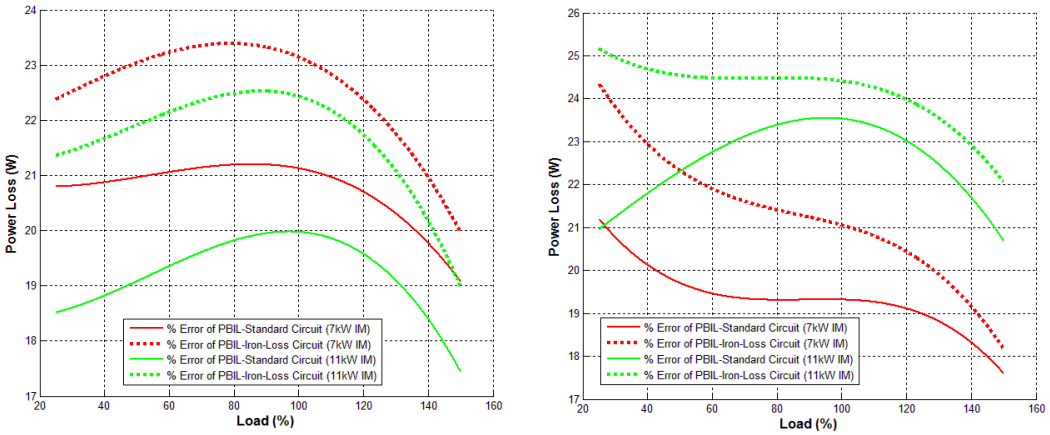

(a) Standard Efficiency IMs (b) Premium Efficiency IMs

Figure 8.18: Error of Measured against Estimated Rotor Copper Losses

Stray Load Losses

As with the aforementioned losses, the effect of repeated PBIL runs on stray load losses is determined and shown in Figure 8.19. As shown, the stray load loss estimate is consistent throughout repeated NIEE-PBIL algorithm runs regardless of the circuit implementation used.

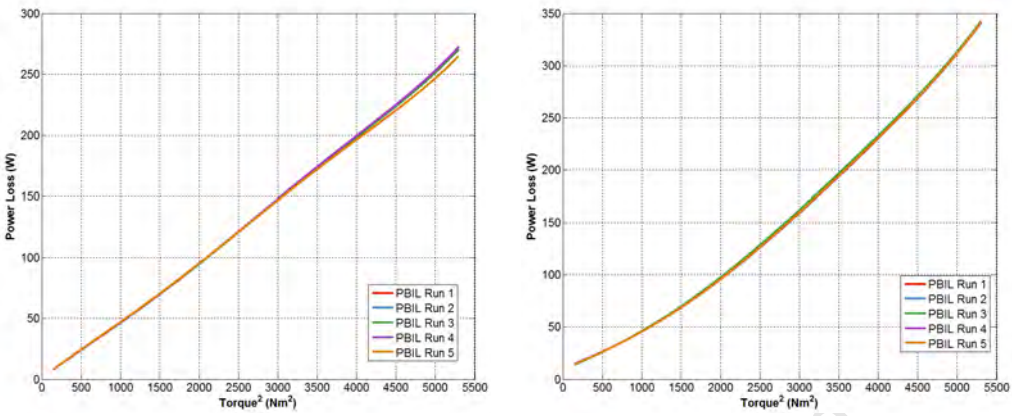

(a) Standard Circuit (b) Iron-Loss Circuit

Figure 8.19: Effect of NIEE-PBIL Repeatability Run on Stray Load Losses in the 7.5kW Standard Efficiency IM

When considering the measured and estimated stray load losses (as shown in Figure 8.20), and upon reviewing the stray load loss estimates between the NIEE-PBIL methods, there appears to be no correlation between the NIEE-PBIL method and the IEEE and IEC methods when comparing the various machines tested. All the other losses uniquely compare across machines, i.e.: NIEE-PBIL stator copper losses were overestimated, rotor copper losses were equal/underestimated, no-load losses were underestimated).

The difference in trends and estimates between the NIEE-PBIL implementations are caused by the introduction of a slip dependent rotor stray load loss resistor in the Iron-Loss NIEE-PBIL implementation. This results in an non-linear increase in the stray load loss estimate with respect to the square of the load torque. Thus, the Standard circuit PBIL implementation gives a lower loss estimate and accounts for stray load losses in a similar manner to the IEEE and IEC standards, albeit in different scale.

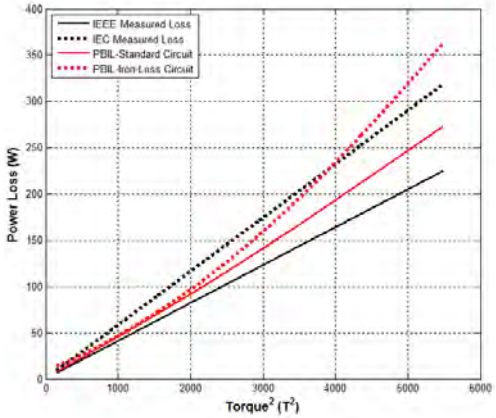

(a) 7.5kW Standard Eff. IM

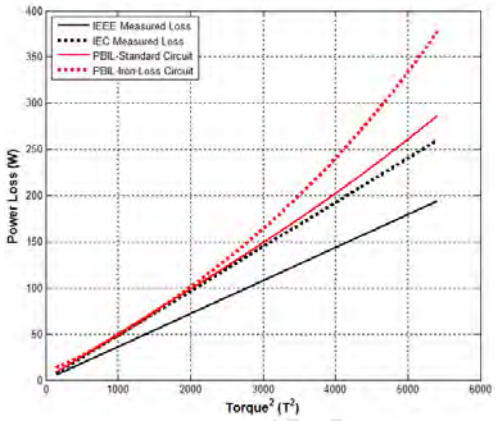

(b) 7.5kW Premium Eff. IM

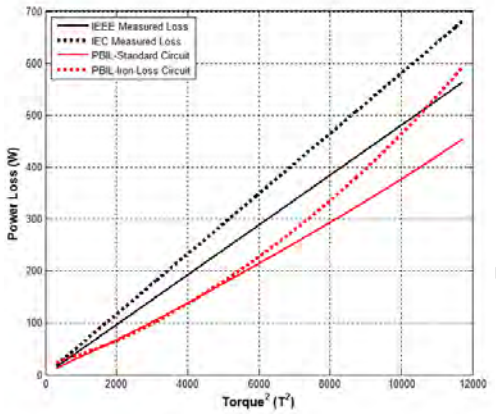

(c) 11kW Standard Eff. IM

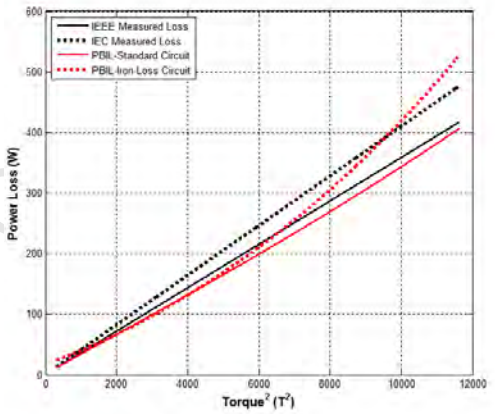

(d) 11kW Premium Eff. IM

Figure 8.20: Comparison Between Measured and Estimated Stray Load Losses

Summary

The NIEE-PBIL estimation method cannot provide a realistic estimate of the core loss due to the variations in estimating the core loss resistor. However, based on the deviation of efficiency estimated between PBIL runs, the NIEE-PBIL algorithm solves for parameters co-dependently where incorrect core loss solutions are compensated for when determining the remaining parameters.

The core losses are the only losses affected by repeated NIEE-PBIL runs and the

variations between core losses are constant (as seen in Figure 8.12). Therefore, as shown in Figure 8.21, the largest efficiency variations caused by inconsistent core loss estimates occur in the lower loading ranges of an induction machine.

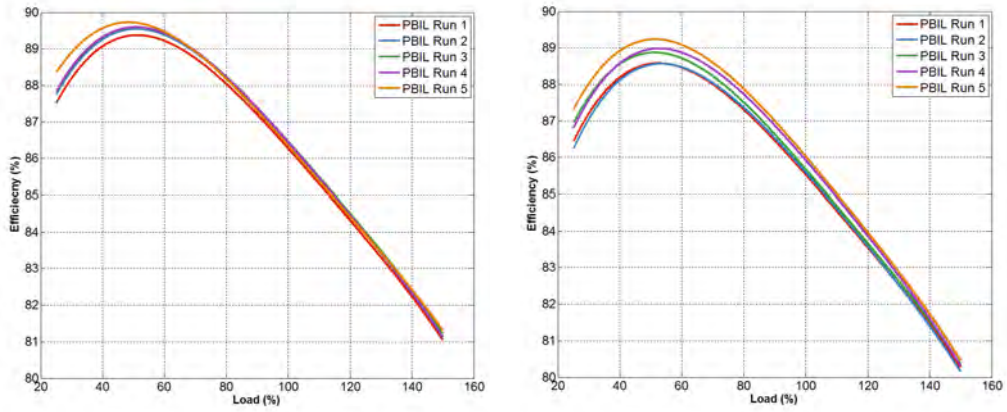

(a) Standard Circuit (b) Iron-Loss Circuit

Figure 8.21: Effect of NIEE-PBIL Repeatability Efficiency in the $7.5kW$ Standard Efficiency IM

However, referring to Figure 8.21, it is shown that at highest core loss deviation impact point (at 25% load), the NIEE-PBIL algorithm has an efficiency deviation of $\pm 0.25\%$ and $\pm 0.5\%$ (when considering the range of the deviations) for the Standard and Iron-Loss circuit implementations respectively .

Therefore, if the variation between efficiency estimates for each NIEE-PBIL run are regarded as insignificant when compared to the variation in the solved value of the core loss resistor, it can be concluded that the entire set of PBIL parameters are codependent where deviations in the **implied** temperature estimation of the no-load loss parameters will lead to inconsistent iron loss resistor values. A similar phenomenon of inconsistently deducing core loss resistor values was recognized in [42]; whereby [42] explained the inconsistency as a result of the relatively small impact that core loss current has on input/stator current.

Thus, considering the results presented, the NIEE-PBIL algorithm offers a viable, non-intrusive alternative for estimating the efficiency of an induction motor to a high degree of accuracy when compared to the IEEE 112-B and IEC

60034-2-1 standards. This is true more-so when selectively referring to the Iron-Loss implementation at lower machine load conditions and the Standard Circuit implementation at higher machine load conditions.

8.3.3 Algorithm Sensitivity to NIEE-PBIL Model Assumptions

In order to reduce the number of equivalent circuit parameters that are required to be solved by the NIEE-PBIL algorithm, simplifying assumptions were made with regards to an induction machines performance as described in Chapter 5.2. However, these assumptions may not hold true for an induction machine as some of the generalizations, such as the percentage of losses attributed to friction and windage are based on empirical data [18]. Therefore, the effect of these assumptions on efficiency estimation are investigated in this section. The assumptions investigated include the impact of the stator-to-rotor leakage reactance ratio, the effect of percentage of rated power assigned to stray-load loss as well as the percentage of rated input power relating to friction and windage losses.

Effect of X_s/X_r Ratio

Based on the recommendations of the IEEE 112-Std, the ratio of the stator to rotor reactance ratio is determined by the design class of the machine (found on the machine's nameplate data). Whilst it is simple to incorporate this ratio in the Standard Equivalent circuit implementation of the NIEE-PBIL, due to the relationship in defining the stray load loss resistors in the Iron-Loss NIEE-PBIL implementation (from Equation 5.11), varying the X_s/X_r ratio would affect stray load loss estimates. Thus, the effect of various leakage reactance ratios are only investigated in the Standard Equivalent circuit method as see in Figure 8.22.

As can be seen from Figure 8.22, the impact of varying the leakage reactance ratios is negligible when considering the variations in repeatedly running the

NIEE-PBIL algorithm as mentioned and illustrated in Table 8.7.

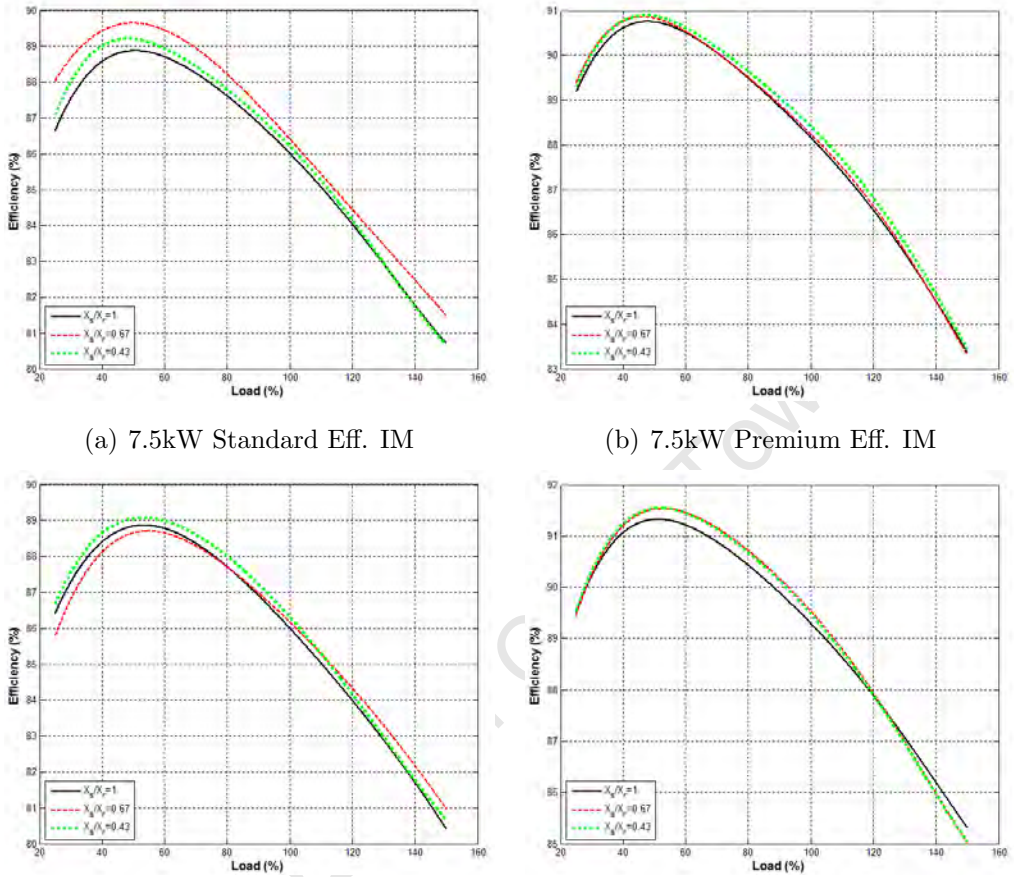

(a) 7.5kW Standard Eff. IM

(b) 7.5kW Premium Eff. IM

(c) 11kW Standard Eff. IM

(d) 11kW Premium Eff. IM

Figure 8.22: Efficiency Estimate Sensitivity to Leakage Reactance Ratio

Effect of Stray-Load Loss Assignment

Based on the design class of an induction machine, the IEEE 112 standard recommends a percentage value of the rated output power be attributed to stray load losses. Referring to Figure 8.23, it can be seen that varying recommended percentage of stray load loss by ±25% (in this instance 1.8% ± 0.45% for all machines) yields no discernible impact on the Standard Equivalent Circuit implementation of the NIEE-PBIL efficiency estimate (except in the case of the $11kW$ premium efficiency motor). However, the

Iron-Loss equivalent circuit implementation is affected by changes in the stray load loss designation especially at lower machine load points where the efficiency estimate varies by ±1%. This may be due to the nature in which the Iron-Loss equivalent circuit accounts for stray load losses in the stator side of the circuit as well as the rotor side (unlike the Standard Equivalent circuit implementation which only accounts for stray load losses on the rotor side). Additionally, the stray load losses accounted for on the rotor side are slip dependent, thus it can be concluded that at lower load points (or higher speed points) the efficiency estimate is sensitive to variations in stray load loss assignment (if a variation of ±1% is considered significant).

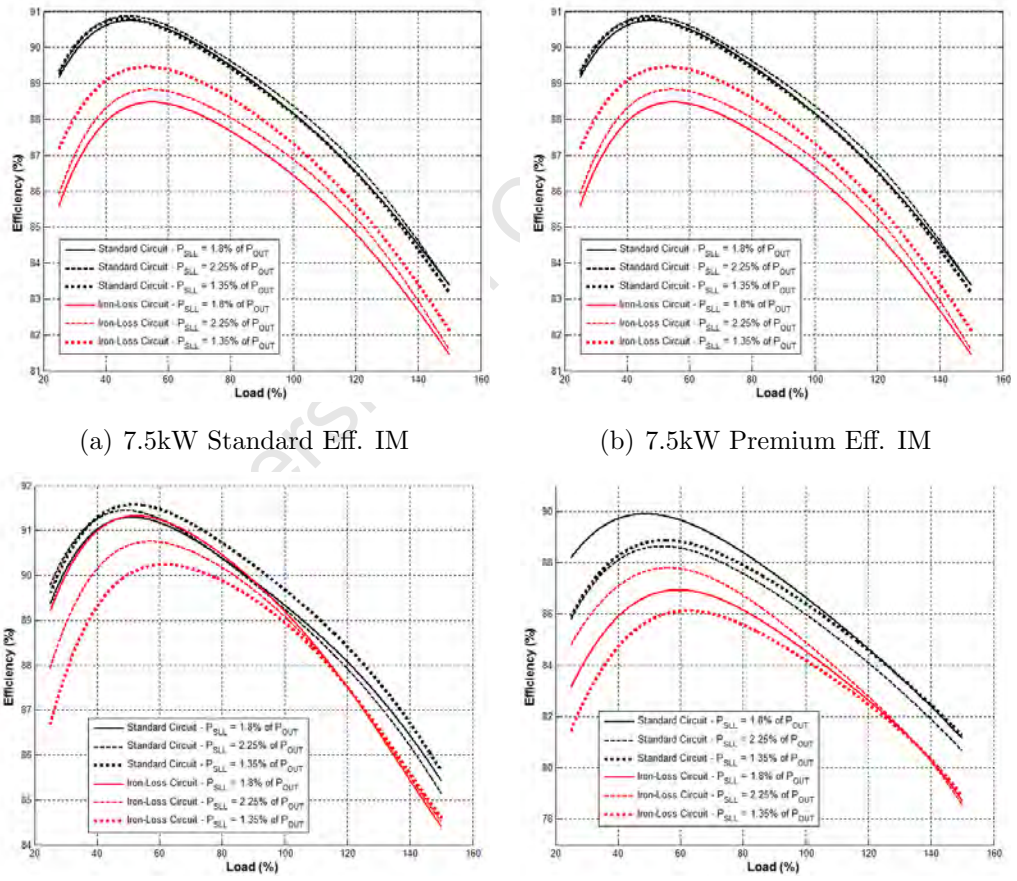

(a) 7.5kW Standard Eff. IM

(b) 7.5kW Premium Eff. IM

(c) 11kW Standard Eff. IM

(d) 11kW Premium Eff. IM

Figure 8.23: Efficiency Estimate Sensitivity to Variations in Stray Load Loss Values

Effect of Friction and Windage Loss Assignment

When considering a variation in the recommended friction and windage loss value by $\pm 25\%$ (in this instance $1.2\% \pm 0.3\%$ for all machines), there is no discernible pattern in the variation of the efficiency estimate (as seen in Figure 8.24). The largest variation between efficiency estimates is $\pm 1\%$ seen in the $7.5kW$ premium efficiency induction machine at lower load points. This may be explained by the nature in which the friction and windage losses are accounted for where, recalling Equation 5.15, the losses are proportional to the square of speed of the induction machine.

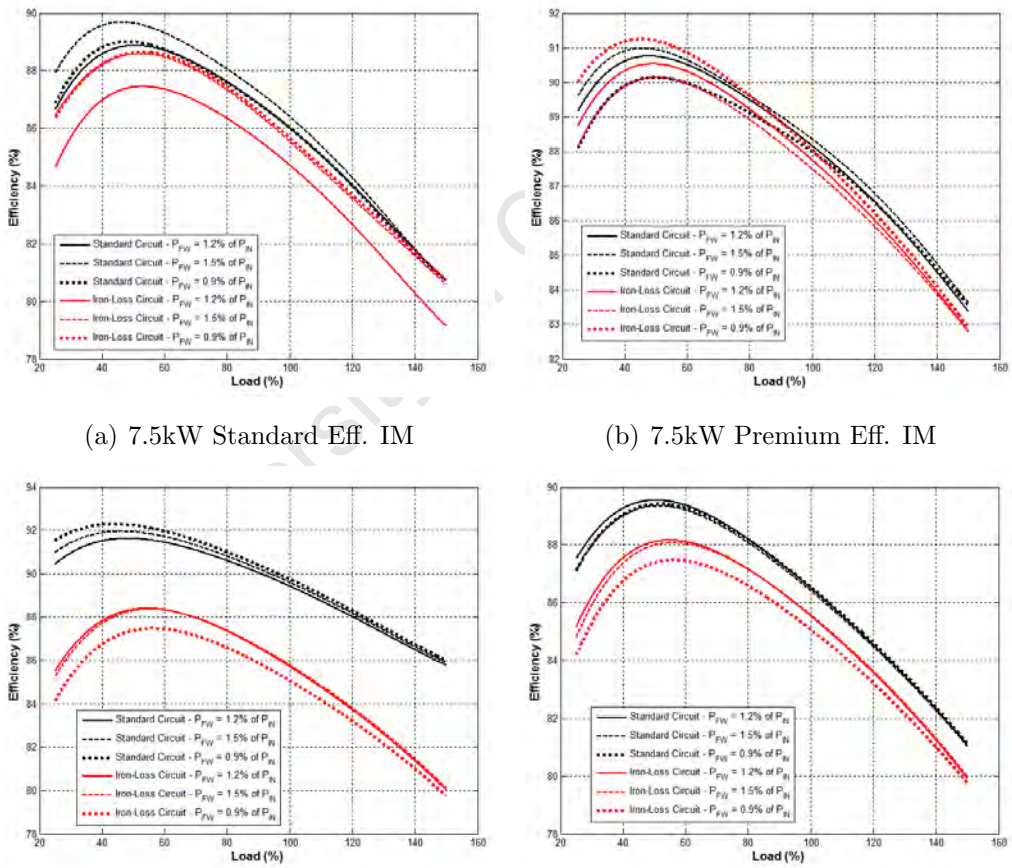

(a) 7.5kW Standard Eff. IM

(b) 7.5kW Premium Eff. IM

(c) 11kW Standard Eff. IM

(d) 11kW Premium Eff. IM

Figure 8.24: Efficiency Estimate Sensitivity to Variations in Friction and Windage Loss Values

Chapter 9

PWM-VSI Supplied IM Efficiency Estimation

Shown in Chapter 8, the greatest absolute error deviation between the Iron-Loss circuit implementation of the NIEE-PBIL algorithm and the IEEE and IEEE standards is 2.59%, the proposed PBIL method is a viable candidate for attempting to estimate a PWM-VSI supplied induction machine if the theoretical alterations to a harmonic equivalent circuit reflects towards an induction machine as the balanced equivalent circuit does. Given that the NIEE-PBIL method has been able to accurately determine the efficiency of an induction machine under balanced sinusoidal power supply, the technique is now applied to a PWM-VSI powered induction machine.

9.1 PWM-Modified Efficiency Estimation Methodology

The VSI used for experiments synthesizes a sine wave using a PWM voltage signal for each phase. In the tests conducted, the drive was setup to ensure that the fundamental frequency of the PWM signal generated was $50Hz$ whereby the switching frequency of the PWM wave could be altered manually. Two tests were conducted on a $7.5kW$ Standard efficiency induction machine at switching frequencies of $1250Hz$ and $3500Hz$.

At each of the set switching frequencies the induction machine was set to operate at it's rated load under open-loop control until the measured stator temperature stabilized to a variation of less than $1°C$ over 30 minutes. The machine load was then temporarily varied to 4 other load points during which instantaneous voltage and current readings were taken. In the absence of a final draft of the IEC 60034-2-3 standard, the direct method is used as a benchmark for evaluating the efficiency estimate from the NIEE-PBIL technique. Thus, in addition to input power measurements, shaft torque and speed measurements were taken at each load point.

9.2 Harmonic Power Analysis

The power analyzer utilized in experiments returns instantaneous voltage and current waveforms sampled at $16kHz$ and the time required for speed estimation is 5 seconds. Therefore, the minimum time required to assess the efficiency of an induction machine under the proposed algorithm is 25 seconds for temporal load tests (5 seconds each for 5 different load point measurements).

As the harmonic components of voltage and current are required in the fitness functions defined in Chapter 5.3, the individual harmonic components need to be determined as accurately as possible. In order to assess the accuracy of extracting the values of each harmonic component, the measured input power is used as a benchmark where the total input power is compared against the input power calculated by means of the harmonic voltage and current components. This is shown mathematically for a 3-phase system in Equation 9.1.

$$P_{in} = \sum_{h=1} \left(|\vec{V}_{A,h}||\vec{I}_{A,h}| \cos(\angle\vec{V}_{A,h} - \angle\vec{I}_{A,h}) \right) + \sum_{h=1} \left(|\vec{V}_{B,h}||\vec{I}_{B,h}| \cos(\angle\vec{V}_{B,h} - \angle\vec{I}_{B,h}) \right) + \sum_{h=1} \left(|\vec{V}_{C,h}||\vec{I}_{C,h}| \cos(\angle\vec{V}_{C,h} - \angle\vec{I}_{C,h}) \right) \quad (9.1)$$

Using all three phases in the estimation algorithm would greatly increase the algorithms complexity as each phase current would have to be optimized. Therefore, as the PWM-VSI and the induction machine are both assumed to be balanced, the 3-phase input power can be defined in terms of a single phase voltage and current as shown in Equation 9.2. As a precaution against instrumentation error the single phase voltage and current is determined from the averages of the three measured voltage and current phases for each appropriate harmonic order.

$$P_{in} = \sum_{h=1} \left(3|\vec{V}_{A,h}||\vec{I}_{A,h}| \cos(\angle\vec{V}_{A,h} - \angle\vec{I}_{A,h}) \right) \quad (9.2)$$

where:

$$\left.\begin{array}{l}\vec{V}_{P,h} = \frac{\vec{V}_{A,h}+\vec{V}_{B,h}+\vec{V}_{C,h}}{3} \\ \vec{I}_{P,h} = \frac{\vec{I}_{A,h}+\vec{I}_{B,h}+\vec{I}_{C,h}}{3}\end{array}\right\} for\ h = 1, 5, 7, 11, 13, ... \tag{9.3}$$

As stated previously, the voltages and currents are sampled at a frequency of $16kHz$ or $32kHz$ for a period of 0.1 seconds. This would lead to a frequency spectrum with a $10Hz$ resolution for each sampled wave. To improve the frequency resolution and accuracy in determining the harmonic components, zero-padding and a peak detection algorithm is applied to data as shown in Appendix A.2 where the fundamental signal processing theory is identical to that discussed in the speed estimation technique outlined in Chapter 4. The fundamental harmonic is found using a global maximum search and parabolic interpolation. The magnitude and angles of the fundamental and other harmonic orders are found using **MATLAB**'s inbuilt *spline interpolation* function.

The effect of extracting harmonic data from the voltages and currents is illustrated in Figure 9.1 for an induction machine powered by a PWM-VSI at $1250Hz$ switching frequency at rated load. The associated power factor (and thus phase angle) associated with each of the extracted relevant harmonics is shown Figure 9.2. As seen in Figure 9.2, due to the sampling frequency being limited to $16kHz$, the 151st harmonic ($7550Hz$) is the highest relevant harmonic order that can be analyzed due to the Nyquist sampling frequency theorem.

The effectiveness of the results obtained from harmonic extraction method which are then implemented in Equations 9.2 and 9.3 to determine input power can be seen in Figure 9.3. From Figure 9.3 where the machine is powered by PWM-VSI, the measured input power differs from the calculated harmonic input power by less than 0.5% for various machine load conditions. The reason for an accurate power estimation is that despite sampling signals at only $16kHz$, in a PWM-VSI, the current induced in an machine closely matches a pure sine wave, thus higher order harmonics have negligible magnitudes (and thus power associated

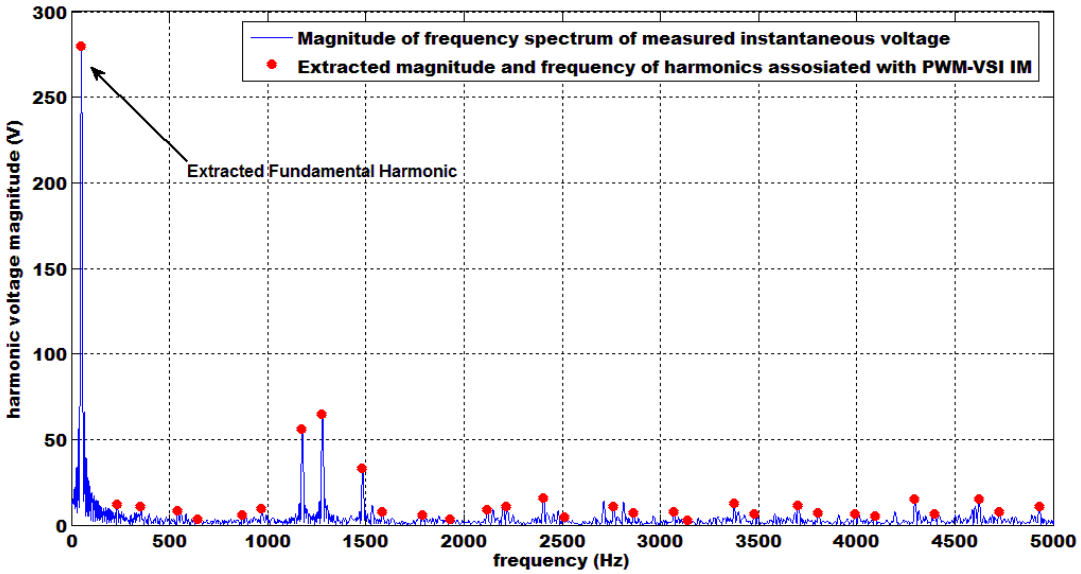

Figure 9.1: Extracting the Harmonic Components from a Sampled PWM-VSI Voltage Signal

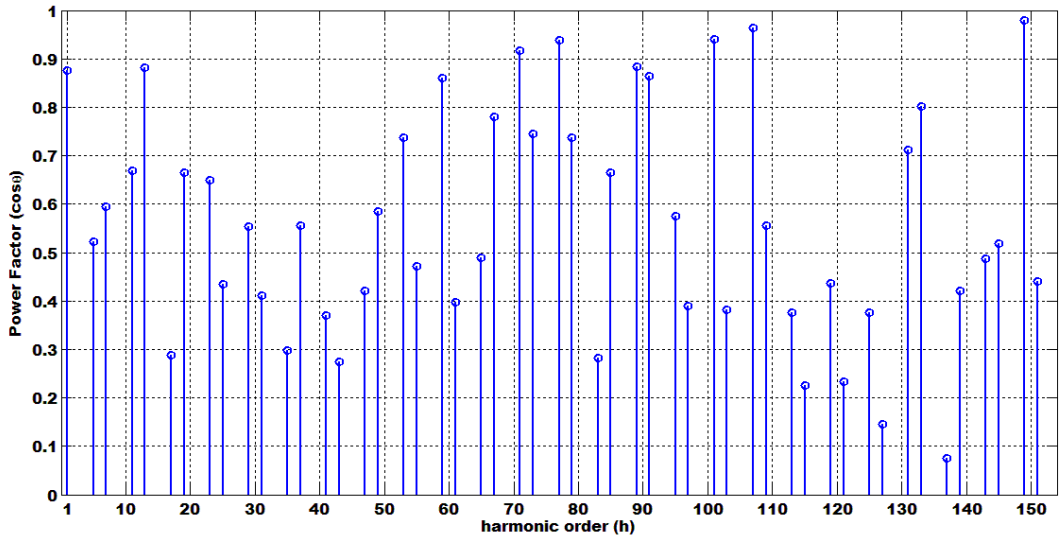

Figure 9.2: Power Factor of Harmonics of PWM-VSI Driven 7.5kW IM Operating at Rated Load

at higher magnitudes decreases).

As seen from Figures 9.1 and 9.2, the magnitudes and power factors of the

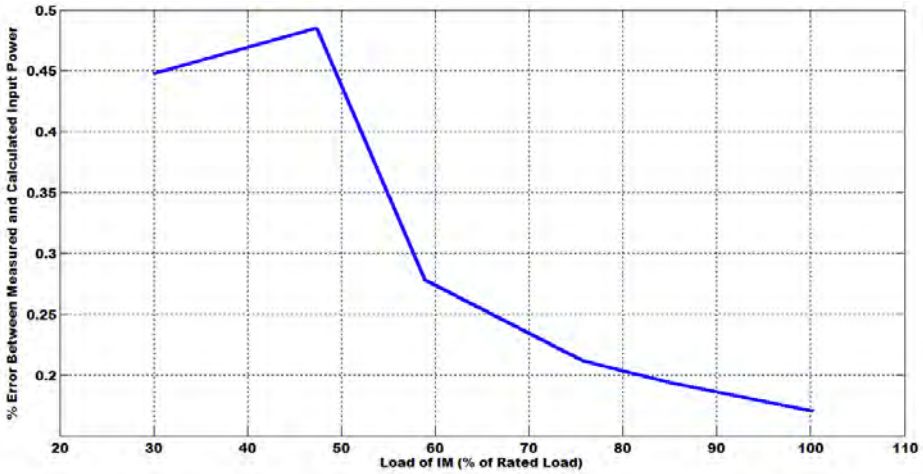

Figure 9.3: Error Between Measured and Harmonic Derived Input Power @ $1250Hz$ Switching Frequency

harmonics do not follow a set of rules based on the harmonic orders (as inferred from Figures 3.4, 3.5 and [5]). Taking this into consideration along with [7] and [31] stating that the harmonic adjustments for the iron-loss resistors are based on an *eddy-hysteresis* ratio (see Chapter 3.1.2), attempting to solve for the equivalent circuit parameters in addition to an eddy-hysteresis ratio would not yield meaningful results. Additionally, the problem is exasperated given the fact that the NIEE-PBIL algorithm cannot determine individual parameters in a sinusoidal power induction machine (as shown in the previous chapter).

As most of the power loss and power transfer in an induction machine is associated with the fundamental harmonic, the equivalent circuit parameters are solved using the fundamental harmonic with the exception of the temperature estimation algorithm (where the influence of harmonics is intrinsic). Once the fundamental equivalent circuit has been solved, the harmonic circuit model can be used for efficiency estimation (where the harmonic stray load and core loss components a defined in Chapter 5.2 (Equations 5.5 and 5.7).

9.3 Efficiency Estimation Test Results

Based on a methodology similar to the IEEE and IEC standards, the tests carried out on a PWM-VSI supplied induction machine are based around the machine operating at rated load. Once temperature has stabilized, measurements were taken at decreasing load points. The experimental results for a $7.5kW$ induction machine under two different switching frequency settings are shown in Table 9.1. The motivation behind analyzing two different switching frequencies is to investigate the impact of various harmonic losses on the proposed efficiency estimation algorithm as the fundamental frequency (and thus fundamental losses) of both PWM-VSI tests are equal. Any differences noted between the efficiency estimates ensure that harmonics are taken into consideration (and not neglected) when deducing a machines efficiency.

Table 9.1: Test Data of Induction Machines Under PWM-VSI Supply

(a) 7.5kW Standard Efficiency IM @ 1250Hz Switching Frequency

% of rated load	$V_{s,fundamental}$ (V)	$I_{s,fundamental}$ (A)	P_{in} (W)	$Freq_{fundamental}$ (Hz)	$Speed$ (rpm)
97.63	391.41	14.39	8687.50	51.16	1490.13
82.62	390.15	12.68	7217.32	51.07	1492.67
57.49	407.27	9.83	5176.06	50.84	1508.85
38.62	410.00	8.38	3604.87	50.78	1513.28
28.72	411.99	7.83	2792.67	50.64	1513.25

(b) 7.5kW Standard Efficiency IM @ 3500Hz Switching Frequency

% of rated load	$V_{s,fundamental}$ (V)	$I_{s,fundamental}$ (A)	P_{in} (W)	$Freq_{fundamental}$ (Hz)	$Speed$ (rpm)
98.45	375.32	14.98	8793.86	51.17	1483.79
87.50	374.94	13.33	7783.07	51.11	1490.35
66.20	369.10	10.32	5784.06	51.06	1498.57
58.03	368.49	9.38	5152.84	50.97	1501.30
28.45	375.42	6.15	2799.69	50.77	1512.20

Using the test data from Table 9.1, the results attained from each of the implemented NIEE-PBIL methods are compared against the efficiency determined from the *Direct-Method* as discussed in Chapter 6.1 (and earlier in this chapter). The results are shown in Figures 9.4 and 9.5, where the efficiency at the load points have been fitted to a 5-order polynomial curve. Additionally, the results are summarized in Tables 9.2 and 9.3.

Referring to Figures 9.4 and 9.5, it is shown that regardless of the switching frequency applied or the NIEE-PBIL circuit implementation used, the efficiency estimate at low load conditions is highly inaccurate when compared to the direct method. Referring to the Iron-Loss circuit implementation, the error compared to the Direct-Method at 30% load is 8% and 5% for the $1250Hz$ and $3500Hz$ switching frequencies respectively. Considering that a similar phenomenon occurred during sinusoidal balanced power supply testing, the error in efficiency estimates at low load conditions can be attributed to the NIEE-PBIL's focusing on the fundamental harmonic to solve for parameters. Additionally, the Direct Method does not account for temperature compensation whereas the NIEE-PBIL method does further contributing to higher discrepancies at low load points.

Due to the nature of the algorithm compensating for specific losses (as described in 8.3.2), a loss analysis cannot be performed to definitively explain the error in the efficiency estimate at lower load points due to inaccurate core loss resistance estimates.

Considering that the average loading conditions for $7.5kW$ induction machines is 57% [56], Tables 9.2 and 9.3 focus on summarizing the efficiency estimate and associated errors between 40% and rated load.

From the results it can be seen that the NIEE-PBIL algorithm closely estimates the efficiency of a PWM-VSI supplied induction machine at higher loading points with an error of 2.17% and 1.92% when referring to the Iron-Loss circuit implementation at rated load for $1250Hz$ and $3500Hz$ switching frequencies respectively.

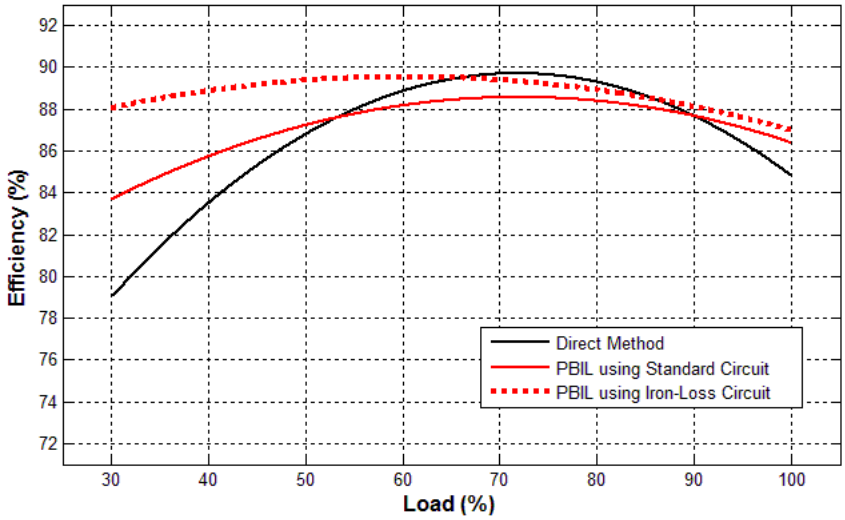

Figure 9.4: Efficiency Estimate of PWM-VSI Supplied 7.5kW IM @ 1250Hz Switching Frequency

Table 9.2: Efficiency Estimate of PWM-VSI Supplied 7.5kW IM @ 1250Hz Switching Frequency

	Direct Method	**PBIL - Standard Crct.**		**PBIL - Iron-Loss Crct.**	
% of rated load	Efficiency (%)	Efficiency (%)	Error (%)	Efficiency (%)	Error (%)
100.00	84.83	86.39	-1.56	87.00	-2.17
85.00	88.69	88.10	0.59	88.56	0.13
70.00	89.68	88.56	1.12	89.39	0.29
55.00	87.97	87.76	0.21	89.50	-1.53
40.00	83.50	86.54	-3.04	89.15	-5.65

From Figures 9.4-9.5 and Tables 9.2-9.3; when analyzing only the Standard-Circuit implementation of the NIEE-PBIL algorithm, the efficiency estimate of an induction machine with a PWM supply is accurate (to within 1.56% error) for loads higher than 50% of rated load regardless of the switching frequency.

Comparing the trend of the results to those found during sinusoidal power supply testing, the efficiency estimates from the NIEE-PBIL circuit implementations do not correspond to results found in the PWM-VSI tests. In the NIEE-PBIL sinusoidal supply efficiency estimate, the Standard Circuit

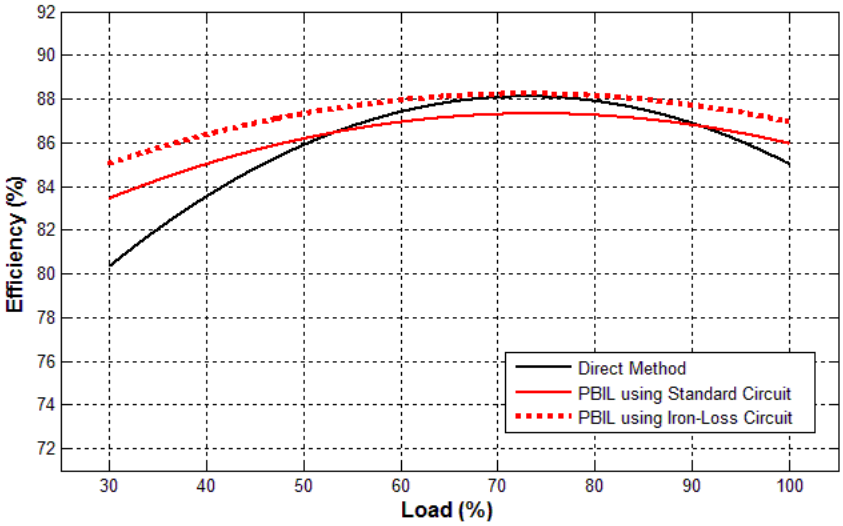

Figure 9.5: Efficiency Estimate of PWM-VSI Supplied 7.5kW IM @ 3500Hz Switching Frequency

Table 9.3: Efficiency Estimate of PWM-VSI Supplied 7.5kW IM @ 3500Hz Switching Frequency

	Direct Method	**PBIL - Standard Crct.**		**PBIL - Iron-Loss Crct.**	
% of rated load	Efficiency (%)	Efficiency (%)	Error (%)	Efficiency (%)	Error (%)
100.00	85.03	85.95	-0.92	86.95	-1.92
85.00	87.49	87.08	0.41	87.97	-0.48
70.00	88.07	87.29	0.78	88.21	-0.14
55.00	86.74	86.60	0.14	87.67	-0.93
40.00	83.52	85.00	-1.48	86.34	-2.82

implementation provides a higher efficiency estimate when compared to the Iron-Loss circuit implementation. However, as shown in Figures 9.4 and 9.5, when solving for harmonics, the Iron-Loss implementation provides a higher efficiency estimate then the Standard Circuit implementation. Therefore, by comparing the circuit differences, if the assumption that fundamental harmonic losses are treated in a similar manner to sinusoidal losses, it can be concluded that the Iron-Loss implementation underestimates core and/or stray-load losses when compared to the standard circuit implementation. This may be due to the effect of the assumptions made on the impact of harmonics on the

stray-load and core loss resistors. In the Standard Circuit implementation core loss is assumed not to be affected by harmonics whereas they are in the Iron-Loss circuit implementation. Alternatively, in the Iron-Loss implementation, stator stray-load losses are taken into account whereas the Standard Circuit implementation only considers harmonic impact of stray-load losses on the rotor side.

Additionally, as seen in Table 9.1, the fundamental RMS harmonic voltage magnitudes differ between the two tests as well as differ from the machines rated voltage. Thus, whilst higher switching frequencies are expected to yield and increase in machine efficiency, this cannot be seen in the efficiency test results which is due to the differing voltage levels and current levels (proportional to switching frequency and fundamental voltage). As PWM fundamental voltage levels differ from the rated voltage, the sinusoidal test results attained in the previous chapter (which used rated voltages) cannot be used for meaningful comparison purposes.

The aim of testing an induction machine under various PWM-VSI switching frequencies was to ensure that harmonics are taken into consideration when determining efficiency. Comparing the results in Figures 9.4-9.5 and Tables 9.2-9.3, it is shown that both the Standard Circuit and Iron-Loss implementations differ in efficiency estimation between the two switching frequencies implemented. Whilst this may be due to the NIEE-PBIL algorithm taking harmonics into consideration, the variations may be a result of the uncontrollable differences in the fundamental supply voltage delivered by the PWM-VSI as seen in Table 9.1.

When considering the Standard Circuit PBIL efficiency errors between the two switching frequency tests (and to some degree the Iron-Loss circuit implementation), the efficiency errors for the $3500Hz$ are much lower (more accurate when compared to the direct method) than the efficiency errors associated with the $1250Hz$ test. Referring to Tables 9.2-9.3, the errors between 40% and rated load for $3500Hz$ test is in the range of $0.14 - 1.48\%$ and $0.14 - 2.82\%$ for the Standard and Iron-Loss circuit implementations

respectively whereas the same respective error ranges for the $1250Hz$ test are $0.21 - 3.04\%$ and $0.13 - 5.65\%$. This may due to the prevalent fundamental harmonic under-voltage supply (when compared to the machines rated voltage of 380V) in the $3500Hz$ switching frequency test compared to the prevalent fundamental harmonic over-voltage supply in the $1250Hz$ switching frequency test. Alternatively, the differences in efficiency estimation errors may be based on the switching frequencies themselves and their impact on the harmonic losses determined in the NIEE-PBIL.

Chapter 10

Conclusions and Recommendations

Based on analysis of the test results presented in Chapters 7-9, the following conclusions and recommendations for future work can be drawn:

10.1 Conclusions

This research proposed a non-intrusive estimation technique to determine an induction machines efficiency under sinusoidal and PWM-VSI power supplies. The main focus was based on the investigation, implementation and experimental analysis of determining efficiency through parameter identification of an induction machine's equivalent circuit parameters and thermal coefficient. The parameters were identified by applying an evolutionary intelligent algorithm to a limited set of test results attained from experiments. The solved parameters were then used to estimate an induction machines efficiency over a range of loading conditions.

Efficiency tests were conducted on several machines under various power supply conditions based on the IEEE 112-B, IEC 60034-2-1 and Direct methods. The efficiency measurements were then compared to the proposed efficiency estimation algorithm.

Based on the analysis of results from the experiments, the following conclusions can are made.

10.1.1 Speed Estimation

Vibration analysis combined with signal analysis methods provide an accurate rotor speed estimate within an error of $1rpm$. This error is the same as that of the instrumentation error used to benchmark speed and is obtained regardless of the type of power supply used (balanced sinusoidal and PWM-VSI).

Given that the speed estimation method proposed is the most time consuming data acquisition procedure implemented in the NIEE-PBIL technique, a data acquisition time of 5 seconds per load test offers the lowest possible level of

intrusiveness. This can be concluded when considering the overall effect of temporal load changes on machine productivity and the test requirements in the efficiency estimation process.

10.1.2 Sinusoidal Supply Efficiency Estimation

The proposed Standard Circuit NIEE-PBIL determines a machines efficiency with an accuracy of $0.02 - 0.44\%$ and $0.07 - 1.04\%$ at high loading conditions ($125 - 150\%$) when compared to the IEEE 112-B and IEC 60034-2-1 standards respectively and $1.27 - 5.85\%$ and $0.04 - 5.37\%$ at low loading conditions ($25 - 50\%$). Alternatively, the proposed Iron-Loss Circuit NIEE-PBIL determines a machines efficiency with an accuracy of $0.18 - 2.12\%$ and $0.09 - 1.64\%$ at low loading conditions ($25 - 50\%$) when compared to the IEEE 112-B and IEC 60034-2-1 standards respectively and $1.37 - 2.17\%$ and $1.22 - 2.59\%$ at high loading conditions ($125 - 150\%$). Thus, the Standard Circuit implementation should be used at higher loading conditions and the Iron-Loss implementation at lower loading conditions.

Due to the inconsistencies in attaining core loss resistor values, the NIEE-PBIL incorrectly assesses core losses. However, whilst, all other estimated losses are consistently assessed, and in the case of copper losses, matching the trends of measured losses, the estimated losses are nevertheless incorrect/inaccurate when compared to the measured losses. The deviations caused by inconsistent core loss estimates results in a deviation of $\pm 0.25\%$ and $\pm 0.5\%$ in the efficiency estimate of the Standard and Iron-Loss circuit implementations respectively at lower machine loading conditions. However, as these core loss deviations have a constant offset, the efficiency estimate deviation at higher loading conditions is negligible. The inconsistencies in determining core losses are due to faults in the NIEE-PBIL's method of implicitly determining the impact of current losses (and thus temperature) in the machines core.

The NIEE-PBIL algorithm is incapable of identifying a single unique set of equivalent circuit parameters despite accurately (depending on the circuit

implementation and load rage considered) determining the sum of all losses incurred in an induction motor. If an efficiency estimate deviation of 1% is considered negligible, the proposed NIEE-PBIL technique is immune to incorrect assumptions on stray-load loss and friction and windage loss assignments. Additionally, the NIEE-PBIL algorithm is also immune to stator and rotor leakage reactance ratios. Therefore, it can be concluded that parameter identification in the NIEE-PBIL algorithm is solved co-dependently where an incorrect loss assessment in the core segment of the machine is compensated for in another segment or segments.

Given that the NIEE-PBIL technique inaccurately determines independent losses that are incurred in an induction machine whilst accurately determining efficiency, it can be concluded that the total losses estimated by the technique is accurate (again, ignoring 1% deviation at lower loading conditions). Therefore, as rotor and stator copper losses are a function of the temperature, it can also be concluded that inaccurately identifying these losses whilst consistently determining k_{TH} with a low standard deviation means that the temperature estimated by the algorithm at each load point is also incorrect/inconsistent. Thus, despite the high degree of machine efficiency estimation, the NIEE-PBIL cannot be used for machine load temperature estimation purposes.

The efficiency estimate error range between 50% and 75% of rated load when considering all machines tested is $0.53 - 2.98\%$ $\pm 0.25\%$ and $0.04 - 2.57\%$ $\pm 0.25\%$ when referring to the Standard Circuit implementation compared against the IEEE 112-B and IEC 60034-2-1 methods respectively. Similarly, the efficiency estimate error range between 50% and 75% of rated load when considering all machines tested is $0.13 - 0.70\%$ $\pm 0.5\%$ and $0.11 - 1.73\%$ $\pm 0.5\%$ when referring to the Iron-Loss Circuit implementation compared against the IEEE 112-B and IEC 60034-2-1 methods respectively. Therefore, it can be concluded that, when considering most induction machines operate at 57% of their rated load [56], regardless of the international standard being referred to (IEEE or IEC), the Iron-Loss circuit implementation provides the highest accuracy of the two NIEE-PBIL circuit implementations and thus should be referred to when non-intrusively estimating efficiency under sinusoidal

conditions.

10.1.3 PWM-VSI Supply Efficiency Estimation

With regards to PWM-VSI testing, the proposed algorithm accurately estimates a machines efficiency by $0.14 - 3.04\%$ and $0.13 - 5.65\%$ for the Standard and Iron-Loss NIEE-PBIL implementations respectively.

From the sinusoidal and PWM-VSI trends in the relationship between the efficiency estimates of the Standard circuit implementation compared to the Iron-Loss circuit implementation, it can be concluded that harmonics play a influential role in VSD supply loss determination. However, in the absence of an in-depth loss analysis into the harmonic efficiency estimates (due to the nature of the Direct Method and unrated fundamental voltages implemented) the nature of the impact of harmonics is indiscernible.

In the absence of understanding the effects of how over and under voltage supply affect the NIEE-PBIL algorithm, any conclusions drawn on the impact of harmonic over and under voltage supply would be premature. Additionally, due to the control scheme implemented in the PVM-VSI tests, speed ranges over loading conditions differed from those performed in the sinusoidal power supply experiments further alienating any comparison between the two.

The efficiency estimate error range between 55% and 70% of rated load when considering the two tested switching frequencies is $0.14 - 1.12\%$ and $0.14 - 1.53\%$ when referring to the Standard and Iron-Loss circuit implementations respectively. Thus, when considering most induction machines operate at 57% of their rated load [56] and taking the results of sinusoidal tests into account, it can be concluded that the Iron-Loss circuit implementation of the NIEE-PBIL algorithm be used when estimating induction machine efficiency under the two different power supplies investigated.

10.1.4 Evolutionary Algorithm Assessment

During the course of repeated tests and PBIL runs, the average generation run time of the NIEE-PBIL algorithm was measured and is 83.56 and 101.07 for the Standard and Iron-Loss implementations respectively. If 2 parallel PBIL probability vectors with 10 independent populations each is taken into consideration (as was implemented in the NIEE-PBIL), the average run-time of the algorithm in linear generational processing time would be 1671.2 and 2021.4 generations for the Standard and Iron-Loss implementations respectively. Compared to the method described in [42] which runs for 10,000 generations, the PBIL proves to be a more robust optimization tool for solving equivalent circuit parameters of an induction machine in terms of computational power.

10.2 Recommendations

Based on the above conclusions, the following recommendations can be made.

10.2.1 Speed Estimation

The disadvantage of the proposed speed estimation method is the requirement of additional equipment in attaining vibration data when compared to methods of determining speed estimation by current signature analysis. As current measurement is required in the efficiency estimation process, it is recommended that speed estimation by current signature analysis be investigated in conjunction with the effect of increasing temporal load change times and decreasing speed estimation accuracy. Thus, if a threshold limit is found where increased temperature deviation caused by increased load time changes does not affect the efficiency estimation accuracy; and, a decrease in speed estimation accuracy does not affect efficiency estimation accuracy, current signature analysis may be a cost-effective alternative to vibration analysis.

10.2.2 NIEE-PBIL Technique

Based on analysis of results on sinusoidal power supplied induction machines, further improvements can be made to the proposed NIEE-PBIL algorithm. As the Standard Circuit implementation has a better efficiency estimate at higher load points and the Iron-Loss implementation has a better efficiency estimate at lower load points, a combination of the two implementations should be formed. This may be achieved by analyzing the input current and measured slip in collaboration with the rated input current and slip given in the machines-nameplate data to give an estimate on the machines loading condition. This estimated value could then be used to determine the use of the Standard circuit implementation at higher load points, or alternatively, the Iron-Loss circuit implementation at lower load points.

If estimating temperature or accurately determining each of the machine parameters is required, a more suitable model/method should be implemented whereby core losses are accurately determined. This could include an extension of the NIEE-PBIL method that would extrapolate and estimate the no-load losses without a no-load test from data collected at temporal load points from the numerous temporal load tests. As mentioned above, non-intrusive slip/current methods could be used in collaboration as rough estimates of machine performance.

10.2.3 Experimental Tests

As the IEEE and IEC standards require the machines to be tested at their rated temperature, for a meaningful comparison, a similar approach was adopted in the NIEE-PBIL tests. However when considering that most induction machines operate between 57% of their rated load, the NIEE-PBIL algorithm should be tested at these load points rather than at rated to ensure that the method not only works in realistic conditions, but additionally reduces the intrusiveness of requiring the machine to be at rated load in order to determine the efficiency-load profile.

In order to comprehensively assess the efficiency estimation of PWM-VSI inductions machines, methods similar to the IEEE and IEC loss segregation should be employed (such as the draft IEC 60034-2-3). However, as the IEC 60034-2-3 requires a balanced sinusoidal supply analysis in addition to a harmonic, a voltage control scheme should be developed for the PWM-VSI drive to ensure that the sinusoidal and fundamental harmonic voltage levels are equal and thus the test results comparable.

With regards to estimating the efficiency of PWM-VSI supplied motors, the testing of numerous motors under various switching frequencies was not included and thus should be performed. Tests should also be conducted on various VSD control implementations (such as closed loop control, current source inverters) in order to increase the versatility of the proposed method. Similarly, balanced supply conditions are improbable in uncontrolled environments [19], thus test should be conducted on deformed and unbalanced supply conditions with circuit implementations suggested in [19] as well as other sources investigated. Following from this, an additional modification can be made to the method whereby the power supply is analyzed prior to parameter identification so that an appropriate model (balanced/unbalanced/PWM/...) may be used to determine a machines efficiency to the highest possible accuracy.

Additionally, discrepancies in the efficiency estimate of PWM-VSI supplied motors at lower load points may be due to the fundamental harmonic voltage being higher than the machines rated voltage level. Thus, additional tests for balanced over and under sinusoidal supply voltage conditions should be conducted. Furthermore, once the core loss estimates suggested for the sinusoidal power supply application is solved, a meaningful loss analysis may be carried out for PWM-VSI supplied induction machines.

Appendix A

Software Source Code

A.1 Parabolic Interpolation for Speed Estimation

```
function [speed] = csg_speed_estimator(data, f_sampl_rate,...
                                                    zero_pad_fact)

% CSG_SPEED_ESTIMATOR
%
% function [speed] = csg_speed_estimator(data, f_sampl_rate,...
%                                                    zero_pad_fact)
%
% Estimate IM operating speed by analyzing vibration data
%
% Output: speed - estimated rotor speed in RPM
%
% Input: data          - vibration data
%        f_sampl_rate  - sample rate of vibration data
%        zero_pad_fact - zero pad factor employed
%                        -> -1 if zero pad unwanted
%

% adjust data for DC offset
data = data - mean(data);

% adjust data for zero padding if 'zero_pad_fact' is wanted
if zero_pad_fact > -1
    pad_fact = nextpow2(length(data))+zero_pad_fact;
    pad_effect = 2^(pad_fact);
else
    pad_effect = length(data);
end

% perform Fourier transform
wave_fft = fft(data, pad_effect)/length(data);


% convert FFT to PSD scale
```

```
35 PSD_fft = 20*log10(wave_fft.*conj(wave_fft)./(2*pi));
36
37 % create frequency axis
38 freq_axis = linspace(0,f_sampl_rate,length(wave_fft));
39
40 % adjust axis for vibration harmonic boundaries
41 f_sync = 2*50/4;      % sync speed vibration frequency
42                       % for 50Hz, 4-pole IM
43
44 bin_sync = ceil(f_sync/freq_axis(2));   % find sync speed bin
45
46 freq_axis = freq_axis(1:bin_sync);   % adjust frequency boundaries
47 PSD_fft = PSD_fft(1:bin_sync);       % adjust PSD boundaries
48
49 % find peak point and adjacent point
50 [PSD1 bin1] = max(PSD_fft);
51 f1 = freq_axis(bin1);
52
53 PSD2 = PSD_fft((bin1-1));
54 f2 = freq_axis((bin1-1));
55
56 PSD3 = PSD_fft((bin1+1));
57 %f3 = freq_axis((bin1+1));
58
59 % parabolic interpolation
60 f_interp = f1 + ((f1-f2)*(PSD2-PSD3))/(2*(PSD2+PSD3-(2*PSD1)));
61
62 % return estimated speed
63 if zero_pad_fact == -2   % interpolation not wanted
64     speed=f1*60;
65 else
66     speed=f_interp*60;
67 end
68
69 end
```

A.2 Extracting Harmonic Data for Voltage/Current Wave

```
function [data] = csg_get_harmonic_data_single_wave(wave, file_st)

% get_harmonic_data_single_wave
%
%   gets harmonic data from a single wave
%
%   Inputs : single wave data,
%            file_st-> sample rate 0 for 16kHz, 1 for 32kHz
%
%   Outputs: data structure as follows
%               .fund_mag  > fundamental magnitude of FFT
%               .fund_freq > frequency of fundamental magnitude
%               .fund_angl > angle of fundamental magnitude
%               .fund_idx  > index of fundamental magnitude
%               .harm_mag  > harmonic magnitude of FFT
%               .harm_freq > frequency of harmonic magnitude
%               .harm_angle > angle of harmonic magnitude
%               .harm_idx  > index of harmonic magnitude


% sample rate: 0 for 16kHz, 1 for 32kHz
if (file_st)
    sample_rate = 32000;
    harm_order=zeros(1,100);
else
    sample_rate = 16000;
    harm_order=zeros(1,50);
end

% create harmonic index
for count = 1:(length(harm_order)/2)
    harm_order(count*2-1) = (6*count-1);
    harm_order(count*2) = 6*count+1;
end
```

```
35
36 % perform zero padding and fft
37 pad_fact = nextpow2(length(wave))+2;
38 wave_fft = fft(wave, (2^pad_fact))/length(wave);
39
40 % create frequency axis
41 freq_axis = linspace(0,sample_rate,length(wave_fft));
42
43 % adjust axis for nyquist rate
44 freq_axis = freq_axis(1:end/2);
45 wave_fft = wave_fft(1:end/2);
46
47 % find fundamental frequency, magnitude and index
48 [max_val, max_indx] = max(abs(wave_fft));
49 fund_mag = max_val;
50 fund_freq = freq_axis(max_indx);
51
52 % find nearest index for harmonic frequencies
53 m=harm_order*fund_freq;
54 [ix,ix]=min(abs(bsxfun(@minus,m,freq_axis.')));
55
56 % perform  harmonic peak search
57 bin_width_srch = floor((max_indx-1)/2);
58 for count = 1:length(harm_order)
59
60     idx = ix(count);
61     [~ max_indx2] = max(abs(wave_fft((idx-bin_width_srch):...
62         (idx+bin_width_srch))));
63
64     ix(count) = (max_indx2-1-bin_width_srch)+idx;
65
66 end
67
68 % perform parabolic interpolation
69 [peak1, peak1_indx] = max(abs(wave_fft));
70 f1 = freq_axis(peak1_indx);
71
72 peak2 = abs(wave_fft((peak1_indx-1)));
73 f2 = freq_axis((peak1_indx-1));
```

```
74
75 peak3 = abs(wave_fft((peak1_indx+1)));
76
77 % interpolte with spline algorithm for harmonics
78 f_interp=f1+((f1-f2)*(peak2-peak3))/(2*(peak2+peak3-(2*peak1)));
79 m=harm_order*f_interp;
80
81 % assign harmonic values of waveform
82 data.harm_mag = interp1(freq_axis, abs(wave_fft), m, 'spline');
83 data.harm_freq = m;
84 data.harm_angl = angle(interp1(freq_axis,wave_fft,m,'spline'))...
85     *180/pi;
86
87 % assign fundamental values of waveform
88 data.fund_mag = fund_mag;
89 data.fund_freq = fund_freq;
90 data.fund_angl = (angle(wave_fft(max_indx))*180)/pi;
91 data.fund_idx = max_indx;
92
93 % assign harmonic order values of waveform
94 data.harm2_mag = abs(wave_fft(ix));
95 data.harm2_freq = freq_axis(ix);
96 data.harm2_angl = angle(wave_fft(ix))*180/pi;
97 data.harm2_idx = ix;
98
99 end
```

Appendix B

Figures and Tables

B.1 Speed Estimation Test Results

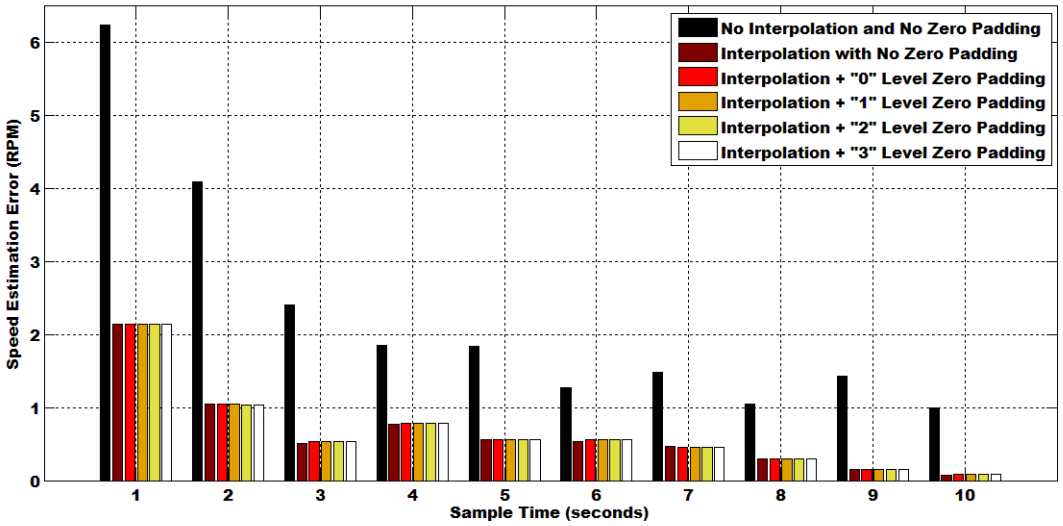

Figure B.1: 7.5 kW IM Speed Estimation Error Analysis @ 100% of Rated Load

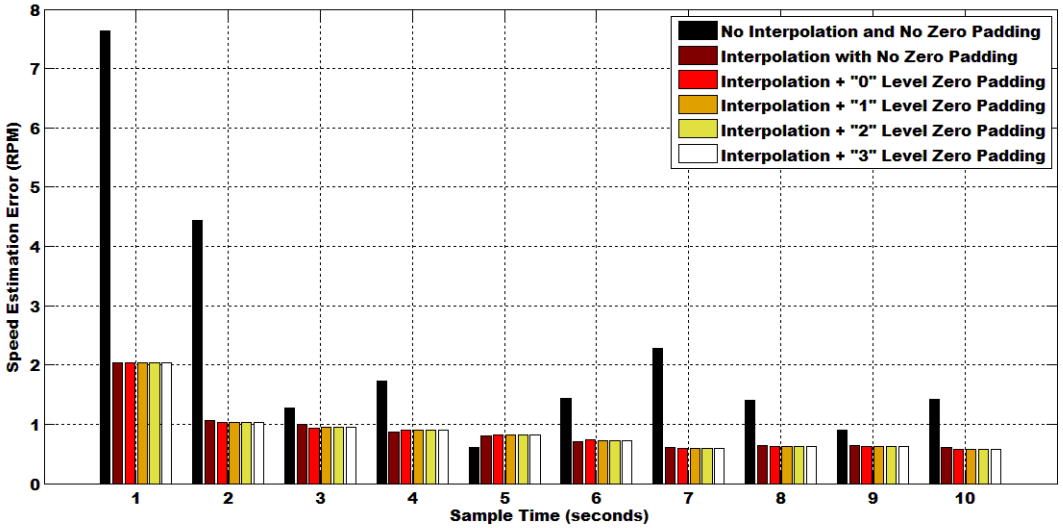

Figure B.2: 7.5 kW IM Speed Estimation Error Analysis @ 75% of Rated Load

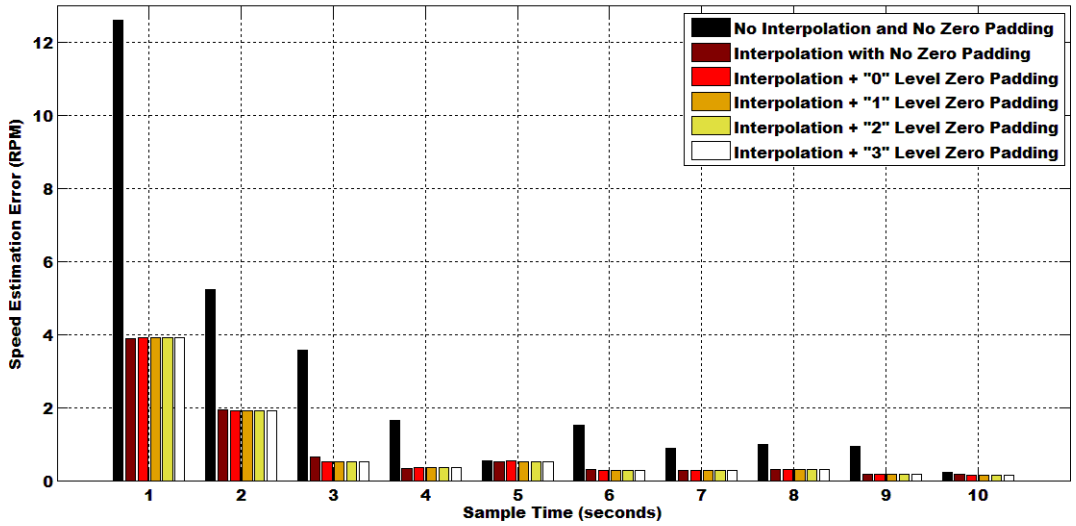

Figure B.3: 7.5 kW IM Speed Estimation Error Analysis @ 50% of Rated Load

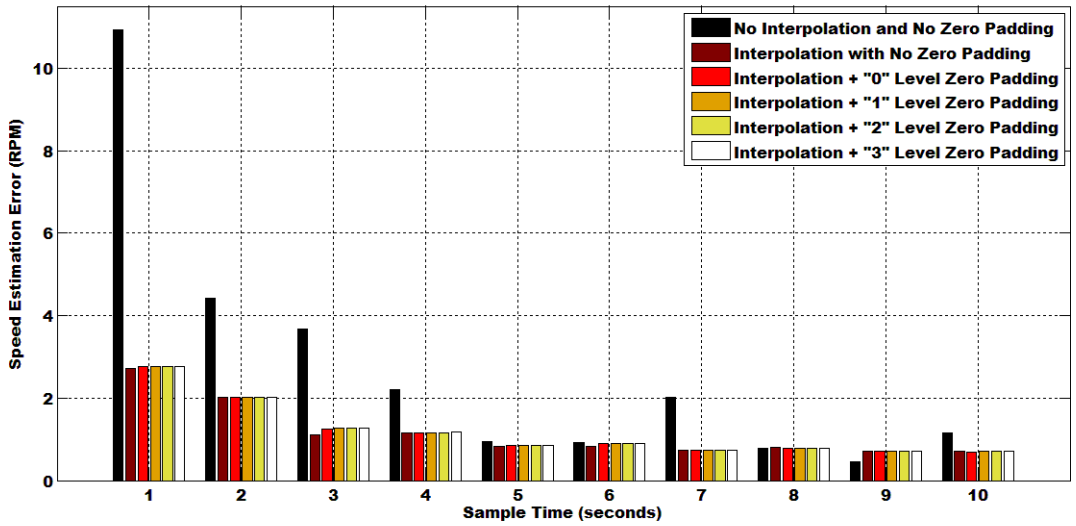

Figure B.4: 7.5 kW IM Speed Estimation Error Analysis @ 25% of Rated Load

Table B.1: 7.5kW IM Speed Estimation Repeatability Analysis @ 100% of Rated Load

		Sample Time of Vibration Data (seconds)									
		1	2	3	4	5	6	7	8	9	10
No Interpolation	$\overline{n_{err}}$	6.2463	4.0973	2.4041	1.8526	1.8457	1.2665	1.4797	1.0544	1.4354	0.9959
with No Z_{PF}	σ	3.0730	2.7465	1.2736	0.9175	0.3334	0.4155	0.5297	0.4533	0.6094	0.4847
Interpolation	$\overline{n_{err}}$	2.1418	1.0460	0.5141	0.7734	0.5548	0.5282	0.4664	0.2980	0.1560	0.0763
with No Z_{PF}	σ	1.7898	0.3175	0.3724	0.2028	0.3552	0.2458	0.1225	0.0493	0.0648	0.0792
Interpolation	$\overline{n_{err}}$	2.1411	1.0454	0.5333	0.7846	0.5609	0.5592	0.4604	0.2918	0.1556	0.0855
with $Z_{PF} = 0$	σ	1.7875	0.3444	0.2527	0.2293	0.3861	0.2707	0.1162	0.0468	0.0569	0.0689
Interpolation	$\overline{n_{err}}$	2.1386	1.0431	0.5358	0.7832	0.5555	0.5564	0.4607	0.2906	0.1543	0.0849
with $Z_{PF} = 1$	σ	1.7813	0.3374	0.2503	0.2320	0.3882	0.2662	0.1165	0.0467	0.0577	0.0685
Interpolation	$\overline{n_{err}}$	2.1387	1.0415	0.5339	0.7835	0.5545	0.5571	0.4608	0.2904	0.1541	0.0852
with $Z_{PF} = 2$	σ	1.7773	0.3369	0.2493	0.2335	0.3897	0.2663	0.1165	0.0471	0.0581	0.0684
Interpolation	$\overline{n_{err}}$	2.1380	1.0410	0.5334	0.7834	0.5542	0.5573	0.4608	0.2904	0.1541	0.0853
with $Z_{PF} = 3$	σ	1.7758	0.3362	0.2486	0.2342	0.3901	0.2661	0.1165	0.0474	0.0584	0.0684

$\overline{n_{err}}$ represents the average error between actual and estimated speeds (in rpm)

σ is the standard deviation for the repeatability tests

Table B.2: 7.5kW IM Speed Estimation Repeatability Analysis @ 75% of Rated Load

		Sample Time of Vibration Data (seconds)									
		1	2	3	4	5	6	7	8	9	10
No Interpolation	$\overline{n_{err}}$	7.6301	4.4378	1.2800	1.7359	0.6145	1.4311	2.2723	1.4060	0.9056	1.4256
with No Z_{PF}	σ	4.3996	0.5623	0.4338	1.3137	0.2974	1.1045	0.3410	0.4172	0.0881	0.4322
Interpolation	$\overline{n_{err}}$	2.0398	1.0570	1.0011	0.8728	0.8016	0.7067	0.6020	0.6404	0.6415	0.6077
with No Z_{PF}	σ	1.1007	1.0083	0.7087	0.6621	0.4131	0.3029	0.4252	0.2848	0.3525	0.4371
Interpolation	$\overline{n_{err}}$	2.0341	1.0257	0.9343	0.8935	0.8243	0.7333	0.5908	0.6240	0.6198	0.5782
with $Z_{PF} = 0$	σ	1.0964	1.0174	0.7903	0.6611	0.4294	0.3514	0.4249	0.2865	0.3605	0.4508
Interpolation	$\overline{n_{err}}$	2.0381	1.0281	0.9426	0.8952	0.8218	0.7288	0.5904	0.6227	0.6180	0.5769
with $Z_{PF} = 1$	σ	1.0889	1.0104	0.7879	0.6604	0.4278	0.3490	0.4242	0.2855	0.3620	0.4534
Interpolation	$\overline{n_{err}}$	2.0419	1.0291	0.9442	0.8956	0.8213	0.7286	0.5898	0.6221	0.6175	0.5758
with $Z_{PF} = 2$	σ	1.0833	1.0074	0.7868	0.6594	0.4278	0.3491	0.4241	0.2854	0.3622	0.4538
Interpolation	$\overline{n_{err}}$	2.0434	1.0296	0.9447	0.8958	0.8211	0.7284	0.5895	0.6218	0.6170	0.5754
with $Z_{PF} = 3$	σ	1.0804	1.0060	0.7855	0.6589	0.4278	0.3487	0.4241	0.2854	0.3623	0.4540

$\overline{n_{err}}$ represents the average error between actual and estimated speeds (in rpm)

σ is the standard deviation for the repeatability tests

Table B.3: 7.5kW IM Speed Estimation Repeatability Analysis @ 50% of Rated Load

		Sample Time of Vibration Data (seconds)									
		1	2	3	4	5	6	7	8	9	10
No Interpolation with No Z_{PF}	$\overline{n_{err}}$	12.6246	5.2337	3.5661	1.6488	0.5478	1.5159	0.8799	0.9947	0.9242	0.2370
	σ	5.3728	0.8695	1.4776	1.6708	0.1876	0.2239	0.2923	0.2538	0.0535	0.0251
Interpolation with No Z_{PF}	$\overline{n_{err}}$	3.8886	1.9440	0.6390	0.3236	0.5095	0.3052	0.2713	0.3074	0.1749	0.1618
	σ	1.3164	1.1956	0.2308	0.1171	0.3679	0.1704	0.1166	0.1610	0.1700	0.1548
Interpolation with $Z_{PF} = 0$	$\overline{n_{err}}$	3.9241	1.9058	0.5175	0.3490	0.5278	0.2814	0.2676	0.3029	0.1757	0.1497
	σ	1.3147	1.2271	0.1856	0.0978	0.3614	0.1994	0.1119	0.1593	0.1514	0.1439
Interpolation with $Z_{PF} = 1$	$\overline{n_{err}}$	3.9222	1.9028	0.5197	0.3526	0.5265	0.2815	0.2677	0.3030	0.1757	0.1493
	σ	1.3196	1.2286	0.1748	0.1011	0.3658	0.1940	0.1114	0.1593	0.1511	0.1443
Interpolation with $Z_{PF} = 2$	$\overline{n_{err}}$	3.9181	1.9004	0.5182	0.3526	0.5270	0.2805	0.2675	0.3028	0.1749	0.1491
	σ	1.3163	1.2292	0.1742	0.0998	0.3659	0.1935	0.1108	0.1587	0.1510	0.1438
Interpolation with $Z_{PF} = 3$	$\overline{n_{err}}$	3.9167	1.8991	0.5167	0.3528	0.5269	0.2798	0.2674	0.3027	0.1745	0.1490
	σ	1.3143	1.2293	0.1742	0.0994	0.3655	0.1935	0.1106	0.1584	0.1509	0.1436

$\overline{n_{err}}$ represents the average error between actual and estimated speeds (in rpm)

σ is the standard deviation for the repeatability tests

Table B.4: 7.5kW IM Speed Estimation Repeatability Analysis @ 25% of Rated Load

		Sample Time of Vibration Data (seconds)									
		1	2	3	4	5	6	7	8	9	10
No Interpolation with No Z_{PF}	$\overline{n_{err}}$	10.9262	4.4226	3.6735	2.1986	0.9380	0.9289	2.0193	0.7853	0.4575	1.1566
	σ	7.0920	0.7916	1.4058	1.5386	0.5786	1.2358	0.8549	0.0978	0.2543	0.6398
Interpolation with No Z_{PF}	$\overline{n_{err}}$	2.7233	2.0283	1.1010	1.1483	0.8171	0.8375	0.7293	0.7934	0.7184	0.7096
	σ	2.0969	1.3685	0.7587	1.0270	0.6345	0.4714	0.4953	0.5375	0.5193	0.4571
Interpolation with $Z_{PF} = 0$	$\overline{n_{err}}$	2.7730	2.0211	1.2543	1.1606	0.8444	0.8963	0.7243	0.7892	0.7114	0.6996
	σ	2.1558	1.3172	0.6878	1.0360	0.6365	0.4836	0.4970	0.5389	0.5173	0.4504
Interpolation with $Z_{PF} = 1$	$\overline{n_{err}}$	2.7700	2.0151	1.2699	1.1646	0.8454	0.8942	0.7259	0.7915	0.7134	0.7018
	σ	2.1406	1.3149	0.6867	1.0374	0.6383	0.4849	0.4990	0.5411	0.5197	0.4520
Interpolation with $Z_{PF} = 2$	$\overline{n_{err}}$	2.7719	2.0143	1.2735	1.1663	0.8463	0.8960	0.7266	0.7924	0.7142	0.7026
	σ	2.1378	1.3154	0.6876	1.0377	0.6385	0.4852	0.4991	0.5414	0.5196	0.4518
Interpolation with $Z_{PF} = 3$	$\overline{n_{err}}$	2.7724	2.0148	1.2741	1.1670	0.8470	0.8967	0.7270	0.7928	0.7145	0.7030
	σ	2.1358	1.3165	0.6882	1.0377	0.6385	0.4853	0.4992	0.5415	0.5197	0.4518

$\overline{n_{err}}$ represents the average error between actual and estimated speeds (in rpm)

σ is the standard deviation for the repeatability tests

Bibliography

[1] *IEEE Standard Test Procedure for Polyphase Induction Motors and Generators.* IEEE Std 112-2004, IEEE Power Engineering Society, New York, NY.

[2] *Rotating Electrical Machines - Part 2-1: Standard Methods for Determining Losses and Efficiency from Tests (Excluding Machines for Traction Vehicles).* IEC 60034-2-1 (2007), IEC, Geneva, Switzerland.

[3] B. Herndler, "Non-intrusive efficiency estimation of induction machines," Master's thesis, University of Cape Town, Department of Electrical Engineering, Cape Town, 2010.

[4] P. Sen, *Principles of Electric Machines and Power Electronics.* John Wiley & Sons, Inc, 2nd ed., 1997.

[5] N. Mohan, T. Underland, and W. Robbins, *Power Electronics.* John Wiley & Sons, Inc, 2nd ed., 1995.

[6] R. Krishnan, *Electric Motor Drives: Modeling, Analysis, and Control.* Prentice Hall, Inc., 2001.

[7] K. . Venkatesan and J. Lindsay, "Comparitive study of losses in voltage and current source inverted fed induction motors," *IEEE Transactions on Industry Applications*, vol. IA-18, No. 3, pp. 240–246, 1982.

[8] P. Cummings, "Estimating the effect of system harmonics on losses and temperature rise of squirrel-cage motors," *IEEE Transactions on Industry Applications*, vol. IA-22, No. 6, pp. 1121–1126, 1986.

[9] J. I. Smith and X. Serra, "Parshl: An analysis/synthesis program for non-harmonic sounds based on a sinusoidal representation," in *Proceedings of the International Computer Music Conference*, 1987.

[10] C. Gajjar, B. Herndler, P. Barendse, and M. Khan, "Speed estimation of induction machines by means of vibration analysis," in *Southern African Universities Power Engineering Conference (SAUPEC)*, 2011.

[11] A. VanWyk, "Effects of voltage unbalanced supplies on energy-efficient motors," Master's thesis, University of Cape Town, 2010.

[12] P. Walde and C. Brunner, "Energy-efficiency policy opportunities for electric motor-driven systems," tech. rep., InternatIonal Energy Agency (IEA), 2011.

[13] B. Renier, K. Hameyer, and R. Belmans, "Comparison of standards for determining efficiency of three phase induction motors," *IEEE Transactions on Energy Conversion*, vol. 14, No. 3, pp. 512–517, 1999.

[14] A. Boglietti, A. Cavagnino, M. Lazzari, and M. Pastorelli, "International standards for the induction motor efficiency evaluation: a critical analysis of the stray-load loss determination," *IEEE Transactions on Industry Applications*, vol. 40, No. 5, pp. 1294 –1301, 2004.

[15] E. Agamloh, A. Wallace, A. vonJouanne, K. Anderson, and J. Rooks, "Assessment of nonintrusive motor efficiency estimators," *IEEE Transactions on Industry Applications*, vol. 41, No. 1, pp. 127 – 133, Jan./Feb. 2005.

[16] B. Lu, T. Habetler, and R. Harley, "A survey of efficiency-estimation methods for in-service induction motors," *IEEE Transactions on Industry Applications*, vol. 42, No. 4, pp. 924–933, 2006.

[17] J. Hsu, J. Kueck, M. Olszewski, D. Casada, P. Otaduy, and L. Tolbert, "Comparison of induction motor field efficiency evaluation methods," *IEEE Transactions on Industry Applications*, vol. 34, No. 1, pp. 117 – 125, Jan./Feb. 1998.

[18] B. Lu, T. Habetler, and R. Harley, "A nonintrusive and in-service motor-efficiency estimation method using air-gap torque with considerations of condition monitoring," *IEEE Transactions on Industry Applications*, vol. 44, No. 6, pp. 1666 – 1674, Nov./Dec. 2008.

[19] A. Siraki and P. Pillay, "An in situ efficiency estimation technique for induction machines working with unbalanced supplies," *IEEE Transactions on Energy*, vol. 27, No. 1, pp. 85–95, 2012.

[20] A. Siraki, C. Gajjar, M. Khan, P. Barendse, and P. Pillay, "An algorithm for nonintrusive in situ efficiency estimation of induction machines operating with unbalanced supply conditions," *IEEE Transactions on Industry Applications*, vol. 48, No. 6, pp. 1890–1900, 2012.

[21] D. Casada, J. Kueck, H. Staunton, and M. Webb, "Efficiency testing of motors powered from pulse-width modulated adjustable speed drives," *IEEE Transactions on Energy Conversion*, vol. 15, No. 3, pp. 240 – 244, Sept. 2000.

[22] *Rotating Electrical Machines - Part 2-3: Specific Test Methods for Determing Losses and Efficiency of Converter-Fed AC Motors.* IEC 60034-2-3 (Draft Ed. 1), IEC, Geneva, Switzerland.

[23] S. Corino, E. Romero, and L. Mantilla, "How the efficiency of induction motor is measured?," in *International Conference on Renewable Energy and Power Quality (ICREPQ)*, 2008.

[24] E. Hughes, J. Hiley, K. Brown, and I. Smith, *Hughes Electrical and Electronic Technology.* Pearson Education Limited, 10th ed., 2008.

[25] E. Anyang, "The impact of variable speed drives on energy efficient induction motors," Master's thesis, University of Cape Town, Department of Electrical Engineering, Cape Town, 2011.

[26] C. Debruyne, J. Desmet, S. Derammelaere, and L. Vandevelde, "Derating factors for direct online induction machines when supplied with voltage harmonics: a critical view," in *IEEE International Electric Machnines & Drives Conference (IEMDC)*, 2011.

[27] X. Liang and Y. Luy, "Harmonic analysis for induction motors," in *IEEE Canadian Conference of Electrical and Computer Engineering (CCECE)*, 2006.

[28] "Technical guide induction motors fed by pwm frequency inverters," tech. rep., WEG, http://ecatalog.weg.net/files/wegnet/WEG-induction-motors-fed-by-pwm-frequency-converters-technical-guide-028-technical-article-english.pdf, 2009.

[29] J. Murphy and M. Egan, "A comparison of pwm strategies for inverter-fed induction motors," *IEEE Transactions on Industry Applications*, vol. IA-19, No. 3, pp. 363–369, 1983.

[30] P. Sen and H. Landa, "Derating of induction motors due to waveform distortion," *IEEE Transactions on Industry Applications*, vol. 26, No. 6, pp. 1102–1107, 1990.

[31] V. Kinnares, P. Jaruwanchai, D. Suksawat, and S. Pothivejkul, "Effect of motor parameter changes on harmonic power loss in pwm fed induction machines," in *IEEE International Conference on Power Electronics and Drive Systems*, 1999.

[32] A. Boglietti, "Pwm inverter fed induction motor losses evaluation," *Electric Machines and Power Systems*, vol. 22, Ed. 3, pp. 439–449, 1994.

[33] G. Yang and T. Chin, "Adaptive-speed identification scheme for a vector-controlled speed sensorless inverter-induction motor drive," *IEEE Transactions on Industry Applications*, vol. 29, No. 4, pp. 820–825, 1993.

[34] R. Supangat, N. Ertugrul, W. Soong, D. Gray, C. Hansen, and J. Grieger, "Estimation of the number of rotor slots and rotor speed in induction motors using current, flux or vibration signature analysis," in *Australasian Universities Power Engineering Conference (AUPEC)*, 2006.

[35] H. Zhang, K. Bradley, and P. Zanchetta, "A none-intrusive load and efficiency evaluation method for in-service motors using vibration tests with

an accelerometer," in *IEEE Industrial Applications Society Annual Meeting*, pp. 1–6, 2008.

[36] R. Lyons, *Understanding digital signal processing*. Prentice Hall, Inc., 2001.

[37] J. Proakis and D. Manolakis, *Digital Signal Processing - Principles, Algorithms and Applications*. Prentice Hall, Inc., 2007.

[38] "Zero padding does not buy spectral resolution," tech. rep., National Intruments, http://www.ni.com/white-paper/4880/en, 2006.

[39] P. Phumiphak and C. Chat-Uthai, "Non-intrusive method for induction motor field efficiency estimation using on-site measurement and modified equivalent circuit," in *15th International Conference on Electrical Machines and Systems (ICEMS)*, Oct. 2012.

[40] J. Allen and et al., "The effect of repair/rewinding on motor efficiency," tech. rep., Electrical Apparatus Service Association, Inc. (EASA), 2003.

[41] P. Pillay, V. Levin, P. Otaduy, and J. Kueck, "In-situ induction motor efficiency determination using the genetic algorithm," *IEEE Transactions on Energy Co*, vol. 13, No. 4, pp. 326–333, 1998.

[42] B. Lu, W. Cao, I. French, K. Bradley, and T. Habetler, "Non-intrusive efficiency determination of in-service induction motors using genetic algorithm and air-gap torque methods," in *Conf. Rec. IEEE 42nd IAS Annual Meeting*, 2007.

[43] J. Gomez, E. Quispe, M. deArmas, and P. Viego, "Estimation of induction motor efficiency in-situ under unbalanced voltages using genetic algorithms," in *18th International Conference on Electrical Machines (ICEM)*, Sept. 2008.

[44] E. Klingshirn and H. Jordan, "Polyphase induction motor performance and losses on nonsinusoidal voltage sources," *IEEE Transactions on Power Apparatus and Systems*, vol. PAS 87, No. 3, pp. 624–631, 1968.

[45] F. DeBuck, "Losses and parasitic torques in electric motors subjected to pwm waveforms," *IEEE Transactions on Industry A*, vol. IA-15, No. 1, pp. 47–53, 1979.

[46] F. DeBuck, P. Gistelinck, and D. DeBacker, "A simple but reliable loss model for inverter-supplied induction motors," *IEEE Transactions on Industry Ap*, vol. IA-20, No. 1, pp. 190–202, 1984.

[47] J. Hsu, J. Kuech, D. Casada, P. Otaduy, and L. Tolbert, "Comparison of induction motor field efficiency evaluation methods," *Conf. Rec. IEEE 31st IAS Annual Meeting*, vol. 1, pp. 703–712, 1996.

[48] H. Olsson, K. strm, C. de Wit, M. Gfvert, and P. Lischinsky, "Friction models and friction compensation," *European Journal of Control*, vol. 4, No. 3, pp. 176–195, 1998.

[49] S. Baluja, "An empirical comparison of seven iterative and evolutionary function optimization heuristics," tech. rep., Carnegie Mellon University, 1995.

[50] J. Greene, "A role for simple, robust black-box optimisers in the evolution of engineering systems and artefacts," in *Genetic Algorithms in Engineering Systems: Innovations and Applications, IEE Conference Publication*, 1997.

[51] S. Baluja, "Population-based incremental learning: A method for integrating genetic search based function optimization and competitive learning," tech. rep., Carnegie Mellon University, 1994.

[52] E. Hughes, "Optimisation using population based incremental learning (pbil)," in *IEE Colloquium on Optimisation in Control: Methods and Applications*, 1998.

[53] S. Baluja and R. Caruana, "Removing the genetics from the standard genetic algorithm," in *Proceedings of the Twelfth International Conference on Machine Learning*, July 1995.

[54] S. Baluja, *Advances in Neural Information Processing Systems 9*, ch. Genetic Algorithms and Explicit Search Statistics, pp. 319–325. MIT Press, Cambridge, MA., 1997.

[55] *MAGTROL TM 300 Series In-Line Torque Transducers Users Manual*. Magtrol, Inc., 2009.

[56] F. Ferreira and A. deAlmeida, "Method for in-field evaluation of the stator winding connection of three-phase induction motors to maximize efficiency and power factor," *IEEE Transactions on Energy Conversion*, vol. 21, No. 2, pp. 370 – 379, June 2006.